Characterisation of Fluorescent Concentrators in Visible Light Communication

Amna Riaz

Mansfield College

University of Oxford

Supervised by

Prof. Steve Collins

Prof. Dominic O'Brien

A thesis submitted for the degree of

Doctor of Philosophy

Michaelmas 2021

Abstract

Visible Light Communication (VLC) has gained significant attention in the last few years. In VLC, light from existing solid-state light sources is used as a data carrier. The maximum capacity of a VLC channel, like other communications systems, is dependent upon two key factors i.e. the signal-to-noise ratio (SNR) at the receiver and channel bandwidth. VLC systems rely upon light-emitting diode (LED) and lasers as the light sources. Unfortunately, due to the limited bandwidths of most commercial LEDs, a higher data rate can only be achieved by increasing the SNR at the receiver. One simple way to increase SNR is to use a large detector, however, this results in larger capacitance which consequently reduces the bandwidth of the detector. Previously, optical concentrators such as parabolic and compound parabolic concentrators have been coupled to the detectors to concentrate light onto the detector, however, these concentrators are limited by the conservation of etendue. Alternatively, a relatively new approach is to use fluorescent concentrators (FC) which do not conserve etendue and can provide much higher optical gains.

In this thesis, the performance of several types of FC is characterised for use in VLC links which includes gain, bandwidth, absorption-emission spectra, FOV and maximum achievable data rates. The selective absorption of different wavelengths by the FC means that they act as natural filters, therefore, the performance of a blue filter was compared to an FC. Experimental results are presented which show that the FC not only increased the FOV but also increased the maximum achievable data rate. In addition, the feasibility of enabling a wavelength division multiplexing (WDM) system with FCs is discussed. More importantly, a wide FOV receiver for a smartphone that was designed by coupling a commercially available fluorescent fibre to an APD is presented. This receiver provides a wide FOV of ±120°, for a smartphone application. Finally, a method to predict the OOK data rate is described with the experimental results.

Acknowledgements

First and foremost, I would like to express my deep gratitude to my supervisor Professor Steve Collins for valuable guidance, encouraging support, useful critiques, and unlimited patience during my DPhil research journey. I cannot thank him enough for his kindness and insightful feedback, which pushed me to sharpen my analytical skills and brighten my research work to a higher level.

I also would like to thank my co-supervisor Professor Dominic O'Brien for providing me with helpful suggestions and comments. A special thanks to Dr Hyunchae Chun for constructive suggestions and knowledgeful discussions. Meanwhile, I would also like to thank Dr Ravinder, Dr Andy Schreier and Grahame Faulkner for their valuable technical support. My sincere thanks also go to Mr Zubair Ahmed and Mr Paramin Sangwongngam as well as other colleagues for the interesting discussions and sharing ideas. Moreover, I would thank Dr Wajahat Ali, for facilitating me to run my experiments remotely during the COVID-19 lockdown. Moreover, I would like to thank the Pakistan Endowment fund (PEEF) to fund my research and my living cost in the UK. Finally, I wish to thank my parents and my husband for their support and encouragement throughout my DPhil journey. I am out of words to express my gratitude towards our baby girl Fajr Umair who has always been extremely cooperative, patient and understanding towards the study and work commitments of her parents.

Abbreviations

VLC	Visible Light Communication
WLED	White Light Emitting Diode
LED	Light Emitting Diode
LD	Laser diode
LIV	Light-current-voltage
PD	Photodiode
APD	Avalanche Photodiode
AWG	Arbitrary waveform generator
SNR	Signal to noise ratio
ISI	Inter-symbol Interference
BER	Bit Error Rate
BW	Bandwidth
CPC	Compound parabolic concentrator
DFE	Decision feedback equalisation
FC	Fluorescent concentrator
FOV	Field of view
FSO	Free-Space Optical Communication
OWC	Optical Wireless Communication
IM/DD	Intensity Modulation Direct Detection
NRZ	Non-return-to-zero
OOK	On-Off Keying
PAM	Pulse amplitude modulation
QAM	Quadrature amplitude modulation

OFDM	Orthogonal Frequency-Division Multiplexing
QE	Quantum Efficiency
OG	Optical gain
TX	Transmitter
RX	Receiver
ROS	Received output signal
WDM	Wavelength division multiplexing
MIMO	Multiple input multiple output

Contents

List of Figures

List of Tables

1 Literature Review

1.1 Visible light communication

Due to a rapid increase in the demand for wireless services, the unused radio frequency (RF) spectrum is shrinking at an even higher pace [1]. The growing number of mobile users with an increased number of wireless applications suggests that, in the future, it will be challenging to meet users' demands through the existing wireless system [2]. This scarcity of radio spectrum resources is known as 'Spectrum-Drought'[3]. Overcoming this drought will take time and it will be expensive [4].

It is also predicted that a higher number of devices using the RF spectrum will generate higher interference between the devices communicating with a host in a close proximity. A higher level of interference will eventually significantly degrade the service quality [5]. Therefore, new spectrums are required to support the extended wireless capacity [6]. For these reasons, other spectrum bands, such as higher radio frequency (20-90GHz), terahertz, microwave and optical wavelengths (infrared (IR), visible, and ultraviolet (UV) regions) have been investigated [6][7][8].

Optical Wireless Communication uses the visible, infra-red and UV spectrum of light for wireless communication [8]. In particular, communication through visible light is known as visible light communication (VLC). VLC mainly uses light-emitting diodes (LEDs) as a transmitter and it is expected that eventually, LEDs will dominate the general illumination infrastructure by the end of the decade[8][9]. These LED light sources transmit information by the modulation of light [10]. The main advantages of VLC compared to their RF counterpart are (1) VLC uses unlicensed (THz) spectral bands [11], (2) it ensures higher transmission security for indoor applications as the light does not pass through the walls, whereas for RF signals it is not possible, (3) no electromagnetic interference, (4), it is much cheaper as compared to RF communication [12], (5) under-eye safe limits, it is harmless for the human body, (6) it does not influence to the other surrounding sensitive equipment through radio waves, (7) it offers far less energy consumption as the existing illumination

infrastructure can be utilised for data transmission, (8) a huge number of channels are available [13][14][15][16].

A typical VLC system is shown in Figure 1.1. The information in VLC is first encoded and then converted to voltage levels to drive the light source which is either a laser diode (LD) or light-emitting diode (LED). The detected data from the photodiode (PD) on the receiver terminal is then amplified, demodulated and decoded to restore the original data from the received signal [17].

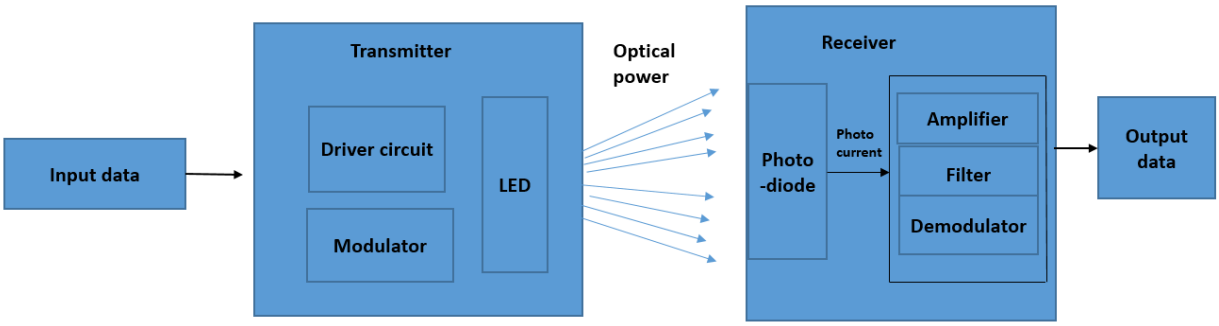

Figure 1.1 The basic architecture of a typical VLC system.

Typically, an LD or LED is used as the source at the transmitter end, and a PIN photodetector or avalanche photodetector is used as a detector in the receiver terminal of the VLC optical link [18]. At the transmitter end, the LD or LED is driven by modulated analogue signal usually generated through a transmitter driver. Laser-based VLC systems have advantages over their LED-based systems, including high bandwidths and long transmission distance [19]. However, due to eye safety requirements, LED is preferred in a commercial environment [19].

The transmission of VLC signal from LED or LD is based upon the “intensity modulation” (IM) principle where information bits are modulated into the optical power or intensity. The signal is then sent over the channel, which is air in wireless VLC where the transmitted signal gets affected by the interference from ambient light and suffers attenuation [20].

In VLC, the control of the phase of an optical carrier is complicated and expensive [21]. In addition to this, the detection of the phase at the receiver terminal is difficult in VLC [22]. In intensity modulation and direct detection (IM/DD), the intensity of the light source (LED or LD), is modulated by the transmitted signal so the information of phase is not required. On-off keying (OOK) is the most commonly used IM/DD modulation scheme in VLC due to its simple implementation [23]. However, OOK-modulated LEDs cannot support high data rate requirements for a VLC link. Multi-level pulse amplitude modulation (PAM) is more popular in visible light communication [24]. There are other modulation schemes such as Orthogonal Frequency-Division Multiplexing (OFDM) [25] which can exploit the bandwidth of a VLC channel by employing adaptive data and power allocation to multiple frequency sub-carriers [26][27][28]. Furthermore, quadrature amplitude modulation (QAM) is another type of modulation scheme which is used in the VLC system, it helps in increasing the spectral efficiency and hence the overall capacity of a transmission system [29].

The receiver recovers the transmitted signal through a “direct detection” (DD) scheme. A photodiode is used to detect the intensity variations. The photodiodes are light-sensitive devices, that generate electric current when optical power is incident on them [30]. Mostly, a PIN photodiode or an avalanche photodiode is used for this purpose [31]. Recently, a photon-counting silicon photomultiplier (SiPM) has been introduced as a replacement for photodiodes [32]. These devices are extremely sensitive, however, in the presence of ambient light, they saturate due to the additional noise from the ambient light [33][34][35].

In communication, signal to noise ratio (SNR) is a technical measurement parameter that compares the level of the desired signal to the amount of background noise. In other terms, SNR is the ratio of desired information or signal power to undesired information or background noise power, with decibels as the standard unit of measurement (dB) [36]. Furthermore, a signal-to-noise ratio larger than 0 dB or greater than 1:1 indicates that there is more signal than noise.

When the data rate is approximately six or seven times the bandwidth of the system, the inter-symbol interference (ISI) power penalty increases exponentially [37]. This means that it is impossible to increase the data rate beyond this value by increasing the SNR [38]. To increase the data rate further, equalisation techniques are usually employed. The channel equalisations are either linear such as zero-forcing equalizer (ZFE) or non-linear such as decision feedback equalization (DFE) [39]. For every symbol decision ZFE forces the ISI to become zero, however, it results in the enhancement of the noise and consequently the performance degrades. The decision feedback equaliser (DFE) is a non-linear equaliser which is needed when the ISI is too high for the linear equalisation to correct the channel impairment. DFE detects the symbol's feedback to estimate the channel output [40]. DFE evaluates the error in each step of iteration and corrects the error by the feedback method which makes it slower than ZFE, however, it can reconstruct the received signal much more accurately.

All equalisation techniques reduce the impact of ISI using multiple samples of the received signal, often known as taps. Since the sampling rate of the signal is proportional to the data rate, the number of samples needed to cover the duration of ISI increases as the data rate increases [40][41].

Due to lower SNR and ISI when the data is transmitted, there is a chance that errors will be introduced into the system. Bit error rate or bit error ratio (BER) is defined as the ratio of a total number of bits in error to the whole length of the transmitted bitstream as given by eq. 1.1 [42]. BER provides an excellent way to achieve this. In digital communications, the BER is used as a measure of how well the receiver can decode the sent data.

$$BER = \frac{\text{Number of Errors}}{\text{Total Number of bits}} \qquad (1.1)$$

According to Säckinger et al, if the noise is Gaussian, the BER could be calculated by

$$BER = \frac{1}{2} erfc\left(\frac{Q}{\sqrt{2}}\right) \qquad (1.2)$$

Where erfc is the error function and Q is the Q parameter, also called Personick Q, is a commonly used measure of the signal-to-noise ratio (SNR). Equation 1.2 suggests that if the value of BER is known then the Q factor can also be calculated by using

$$Q = \sqrt{2} \times erfc^{-1}(2 \times BER) \quad (1.3)$$

where *erfcinv* is the inverse of the complementary error function

With $$Q = \frac{V_{pp}}{2V_{rms}} \quad (1.4)$$

where the numerator is the peak to peak voltage difference between the average receiver output voltage when a zero and a one are transmitted [43] and the denominator is total root mean square noise when a bit zero and a bit one are transmitted. As the difference of mean values of bit one and zero in the received data signifies the received voltage signal, so the numerator in eq. (1.4) could be replaced by the difference between the mean of bit one and the mean of bit zero. Furthermore, the standard deviation (sigma) of bit one and bit zero represents the noise, so the denominator in eq. (1.4) can be replaced by the sum of $sigma_1$ and $sigma_0$. Hence, eq. (1.4) can be written as

$$Q = \frac{\text{Mean}_1 - \text{Mean}_0}{\text{Sigma}_1 + \text{Sigma}_0} \quad (1.5)$$

1.2 Need for Optical concentrators in VLC

According to the Shannon–Hartley theorem, the maximum channel capacity depends upon the bandwidth of the channel and signal to noise ratio at the receiver terminal [44].

$$C = Blog_2\left(1 + \frac{S}{N}\right) \quad (1.6)$$

Where *C* is the channel capacity, *B* is the bandwidth of the channel, *S* is the average received signal power over the bandwidth, *N* is the average noise power over the bandwidth, and *S/N* is the signal-to-noise ratio (SNR) of the communication signal to the noise and interference at the receiver.

If LEDs have to be used as a transmitter in VLC, a higher SNR is particularly desirable as current LEDs have a bandwidth (BW) of 5-20 MHz [45]. Recently, Gallium nitride (GaN) micro-LEDs, which have dimensions less than 175 µm, are presented which have modulation bandwidths of 580 MHz [46]. The laser can be an alternative option as a transmitter that has a bandwidth of hundreds of MHz [47]. However, due to eye safety protocols and the limited use of LD in the lightning infrastructure, they are not a popular choice from the user's perspective [48].

The receiver should also have a higher bandwidth [49]. Several choices are available for photodetectors (PD) which can be used as a receiver in VLC [50]. To achieve a high data rate, if the lasers are used as the transmitters, then to meet the higher bandwidth requirements at the receiver end, the PD's active area has to be smaller (a small active area of PD means high BW) [51]. Typically, optically designed concentrators called parabolic concentrators, and compound parabolic concentrators (CPC) are used with small area detectors for increasing the optical intensity of the PD [52].

1.3 Importance of Field of View

Most of the high-speed detectors have a small collection area as shown in Table 1-1. A list of commercially available APDs with their corresponding active area and BW is provided in Table 1.1.

Table 1-1 The comparison of active area and BW of C8664-02K Hamamatsu APD series.

APD module	Active area	Bandwidth
C8664-02K	0.2 mm^2	700 MHz
C8664-05K	0.5 mm^2	680 MHz
C8664-10K	1.0 mm^2	530 MHz

C8664-02K Hamamatsu APD has an active area of only 0.2 mm^2 which leads to a smaller SNR, however, it has a higher BW of 700 MHz. Similarly, C8664-05K APD has a comparatively larger

active area of 0.5 mm^2, however, due to the increase in the active area the BW decreases to 680 MHz only.

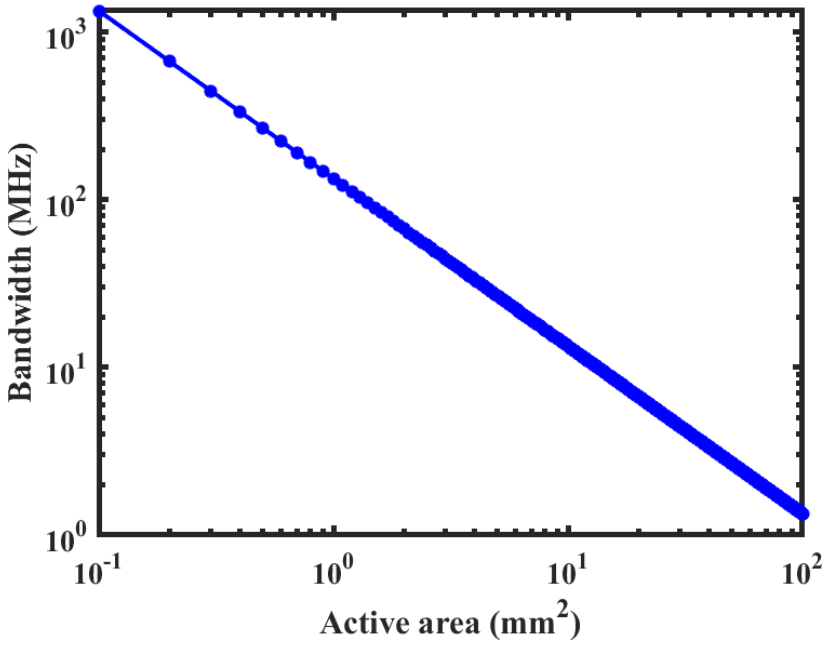

Figure 1.2 The relationship between detector area vs BW from Hamamatsu S8664 series plotted by using equation (1.7).

Increasing the detector's active area increase the light collection ability but it also increases the capacitance. Higher capacitance means a smaller bandwidth which is not desirable. If the BW of the APD is BW_{APD}, then the relation between the active area of the PD and the BW is as follows

$$BW_{APD} = C_{APD}\left(\frac{1}{A_{APD}}\right)^{k} \qquad (1.7)$$

Where is C_{APD} the capacitance and A_{APD} is the area of the APD, whereas k is a constant describing a specific detector technology. This relationship was plotted in Figure 1.2, by using the values of $C_{APD=}7.9 \times 10^4$ and $k = 0.59$ from the data sheet of Hamamatsu S8664. The relationship between the active area and the bandwidth validates that for making the APDs high BW, their active area has to be small.

To achieve higher BW and better SNR, optical concentrators are usually coupled on the receiver side. Optical concentrators, collect the light over a large collection area and focus it to the small size detector. PC and CPC are non-imaging concentrators given the fact that they do not form an image of the source on the detectors [53]. Most CPCs are created by the combination of two symmetric parabolic concentrators.

Concentrators should have two characteristics, first, higher efficiency of concentrating light so that the detector gets higher optical intensity called gain and the second greater acceptance angle which is called Field of View (FOV) [54]. In an optical system, etendue is a geometric property of light, which quantifies how much the light spreads out in terms of area and angle. Conventional optical concentrators such as PC and CPC depend on the process of reflection and refraction which means they have a limiting property called conservation of etendue. The conservation of etendue limits the maximum gain as FOV increases [55]. The maximum achievable geometric gain, in a 2-D concentrator, is given by

$$G_{max} = \frac{n^2}{\sin^2 \theta_{max}} \qquad (1.7)$$

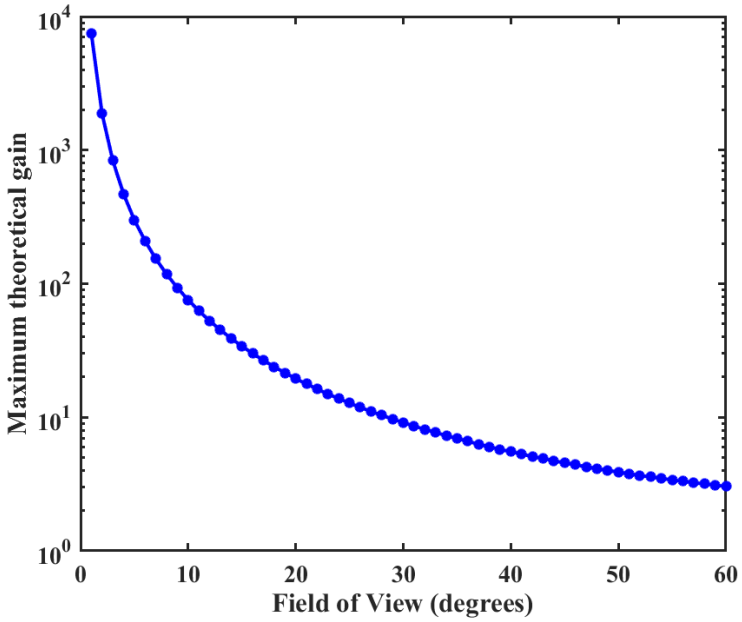

Figure 1.3 Relation between FOV and theoretical gain of a CPC.

where G_{max} is the maximum gain, n is the refractive index and θ_{max} shows the maximum possible incidence angle. It can be seen from equation 1.4 that, if a CPC is made from glass then it has a refractive index of 1.5 and its maximum FOV is 35° with a gain lower than 5 as shown in Figure 1.3. It can be seen that as the FOV increases, the gain of the optical concentrator decreases rapidly.

An alternative to the conventional optical concentrators are the fluorescent concentrators, which have a doping of a fluorophore material and they are not limited by conservation of etendue as reported in [55]. In this thesis, further work on the practicality of different types of commercially available fluorescent concentrators will be discussed.

1.4 Luminescent solar concentrators

The idea of fluorescent concentrators that are not limited by etendue can be traced back to the luminescent solar concentrator (LSC) [56]. They were initially proposed in the 1970s, to replace the expensive large areas of solar cells with inexpensive concentrators. Initially, the development of LSC was limited due to the bad performance of the limited types of dye available at that time [57]. In the later years, the performance of organic dyes and quantum dots was evaluated under a project called 'full spectrum' [58]. These organic dyes are available in a wide range of types with better reabsorption properties. Furthermore, they can have a higher luminescence efficiency. In comparison to them, quantum dots (QD) have a broader absorption spectrum even extending to the UV. The QDs are inherently more stable than dyes. The absorption spectra of QD can be effectively changed by just choosing different nanosize spheres. An important LSC characteristic is a concentration factor (C), defined as the ratio of the output and the input photon flux densities [59]. In the 21st century, LSCs received considerable attention as low-priced sunlight collectors for photovoltaic (PV) cells not only in residential and solar farm-scale PV installations but also in space-based systems. The sunlight collectors were made up of a large-area slab of transparent material containing highly emissive fluorophores and coupled with small PV cells at the edge or the bottom. The fluorophores absorb incident light to them, reemitted at a longer wavelength, and then a portion of the light is guided

toward the PV cells where it is converted into electricity. Large collection areas are preferred to increase the concentrating factor, but the travel time increases which is not desirable. To overcome this problem, a solution to attach PV to the backside of the concentrator is proposed [60].

The emission of light from any substance is called luminescence [61]. It is further divided into two types. First is phosphorescence, in which a substance absorbs photons and emits them after a certain delay (usually seconds) between absorption and emission [62]. The second is fluorescence, which is the same as phosphorescence with the exception that they have a much shorter delay time (in nanoseconds) [63].

1.5 Operation of a fluorescent concentrator

The incident light to an FC undergoes various processes. In general, when the light enters the FC, it gets absorbed by the fluorophore within the FC [64]. After the process of fluorescence, the light gets emitted at a longer wavelength than it was absorbed, called the Stokes shift. Some of the light will be reabsorbed and remitted until it reached the detector by total internal reflection as shown in Figure 1.4. The desirable feature of this FC is that any light which is not reabsorbed by fluorophore

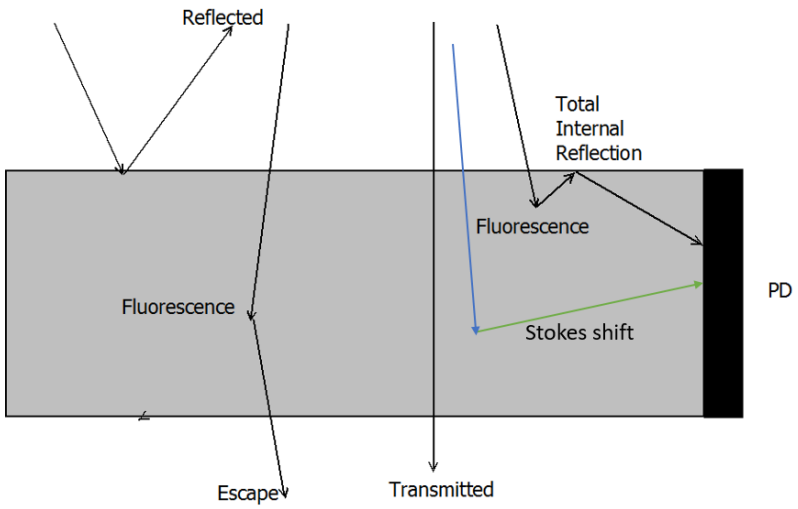

Figure 1.4 Schematic diagram of the physical processes in a fluorescent concentrator with a photodetector PD on its right hand edge.

eventually reaches the detector. Due to these undergoing processes, the performance of FC does not

only depend upon the processes of reflection and refraction only, therefore, FC does not conserve etendue [65].

Furthermore, by emitting light at a longer wavelength than it absorbs, fluorescent concentrators also change the wavelength of the light reaching the photodetector in the receiver. Since the responsivity of many photodetectors is higher at green wavelengths than at blue wavelengths, the wavelength shift (Stokes shift) in the concentrator will create a second increase in the receiver output signal and hence increase the SNR [66].

Like LSC, fluorescent slab concentrators also have a glass or plastic doped with a fluorophore in them [67]. The incident light towards the fluorescent concentrator undergoes several processes. It may get transmitted through the concentrator or reflected from the surface of the concentrator. In addition to this, it may get absorbed, emitted, reabsorbed, and remitted by the fluorophore material and retained by the concentrator by total internal reflection until it reaches the edges where the photodetector can collect it [68].

There are two types of luminescence - phosphorescence has a timescale of milliseconds that is too slow, and so unlike LSCs, fluorescent concentrators (FCs) have to contain fluorophores. To meet the

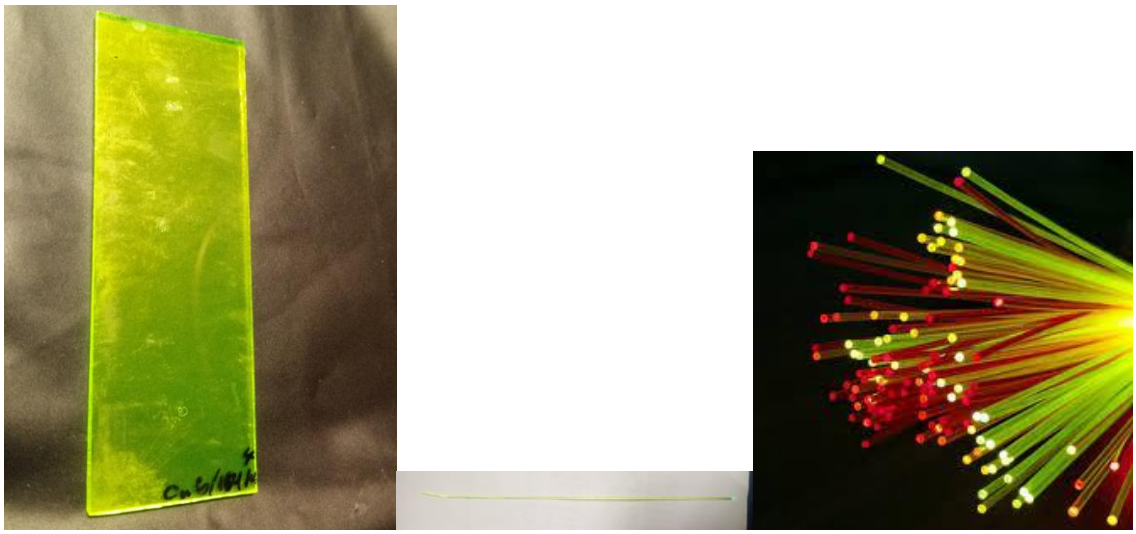

Figure 1.5 Photos of different types of commercially available concentrators.

VLC challenges of achieving higher data rates than RF counterparts, the fluorescent concentrator

must have a delay of nanoseconds or less. Unfortunately, the longer time decay of the phosphorescence in the luminescent materials makes them too slow for VLC, therefore, they cannot be used as a concentrator in an optical communication link. The performance of FC depends on the type of fluorophore present in them [69]. The fluorophore compounds have two discrete energy states, ground and excited, represented as S_o and S_1 respectively. If the photon incident to the fluorophore is absorbed, an electron sitting in the ground state will gain energy and shift to the excited state. The time of stay for an electron in the excited state is called the lifetime. Usually, fluorophores have a lifetime of nano seconds [70]. Fluorophore has the ability to absorb photon depending upon their wavelength. This photon absorption probability depending upon wavelength is called the absorption spectrum. The emitted photons have a longer wavelength due to the non-radiative losses. The wavelength range of the emitted photon is called an emission spectrum. Not every photon absorbed by the fluorophore is emitted as a photon because they may get absorbed and lost. The ratio of the number of photons being emitted to the number of photons absorbed is called quantum yield.

$$\text{Quantum yield} = \frac{\text{number of photons emitted}}{\text{number of photons absorbed}} \qquad (1.8)$$

Unlike a CPC, fluorophores have a lifetime and hence a limited bandwidth. Moreover, the exponential decay of a fluorophore gives rise to a single-pole frequency response.

1.6 Gain of the concentrator

Gain is a product of the concentrating factor and the probability of the number of photons that enter the FC, get converted to another wavelength and finally reach the PD. As explained in the previous section, there are different possibilities for photons falling on the concentrator. Therefore, the efficiency of concentrators can be defined as the ratio of power intensity incident to the antennas to the power intensity coming from the edge of that antenna.

$$\mathrm{G} = \left(\frac{\mathrm{n}}{\mathrm{A_r}}\right) \Big/ \left(\frac{\mathrm{N_i}}{\mathrm{A}}\right) \qquad (1.9)$$

where G is the gain, n is the total number of photons received, A_r is the surface area of the concentrator and A is the total surface area on which the N_i photons are incident.

The gain could be defined either in terms of output power (as optical intensity) or in output voltage. Equation 1.10 quantifies gain in terms of power, where power per unit area is essential for a fair comparison

$$\text{Gain} = \left[\frac{\text{intensity from edge concentrator edge } \left[\frac{\text{W}}{\text{m}^2}\right]}{\text{reference intensity}\left[\frac{\text{W}}{\text{m}^2}\right]}\right] \qquad (1.10)$$

If the gain has to be measured in terms of the output voltage, then certain factors like responsivity of the detector at different wavelengths, the area of the detector and the gain of TIA becomes important. Equation 1.11 gives a relation to measuring the gain in this scenario.

$$\text{Gain} = \frac{\left[(\text{Resposnitivity@green})^{\bar{1}}\left[\frac{\text{W}}{\text{A}}\right] \times \text{TIA Gain}^{\bar{1}}\left[\frac{\text{A}}{\text{V}}\right] \times \text{measured voltage from cont. edge [V]} \times \text{concentrator edge area}^{\bar{1}}\left[\frac{1}{\text{m}^2}\right]\right]}{\left[(\text{Resposivity@blue})^{\bar{1}}\left[\frac{\text{W}}{\text{A}}\right] \times \text{TIA Gain}^{\bar{1}}\left[\frac{\text{A}}{\text{V}}\right] \times \text{measured voltage at the reference plane [V]} \times \text{PD area}^{\bar{1}}\left[\frac{1}{\text{m}^2}\right]\right]} \qquad (1.11)$$

1.7 Bandwidth measurements

The presence of the fluorophore is critical to avoiding the limitations of etendue. However, fluorophores have a finite lifetime and their temporal response is often a single exponential. If this is the case and the lifetime is τ then the corresponding bandwidth will be

$$B = 1/2\pi\tau \qquad (1.12)$$

This is potentially crucial because the capacity of a VLC communication channel is proportional to its bandwidth as suggested by Shannon's theorem given in equation 1.6.

1.8 Previous work on Fluorescent concentrators

The wide FOV fluorescent concentrators have been reported with a FOV of 60^0 [71]. A concentrating factor of 12 and a wide field of view and increasing the data rates by threefold were reported [72]. Facebook has demonstrated the achieved data rates of 2.1 Gbps with a tailored fluorescent

concentrator [73]. However, their work was not user-friendly as they used high power at the receivers which are not eye-safe with the use of complex modulation schemes like OFDM. A simple method to increase the optical gain of the FC in [74]. There is a need to understand the behaviour of FC for their incorporation in a VLC receiver for future usage. A fibre-based receiver with a bandwidth of approximately 85 MHz and a data rate of 250 Mbps suitable for UV-based underwater wireless optical communication has recently been reported [75].

300 Mbps were achieved with an FC-based receiver and with a FOV of ± 60° [76]. Mulyawan et al presented an FC-based two-channel multiple-input multiple-output (MIMO) VLC system in which they demonstrated a data rate of 32 Mbps with a FOV of ±22.5 degrees [77]. Recently, Pavlos et al presented a fluorescent concentrator-based receiver for wavelength division multiplexing (WDM) for data communication [78]. In the presented geometry, the receiver was created with a stack of two FCs for two independent modulated channels. However, the presented matrix has a cross-talk of 30%, which is not desirable. Recently, the bandwidth limitations of fluorescent solar concentrators, which are employed as a detector in optical communication links, were analysed by Portnoi et al [79]. They introduced a low-pass RC filter model, which is verified by Monte-Carlo simulation to demonstrate the importance of mutual optimisation between the time response and the optical gain of the fluorescent solar concentrators [79]. Surampudi et al also presented a method to improve the bandwidth of the FCs which consequently improved the data rate up to three folds [80].

Recently, Ali et al reported 1.45 Gbps data transmission by using a Penta-fluorine concentrator plus a BG3 filter [81]. However, these fluorescent concentrators are not commercially available and the detector was a silicon photomultiplier (SIPM) instead of a photodetector [81]. Furthermore, Ali et al discussed the impact of varying the length of fibre in terms of bandwidth and gain i.e. the longest fibres required the lowest power from the transmitter, however, the bandwidth in the long fibres decreased due to a high transit time of photons in the large concentrator [82]. They suggested that the best length of the fluorescent fibre in an optical link depends upon the desired data rate. In addition

to that, a method to enhance the coupling efficiency by using edge and back reflection of a planar concentrator by using Lambertian-, specular-, and retro-reflectors is demonstrated [83]. They showed an improvement of a factor of two in the received output signal (ROS). Moreover, a smart license plate receiver incorporated with a fluorescent concentrator was proposed for high-speed vehicle-to-vehicle communication [84]. The data rate of more than 500 Mbps was achieved with a FOV of ±25°. Recently, a Quantum dot (QD) fluorescent concentrator combined with power domain multiplexing of a non-orthogonal multiple access (NOMA) scheme was presented with an achievable data rate of 120 Mbps for underwater applications [85].

1.9 Aims of the project

The conservation of etendue has been a bottleneck in the optical receivers. FCs which do not conserve etendue can be a good replacement for conventional optical concentrators. Previous work was mostly focused on the tailored designs of the FCs which are yet not available in the market. The main objective of this work is to characterise the commercially available FC for a VLC link. One definite advantage of fluorescent concentrators when employed in an optical link is that they increase the receiver output signal (ROS) and hence the SNR which plays an important role in determining the maximum achievable data rate.

An important objective of this research is to study the performance of an FC in comparison to different bandpass filters. A detailed investigation will be carried out to evaluate the performance of the low BW fluorescent concentrator in a white light set-up to study their behaviour in an office lighting atmosphere and the robustness of the system. More importantly, the selective absorption of the fluorophore at some wavelengths and the wide field of view mean that they have an ability to practically perform as wide field of view filters. Hence, one fundamental objective of this research was to investigate the benefits of exploiting this filtering property of the FCs to create an RX that detects the blue light from a WLED.

Most of the work in the past has been focused on slab concentrators, however, the fluorescent fibres have a diameter similar to most of the high BW APDs. This suggests more focused light from the edge of the fluorescent fibres can be collected by the APD. Therefore a fundamental aim of the project includes characterising different off-the-shelf fluorescent fibres which vary in absorption, and emission properties along with the different levels of fluorophore doping and the BW. The study will aim to present the performance comparison using FC coupled to a photodetector as a receiver and the photodetector alone as the receiver in terms of optical gains and the maximum achievable data rates.

Moreover, the selective absorption spectra of fluorophores in the FCs create an opportunity to employ wavelength division multiplexing (WDM) in order to increase the link capacity. However, there are several challenges to construct a reliable WDM link such as selecting a suitable combination of the fluorescent concentrator and minimising the cross-talk between the data streams. Previously, two different fluorophores have been incorporated in a rectangular optical element made from microscope slides. However, the H-matrix for this system was far from ideal and indicated 30% of cross-talk. In addition, the field of view of these planar structures is determined by the projected area of a rectangle. In contrast, fluorescence fibres integrated with photodetectors can have a significantly wider FOV and less cross-talk. Therefore one of the key aims of the work presented in this thesis was to exploit the selective absorption of different fluorescent fibres to support WDM. The study includes an evaluation of the performance of different commercially available FCs for their ability to enable a WDM link. An inexpensive, simple and practical receiver that contains different fluorescent fibres and can therefore support WDM will be demonstrated.

In addition, one of the key challenges that are a hurdle in the utilisation of VLC in portable devices such as phones, tablets, and laptops is their constantly changing orientation which creates connectivity issues. In the past, most of the work has been focused on using multiple transceivers for a smartphone to achieve a wide FOV. However, this approach increases the complexity and the cost of the system. A key aim of this thesis was, therefore, to design a fluorescent fibre-based receiver for smartphones

and to investigate its FOV and communication performance at random orientations to evaluate the robustness of the optical link. This work will open a new pathway to large FOV and high gain receivers with a small form factor that could be integrated into mobile devices so that they have a VLC capability. Since the receiver created by coupling the FC to the detector is simple, compact, and inexpensive, it can easily be integrated into remote electronic devices.

There is a need for a method to predict the maximum achievable data rates when an FC is added to the receiver in an optical link. Hence, an important objective of this work will be focused to determine the relationship between the ROS and the data rate that can be achieved by using the OOK modulation scheme. This method will be validated on different wavelength absorbing FCs in a VLC link. The impact of adding an FC into the receiver will be discussed in terms of the increase in data rate and the resulting bandwidth of the FC. This would help the future VLC receiver designer in selecting an FC for a VLC receiver.

1.10 Summary

VLC is a promising candidate to fulfil a growing internet demand. Pulse amplitude modulation such as 2 PAM and 4 PAM are famous simple modulation schemes in VLC. Similar to all other wireless communication, an antenna (concentrator) is used to increase the signal-to-noise ratio (SNR) at the receiver end of the communication link to increase the data rate. In VLC receivers, SNR is typically increased by an optical element, most commonly a lens or a compound parabolic concentrator, however, they are limited by etendue. Luminescent solar concentrators have an ability to shift shorter wavelengths to longer wavelengths and they are used for the collection of sunlight in solar cells. Similarly, fluorescent concentrators, also have wavelength shifting properties and they are independent of conservation of etendue due to the presence of fluorophore in them. These concentrators can be used to concentrate light to APD with a large FOV thereby providing high-speed data rate communications for a VLC link. Fluorescent concentrators with a large FOV of 60° have

been previously presented. Characterisation of different types of fluorescent concentrators needs to be performed to understand their nature and advantages for a VLC link.

Publications

1 Surampudi, A., Singh, R., Riaz, A., Ali, W., Faulkner, G., O'Brien, D. and Collins, S., 2021. A Digital Pre-Equalizer For Optical Wireless Links. Journal of Lightwave Technology, 40(4), pp.961-967.

2 RIAZ, A. and COLLINS, S., A green absorbing fluorescent fibre concentrator for VLC.

3 Riaz, A. and Collins, S., 2020, December. A wide field of view VLC receiver for smartphones. In 2020 European Conference on Optical Communications (ECOC) (pp. 1-4). IEEE.

4 Riaz, A., Faulkner, G., O'Brien, D. and Collins, S., 2020, March. The relationships between the amplitude of receiver output voltage and the maximum achievable OOK data rate. In Free-Space Laser Communications XXXII (Vol. 11272, pp. 278-287). SPIE.

5 Riaz, A. and Collins, S., 2019, November. A slab fluorescent concentrator for visible light communications. In 2019 2nd IEEE Middle East and North Africa COMMunications Conference (MENACOMM) (pp. 1-4). IEEE.

6 Riaz, A., Faulkner, G. and Collins, S., 2019, June. A fluorescent antenna for white light visible light communications. In 2019 Global LiFi Congress (GLC) (pp. 1-4). IEEE.

2 A Comparison of a Blue Filter and commercially available FC for a VLC Link

Visible light communication (VLC) generally uses LED or laser diodes as the source. Most white light-emitting diodes (WLEDs) are made up of a blue LED combined with a yellow phosphor. Phosphor adds a second slower component which ultimately limits the BW of the blue LED (which has a faster response) [86]. An optical filter is typically used to block the yellow component of light before detection [87]. However, the effectiveness of the blue filtering is highly variable and is dependent on some key factors, such as the illumination (Lux level) at the receiver, signal strength and receiver's noise [88][89][90][91].

As an FC absorbs a specific wavelength of light and rejects others, thereby acts as a natural filter. In this chapter, therefore, an experimental demonstration has been presented to investigate the effectiveness of a blue filter. Results are presented which show how the addition of FC improves the performance of commercially available OSRAM OS-PCN-2015-013-A Version 1.2 warm white LED.

In addition, the chapter also contains characterisations of a slab fluorescent concentrator and fibre fluorescent concentrators. Different companies sell wavelength shifter bars (slabs) and fibres made up of solid organic material (polymer) which absorb light at the blue and emit at a green wavelength, which means they can be used as an FC provided they contain a fluorophore rather than a phosphor. These wavelength shifting bars are unaffected by water, which means they can be utilised to create stable VLC receivers. Furthermore, their peak absorptions and emissions are between 400 nm and 700 nm. Due to these characteristics, they can be used as a light collector to reduce the complexity and overall size of the detector. In this chapter, the characterization of a commercially available concentrator and its potential scope in the VLC is also discussed.

The chapter is organised in three halves; the first section contains the measured transmission profile, bandwidth and data transmission experiments performed in an optical link containing WLED with different filters. The performance of the best suitable filter was then compared with a slab fluorescent concentrator and the results are discussed in the second half. Furthermore, experiments to determine the field of view (which is the key feature of this work) and the BW of the concentrator are also described. Finally, the characterisations of various commercially available fluorescent fibre concentrators are described in the 3rd half of the chapter followed by the data transmission result of the best fluorescent fibre. These experiments show that using concentrator results in both an increase in OOK data rate and robustness to ambient light. Finally, the last section of the chapter contains concluding remarks.

2.1 Emission spectra of LED and a blue filter

OSRAM LED uses a Gallium Nitride (GaN) blue LED combined with a yellow phosphor. To investigate the effectiveness of the blue-filtering, initially, the emission of white light from the WLED with and without different filters was measured through an optical spectrum analyser. For a better understanding of the effectiveness of the filtering concept, the results of the blue filter (FB450-40-Bandpass Filter), were also compared with FB500-40 (green filter - Bandpass Filter), and FB550-40 (greenish-yellow filter- Bandpass Filter) separately.

The fibre sensor of the optical spectrum analyser was mounted on a pole and the USB cables connect the PC to the spectrum analyser. Ocean software was used to collect and process the data from the

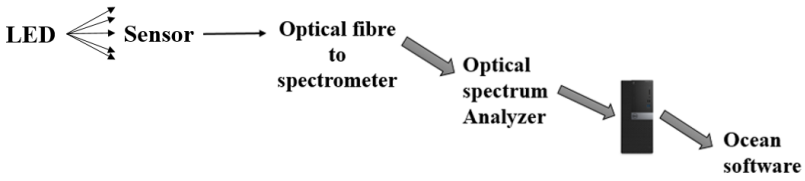

Figure 2.1 Experimental set-up for emission spectrum measurements.

spectrum analyser. The experimental set-up for measuring the spectrum of the concentrator is shown in Figure 2.1.

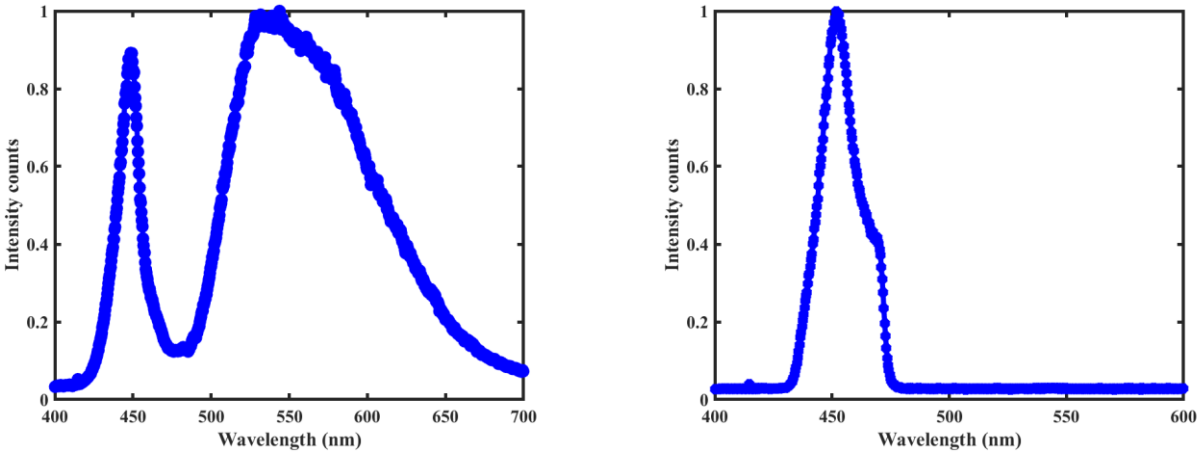

Figure 2.2 (a). Emission spectra of LED (b). Emission spectra of LED with filter FB450-40.

The emission spectra of OSRAM LED, in Figure 2.2 (a), show that it is the sum contribution of two components: blue (with a peak at ~ 450 nm) and yellow (with a peak at ~ 550 nm). It has a different proportion of blue and yellow components as shown in Figure 2.2 (a). An optical filter (FB450-40)

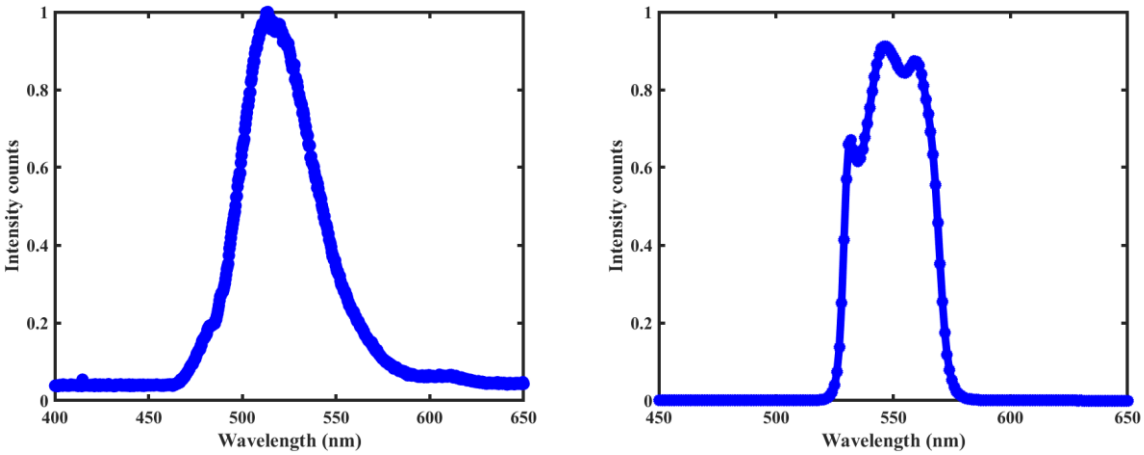

Figure 2.3 (c) Emission spectra of LED with filter FB500-40 (d) Emission spectra of LED with filter FB550-40.

was used to remove the phosphor before reaching the detector. The emission spectra with the blue filter is shown in Figure 2.2 (b) which shows that as expected the blue filter completely rejects the

yellow component of the white light from the LED and transmits only the blue regime. The other two filters used with the WLED allowed the yellow region of the WLED to pass through them as shown in Figure 2.3 (c) and (d).

2.2 A comparison of the measured frequency response of three different optical filters

In this experiment, the 3 dB bandwidth of the WLED with and without filters was measured. The frequency response of the WLED was measured by using a 70 MHz detector (Hamamatsu C1203-04). The frequency was then increased from 1 MHz to 70 MHz and the corresponding frequency response was measured with and without filters in the optical link.

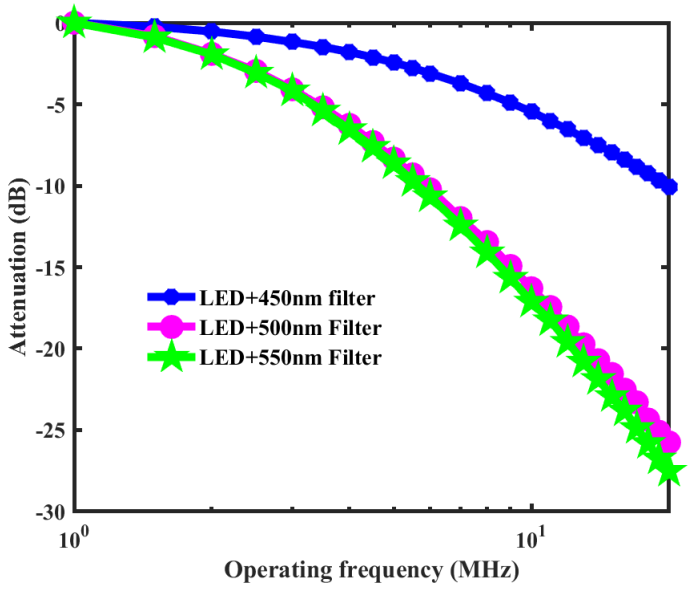

Figure 2.4 BW measurement of LED with different coloured filter.

The BW of LED under these operating conditions was found to be 2.5 MHz. Sequentially, further experiments were performed to measure the frequency response of LED with FB450-40 (blue filter), FB500-40 (green filter) and FB550-40 (greenish-yellow filter) separately. The BW of LED with green and greenish-yellow filters, shown in Figure 2.4, remained the same (2.5 MHz), given the fact that the phosphor was not blocked by these two filters as shown previously in Figure 2.3. However, as expected from the emission profile of the blue filter, the BW of the LED with a blue filter (FB450-40) increased to 6 MHz, shown in Figure 2.4, due to the complete removal of the yellow component

of the white light from the WLED. Due to larger channel BW, Shannon-Hartley Theorem (described in Chapter 1) suggests that the addition of a blue filter to a WLED optical link will support a high data rate, therefore, data transmission experiments were performed with an APD with a blue filter.

2.3 Data transmission when a receiver was created by either an APD alone or an APD with a blue filter

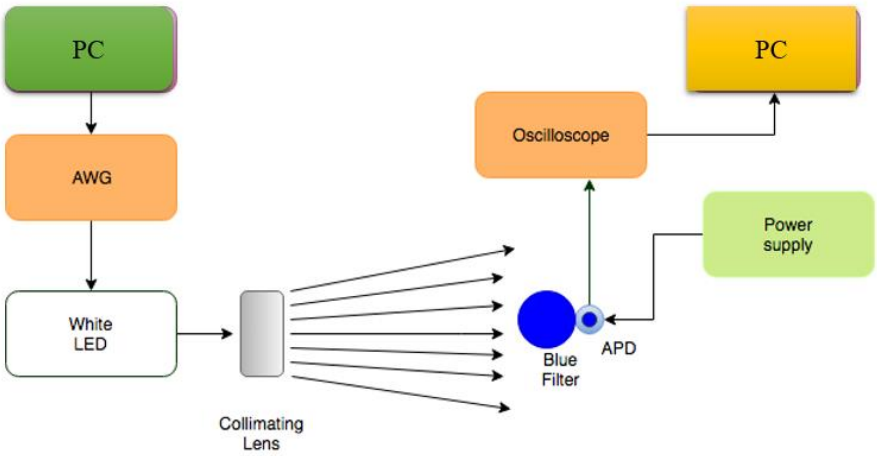

Figure 2.5 Block diagram of the experimental set-up for data transmission experiment.

A data transmission experiment was performed, when an optical link was created by using a WLED as a transmitter and an APD ($C1203-04$) as a receiver. This experiment was performed with and without a blue filter ($FB450-40$) in front of the detector at the receiver terminal at the link distance of 20 cm. A block diagram of the experimental setup for the data transmission experiments is shown in Figure 2.5. OOK data was generated using a pseudo-random bit sequence (PRBS) of 2^{13}. An Agilent AWG (81150A) with a BW of 120 MHz was used to drive the WLED. The detected signal by APD was captured by using an oscilloscope (MSO6414) with a BW of 1 GHz and sent back to the PC for further processing and analysis. The details of the experimental equipment used for various experiments explained in this chapter are given in Table 2-1.

Table 2-1 Detail of the experimental equipment used for the characterisation of the slab concentrator.

Equipment	Part number	Measured bandwidth (MHz)
LED	OS-PCN-2015-013-A Version 1.2	2.5
LD	PL450B	750
AWG	Agilent 81150A	120
AWG	Agilent N8241A	500
Photodiode	Hamamatsu C12702-04	70
PIN photodiode	HSPR-X-I-1G4-SI	1400
Oscilloscope	Agilent MSO6104A	1000

Data rates, ranging from 10 Mbps to 120 Mbps were investigated for two cases: one through the white LED light and the second through the filtered blue light to the APD. In these experiments, the data rates were varied and the corresponding BER was measured at a fixed intensity of light. In Figure 2.6, the BER for data rates up to 120 Mbps is shown for the APD without a filter. In this case, 17 Mbps was achieved with a BER of 1×10^{-3}without equalisation. Due to the limited BW of LED, an adaptive decision feedback equaliser (DFE) was used at the receiver to compensate for the inter-

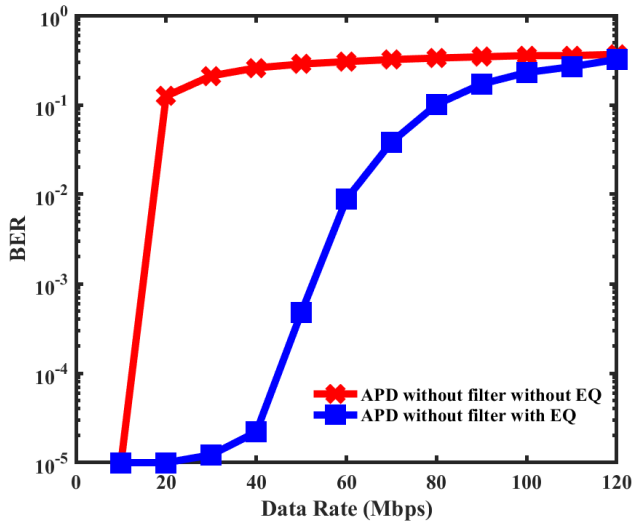

Figure 2.6 Results of OOK data transmission experiments, when the receiver was created with or without the blue filter and when no equalisation scheme was applied.

symbol interference (ISI). The decision circuit estimates whether a bit is a one or a zero by comparing the sampled output voltage signal with the decision threshold voltage (V_{TH}). In the code used to run the experiments each time the code is run, the value of VTH is optimized to the finest scale between the zero and one levels to get a minimum BER. In particular, 10 feed-forward and 2 feedback taps were used with weights determined by the recursive least squares (RLS) adaptive algorithm in MATLAB. Consequently, the data rate increased to 50 Mbps with a BER of 1×10^{-3} with the equalisation as shown in Figure 2.6. The impact of DFE was more evident at higher data rates rather than lower data rates because ISI is more prevalent at higher data rates. At a lower data rate, the signal is mostly distorted by the noise of the receiver.

The eye diagrams at 10 Mbps and 50 Mbps through the APD with and without equalisation are shown in Figure 2.7. A clear eye-opening can be observed in the eye diagrams of the received signal and the signal after applying the decision feedback equaliser at 10 Mbps where the ISI is negligible. On the other hand, Figure 2.7 also demonstrates that at 50 Mbps, the signal recovery is not possible without an equalizer as the eye is completely closed due to the impact of ISI, so DFE was applied to cure ISI.

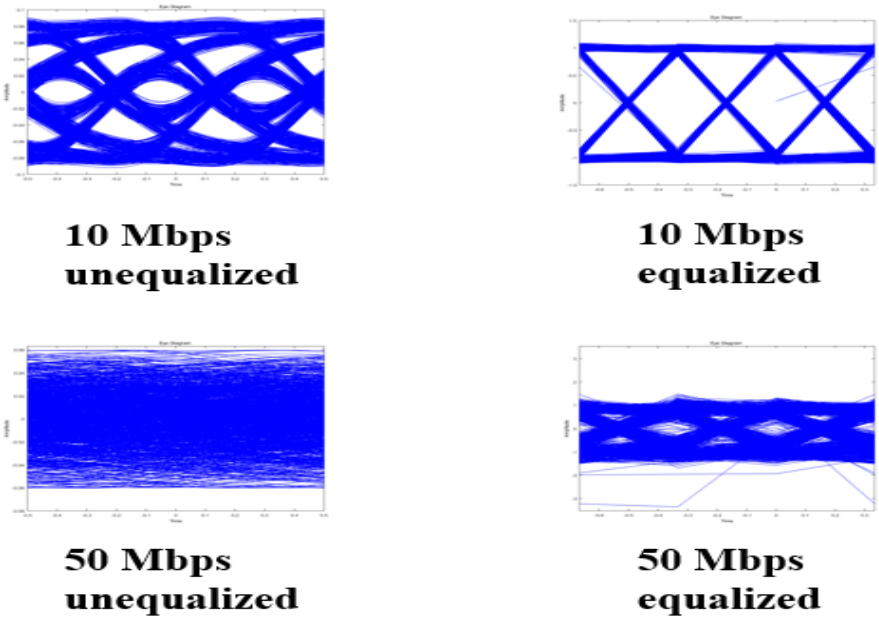

Figure 2.7 Eye diagrams with and without equalisation.

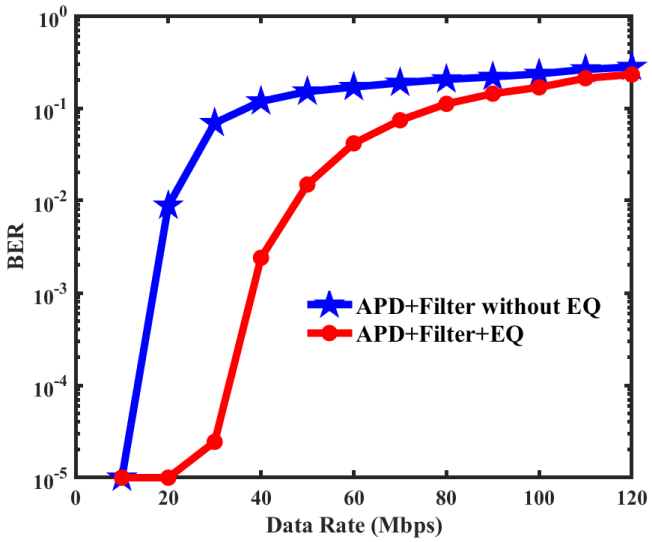

Figure 2.8 Results of OOK data transmission experiments, when the receiver was created with or without the blue filter and when DFE was applied to mitigate the impact of ISI.

To investigate the performance of the blue filter (FB450-40), the same data transmission experiment was repeated by adding the blue filter in front of the APD. For a fair comparison, it was important to keep the intensity and rest of the experimental equipment the same, therefore the experiment was repeated at the same link distance and with the same equipment. Due to the increase in the channel BW, shown in Figure 2.4, it was expected that there will be an increment in the maximum achievable data rate. However, on contrary to this when the blue filter was introduced in the system, the achievable data rate with a BER of 1×10^{-3} dropped to 38 Mbps (with equalisation) rather than increasing as shown in Figure 2.8. The reason for this decrease in the data rate of a link with a blue filter as compared to the link without the filter could be explained in terms of 70% attenuation (the power level of the RX dropped from 300 lux to 90 lux) of the optical power level by using the blue filter at the receiver terminal. The attenuation resulted in a significant loss of the SNR, as according to Shannon Capacity Theorem (described in chapter 1), the SNR is proportional to the optical power at the receiver terminal. Initially, the experiment was set up for a power level of less than 300 lux at the receiver (APD without filter), the filter induces a further decrease in the power level at the receiver. Therefore, the SNR was not large enough to overcome the noise power of the optical link hence BER increased[92]. In other words, it could be inferred that once the bandwidth of the channel

is enough, the achievable data rate of an optical link could only be increased depending on the available SNR [93].

2.4 Commercially available Slab concentrator

Saint Gobain material sells wavelength shifter bars made up of solid organic material (polymer) which absorb light at the blue and emit at a green wavelength. These wavelength shifting bars are unaffected by water, lower alcohols or dilute acid. They have a refractive index of 1.59. Their peak absorption and emission are at 420 nm and 494 nm respectively, which suggests that they have the potential to block the yellow phosphor from the WLED. Furthermore, the decay time BC-482A St. Gobain is 6.6 ns [94]. Due to these characteristics, they can be used as a light collector to reduce the complexity and overall size of the detector. The optical setup for the characterisation of slab florescent antenna is shown in Figure 3-1. According to the experimental requirements, a slab of 75 mm by 25 mm and 1 mm thick wavelength bar is used as an FC in a communication link.

2.5 Absorption and emission spectrum of the Saint Gobain slab concentrator

Like filters, the first experiment on the Saint Gobain concentrator was the investigation of transmission profile. The same method and equipment explained in section 2.1 were used for measuring the transmission profile of the slab concentrator. The results in Figure 2.9, clearly show that the FC blocks the slower yellow component of the light from the WLED. The absorption region

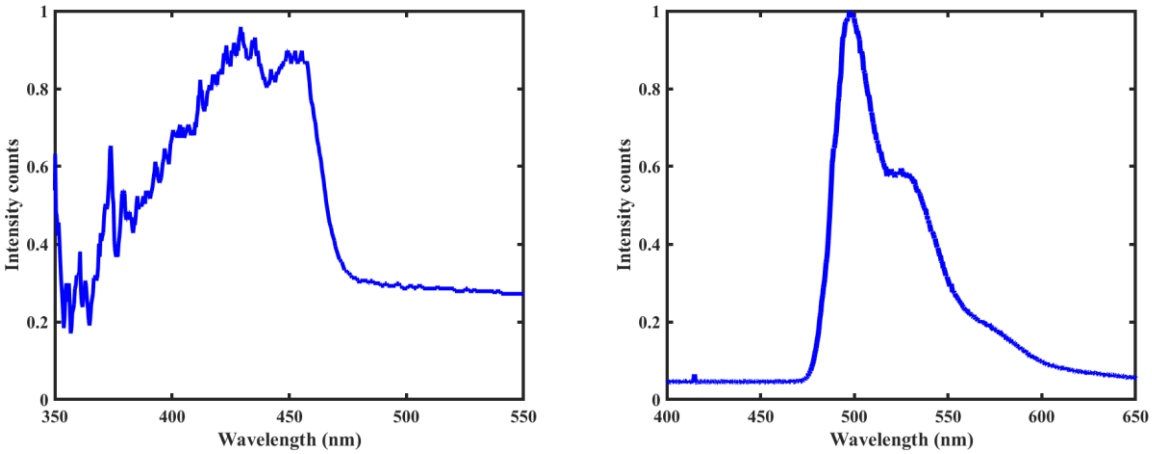

Figure 2.9 Absorption and emission spectrum of Saint Gobain slab concentrator.

for the FC lies between 370 nm to 450 nm, therefore, it does not absorb the yellow wavelength. Furthermore, the emission profile in Figure 2.9, validates the wavelength shifting capability of the FC as it emits light between 480 nm to 550 nm approximately.

2.6 Gain Measurement of fluorescent slab concentrator

A flooded light beam from the WLED was incident on the St.Gobain sample at the link distance (20 cm) where it was fully illuminated. The concentrator was held horizontally with the help of the concentrator holder and two assembly rods as shown in Figure 2.10. APD was coupled to the edge of the concentrator. Due to its small area and narrow FOV, the APD needed optical lenses (aspheric lens- ACL25416U-A) to focus the light into its receiving area. A 3-D printed cover with a slit of 3 mm/200 µm dimensions was used to ensure that the only light entering the APD is from the edge of the slab concentrator. The APD was reversed biased at fixed 5 V and was mounted, over the rotation stage base. The rotation base has X-Y-Z axis control as shown in Figure 2.10. This stage was added to make a better alignment between the concentrator edge and APD active area. It has a locking screw to fix the position of the mount once the optic has been aligned and it allows the smooth adjustment mechanism for precise positioning. The detected signal from APD was then captured by the oscilloscope. The concentrator was fully illuminated by using a uniform beam from the LD. At first,

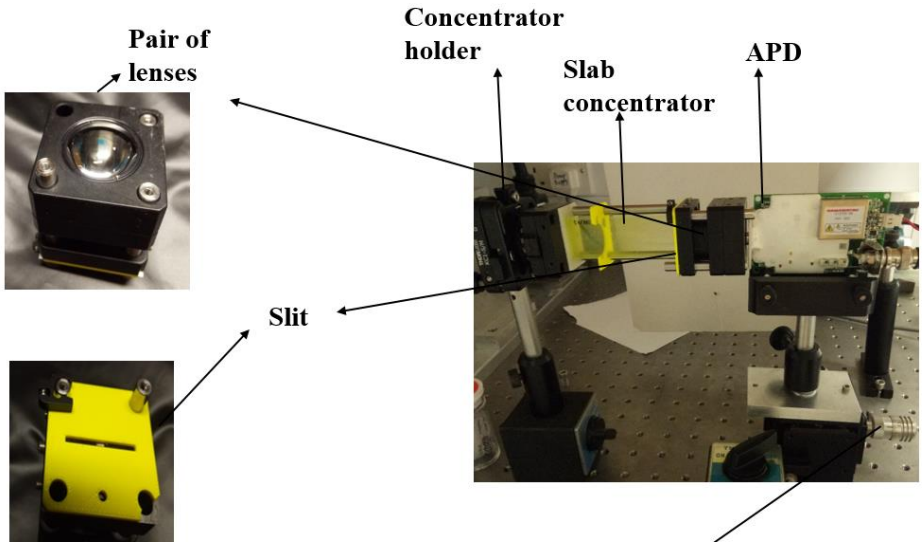

Figure 2.10 Optical-set up for St. Gobain slab concentrator.

the output voltage from the edge of the concentrator was measured, then APD was directly illuminated (without the concentrator), and the output voltage was measured. The gain of the concentrator was calculated using equation 1.10, and the resulting gain of St. Gobain was found to be 1.15.

2.7 Field of view of Saint Gobain slab concentrator

An important advantage of FCs over CPC is their wide FOV. Hence the FOV of the concentrator was measured. In this experiment, the concentrator was held horizontally. The optical post was mounted on a rotating platform with an angular scale and a locking mechanism as shown in Figure 2.11. As the concentrator was offset from the axis of rotation another optical post of a height similar to the height of the concentrator was mounted to keep the distance between the source and the centre of the concentrator constant. The light was shone on the FC at different angles, and the amplitude of the receiver output voltage was measured. The APD and FC were mounted, over a rotation stage base. The rotation base has XY-Z axis control. Both the experimental setup and the rotation stage used for the FOV measurements are shown in Figure 2.11.

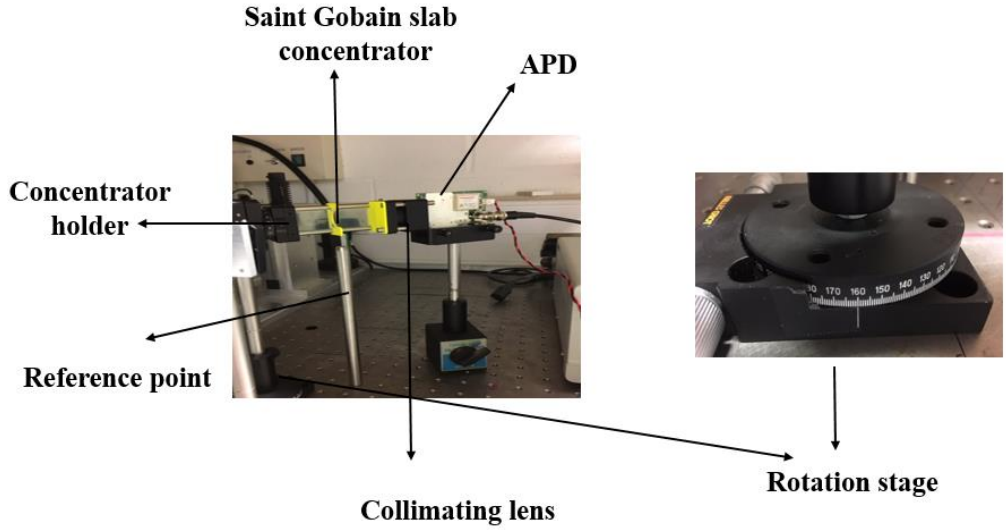

Figure 2.11 Experimental set-up used for FOV measurements.

The concentrator was rotated by increments of 10°(a higher step size was used as the ultimate goal was to measure the maximum FOV) and the output voltage was measured. As the concentrator was offset from the axis of rotation, the rotating base was moved to make sure the centre of the concentrator stays at the same position. This was further ensured by the fixed optical post at the centre which shows where the mean position of the concentrator is required to be. The difficulty, however, was about keeping the correct angle with each measurement as the base is moved. However, the presence of evenly distributed holes on the optical table makes this approximation easier. The receiver output voltage measurements were performed in both clockwise and anti-clockwise directions about the mean position of the concentrator and the whole experiment was repeated twice. The FOV of the Saint Gobain, as shown in Figure 2.12, was found to be 60°.

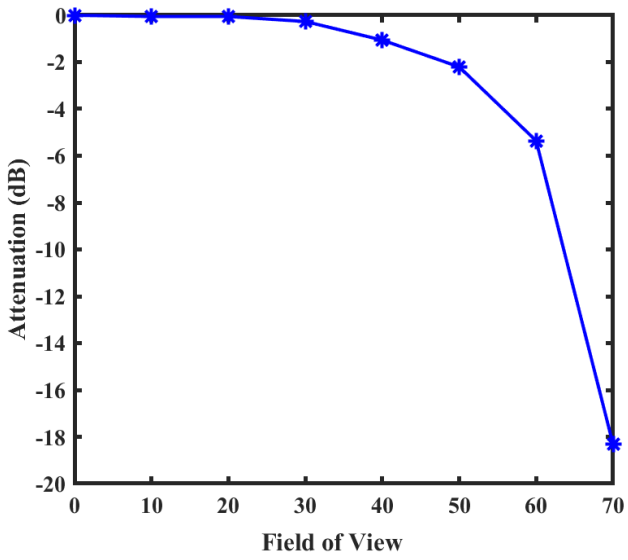

Figure 2.12 Measured results of FOV of the slab concentrator.

2.8 Bandwidth Measurements of Saint Gobain slab concentrator

To ensure that the correct BW of the concentrator is measured, it was important to use the TX and RX with a larger BW. Therefore, an LD module was designed to generate a uniform beam at the receiver. As St. Gobain has a peak absorption at 450 nm wavelength, shown in Figure 2.9, therefore, a violet laser (PL450B, 750 MHz BW) was used as the optical source. LD was initially driven at 30

mV_{PP} and $2V_{DC}$ offset voltage through the AWG to do the precise alignment of the experimental set-up for better results. Once the set-up was done, the amplitude of the voltage and offset was increased to 1 V_{PP} and 3.8 V_{DC}.

A block diagram of the whole laser set-up is shown in Figure 2.14. The laser diode used as a transmitter is a point source and so for its output to cover the whole length of the concentrator it needs to be diverged using optics. The PL450B blue laser diode was therefore mounted on a CP06/M cage plate at one end of four assembly rods (ER4-P4) from a 30 mm cage system, as shown in Figure 2.13. A cage rotation

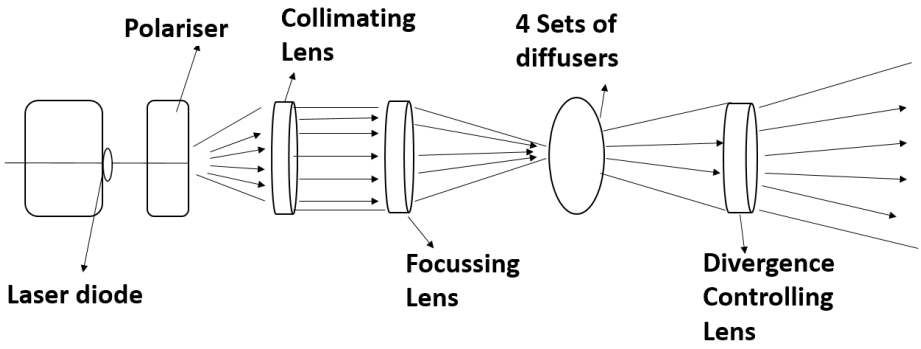

Figure 2.14 Set-up of laser diode.

mount (CRM1/M) and polarizer were added in front of the LD to precisely control the intensity of light falling on the receiver (without changing the driving conditions of the LD). An aspheric lens (ACL25416U-A) was inserted into the set-up to collimate the beam and a second lens (ACL25416U-A) was added to focus the beam. The diffusers from Luminit can only cover an area of 90° angle,

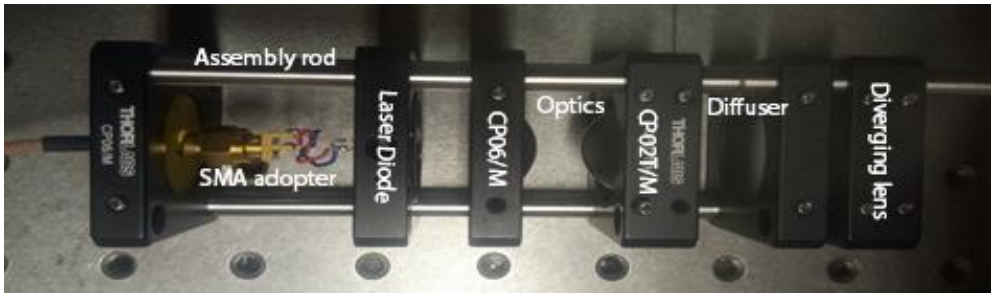

Figure 2.13 A photograph of the laser and associated optics.

therefore, to cover the whole range of a circular beam four diffusers were included in the setup to make the beam uniform. Finally, after the diffuser, another aspheric lens was added to control the divergence of the beam.

A uniform light beam from the laser was incident on the concentrator at the link distance (20 cm) where it was fully illuminated. The concentrator was held horizontally with the help of the concentrator holder and two assembly rods. The APD (Hamamatsu C12702-04,70 MHz BW) was

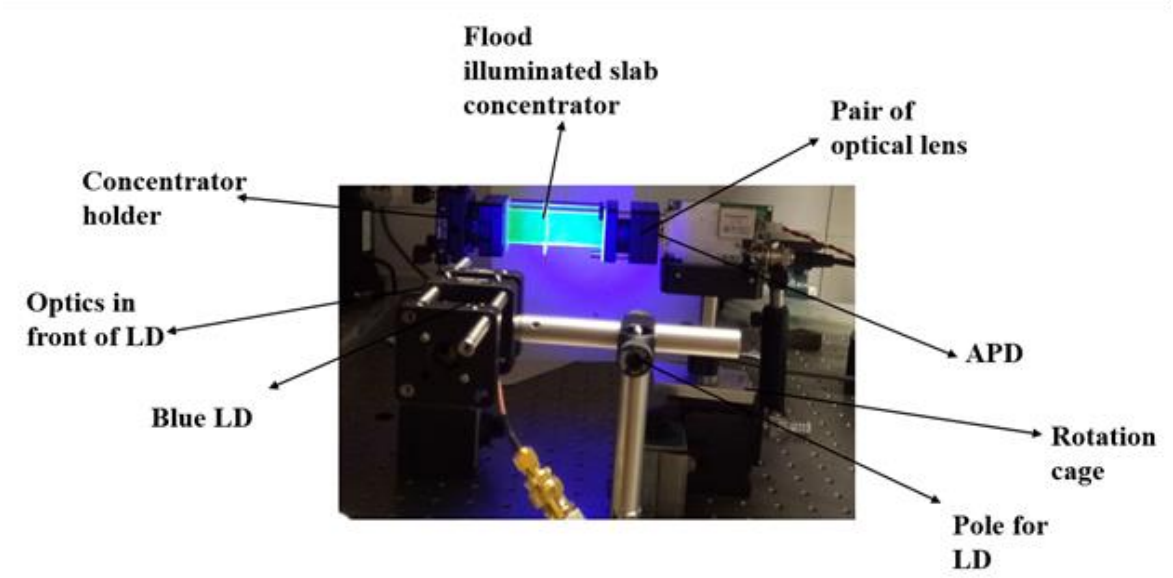

Figure 2.15 Flood illuminated the slab concentrator for BW characterization.

then coupled to the edge of the concentrator. To focus more light from the edge of the concentrator to the APD, a pair of aspheric lenses (ACL25416U-A) were used between the concentrator and the APD. A slit 3 mm by 200 µm was used to block all light sources except the edge of the concentrator to APD. The rotation base stage was used to make a better alignment between the concentrator edge and the APD's active area. It has a locking screw to fix the position of the mount once the optics have been aligned and it allows the smooth adjustment mechanism for precise positioning. The detected signal from APD was then captured by an oscilloscope (MSO6104A,1 GHz BW). The optical setup used for the BW characterisation is shown in Figure 2.15. To measure the BW of the concentrator, the same method which was described in section 2.2 was used.

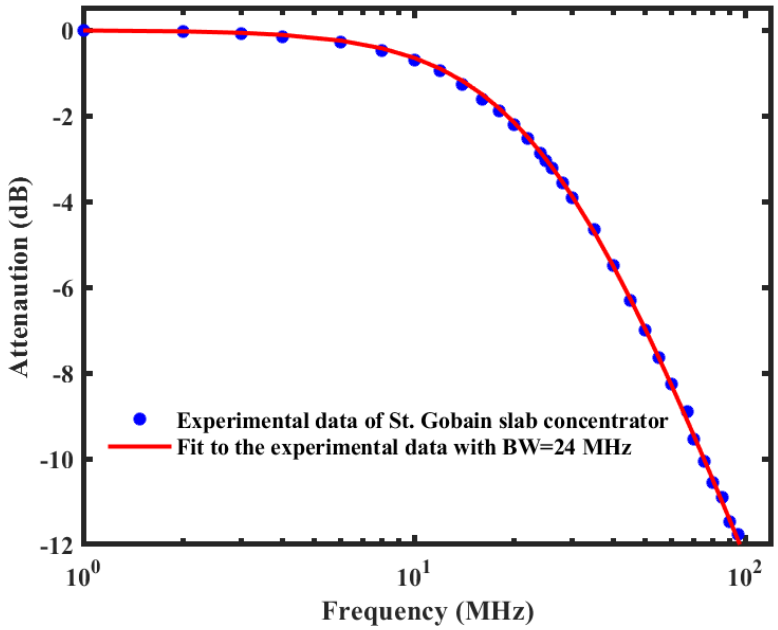

Figure 2.16 Bandwidth of the slab concentrator.

Before performing the BW experiment on the concentrator, the BW characterisation of the whole system itself was performed to make sure that the overall system has a much high BW than the concentrator itself. As shown in Figure 2.16, the frequency response of the concentrator showed a perfect fit to a first-order single-pole response and the 3 dB bandwidth of the concentrator is 24 MHz. Although the bandwidth of the FC depends upon the material and length. Unfortunately, no information about the fluorescent material doped in the commercial fluorescent concentrator was provided by the seller except the decay time. Since the frequency response of the concentrator is a single-pole response, the 3 dB bandwidth can be used to determine the decay time, τ, for the fluorophore, as shown in equation (1.12). By substituting the value of B in equation 1.12 validates that the decay time of the fluorophore doped in the Saint Gobain FC is 6.6 ns.

2.9 Data Transmission experiments when the receiver was created by either APD alone or an APD with the slab concentrator

In the experiments, the same experimental method and equipment as detailed in section 2.3, were used with a few exceptions which are listed below. The modulated light from the WLED was shone onto the receiver, which was either an APD or the same APD coupled to the concentrator. Figure 2.17

shows a block diagram of the experimental setup used for data transmission experiments. For a fair analysis, the experiments were performed with and without the concentrator under the same operating conditions. To minimize the possible impact of ambient light noise when the APD alone was used as the receiver these experiments were performed in dark. The link distance and the optical intensity of the light from the WLED at the receiver were kept constant throughout the experiment.

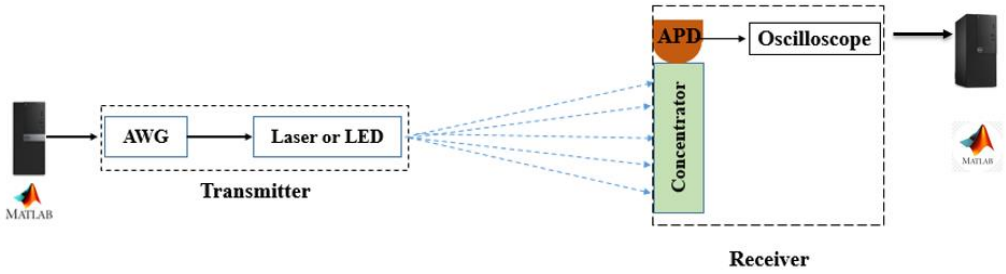

Figure 2.17 Block diagram of the experimental set up being used for the data transmission.

As discussed previously, often a blue bandpass filter is used to block the slower yellow component of the light which results in the reduction of the receiver output signal (ROS) by a factor of two or more. However, due to the removal of the yellow component, as described in section 2.1, section 2.2, and section 2.3, the resulting increase in channel bandwidth did not increase the OOK data rate. The fluorophore in the concentrator means that it also only responds to the blue light from the WLED. However, an interesting observation from these experiments is that using the concentrator was not associated with a significant reduction in the receiver output voltage.

The measured BERs at various data rates are shown in Figure 2.18. These results clearly show that the concentrator increases the data rate at which a particular BER can be achieved. For example, with the APD alone acting as a receiver a BER of approximately 10^{-3} was obtained at around 70 Mbps. However, with the concentrator, the data rate increased to 125 Mbps with a BER of approximately 10^{-3}. Using the concentrator did not result in a significant increase in the receiver output voltage, but if the filter was used, it would have reduced the received output voltage as described in section 2.3.

The increase in data rate must, therefore, be associated with a change in the channel bandwidth combined with no signal attenuation. In this experimental set-up with the APD alone, the bandwidth of the channel was approximately 2.5 MHz. In contrast, when the concentrator was coupled with the same APD the channel bandwidth increased two times. It is this increase in the channel bandwidth, rather than any increase in the received optical signal, which has supported a higher data rate.

In addition to increasing the data rate, another benefit of the filtering action of the fluorophore in the concentrator is the resulting ability to reject ambient light. This beneficial feature of the concentrator

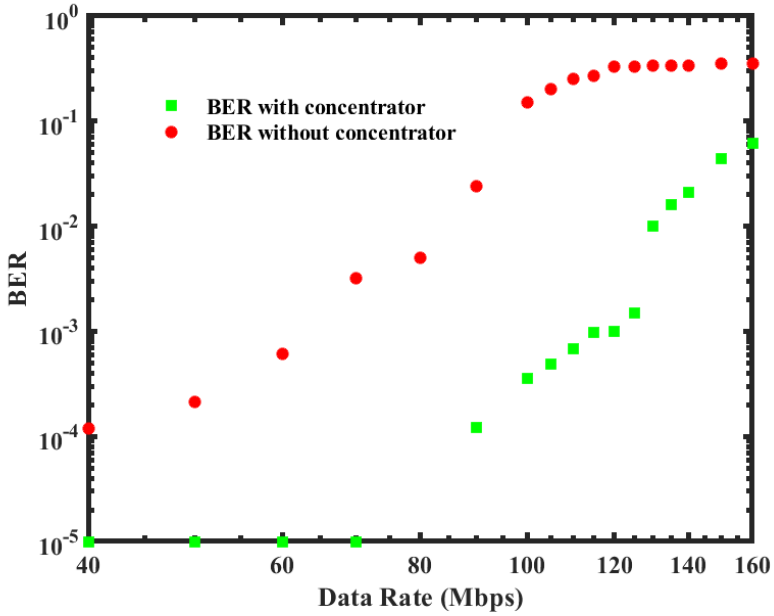

Figure 2.18 Experimental results of OOK data transmission with and without the FC.

has been quantified by determining the impact of ambient light on the BERs of the two receivers. When the APD is used as a receiver the BER at 70 Mbps is 3.2×10^{-3} in the dark. Even though the link is horizontal, so the laboratory lights are not in the receiver's FOV, the BER of this receiver increases by a factor of 4 when the laboratory lights are turned on (500 lux). When the concentrator is employed the BER at 120Mbps is 1×10^{-3}. In contrast to the previous observation, there was no noticeable change in the BER when the laboratory lights were turned on. The concentrator, therefore, makes the receiver more robust to changes in the operating environment.

Furthermore, the larger FOV of fluorescent concentrators suggests that they have the potential to replace parabolic and compound parabolic concentrators for future optical receivers. One possible advantage of employed fluorescent concentrators when used with a laser diode or a coloured LED is that they could increase the receiver output voltage signal and hence the SNR. However, their wide FOV and the selective absorption of some wavelengths by the fluorophore mean that they function as wide field of view filters.

2.10 Fluorescent fibre concentrators

Previous experiments have been performed with concentrators made from a rectangular slab doped with a fluorophore. However, it is also possible to purchase plastic fibres that have been doped with a fluorophore. These fluorescent fibres are commercially available from several different companies that sell through the internet for use in gun sights or decorative lighting. Conveniently they have the same diameter as some fast photodetectors. Due to the efficient coupling capability of fibre concentrators to small area detectors; a wide range of fluorescent fibre concentrators were characterised to investigate their scope in future VLC. A photograph of these fibres is shown in Figure 2.19.

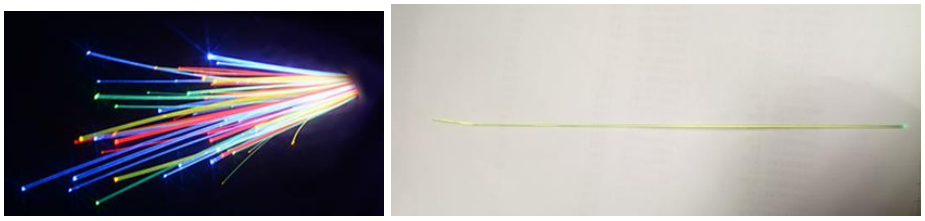

Figure 2.19 Fibre fluorescent concentrators.

2.11 Fluorescent fibres and a concentrator holder

The fibres were bought off a commercial website, they do not have a particular name, so to differentiate they were named after their distinctive colour and shape. They vary in size of the diameters, doping levels of fluorophore and shapes such as circular or rectangular.

In order to characterise these fibres and to determine if they could be used within a receiver, a holder for the fibre was built as shown in Figure 2.20. The holder has been designed to ensure that the fibre is held at the focus of a cylindrical plastic Fresnel lens (from Edmund Optics) attached to its front surface. The purpose of the Fresnel lens is to focus the light beam into the centre of the fluorescent fibre. It is an uncoated lens which has an acrylic substrate and 1.49 index of refraction. The absorption wavelength for this lens lies between 400-1100 nm with a transmission capacity of 92% for this wavelength range which matches the expected transmission profiles of the fibres under test. Furthermore, the fresnel lens allows a large aperture and short focal length with less mass and volume of material as needed by a conventional lens.

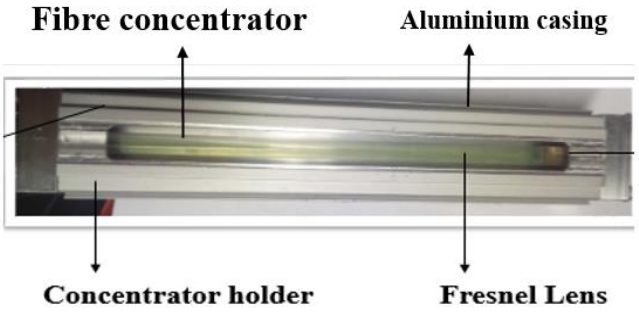

Figure 2.20 The fibre holder with the fibre visible through the plastic Fresnel lens.

The aluminium was used for the casing of the concentrator holder due to its lighter weight, easier moulding capability and cheaper costs. This holder allows one end of the fibre to be optically coupled to detectors as shown in Figure 2.20. Multiple copies of 3-D printed covers, each containing a hole according to the diameter of fibre under-investigations were designed to ensure that the end of the fibre is precisely aligned to the active area of the photodetectors and to block any other light entering the APD. The length of the holder is 17 cm, however, the length of the Fresnel lens is only 13 cm which means the effective length of fibre under test is restricted to 13 cm only.

2.12 Field of View measurements of fluorescent fibre concentrator

Although the Fresnel lens was included in the experiment to increase the achievable signal to noise ratio. However, the operation of a Fresnel lens relies upon processes that conserve etendue and so it

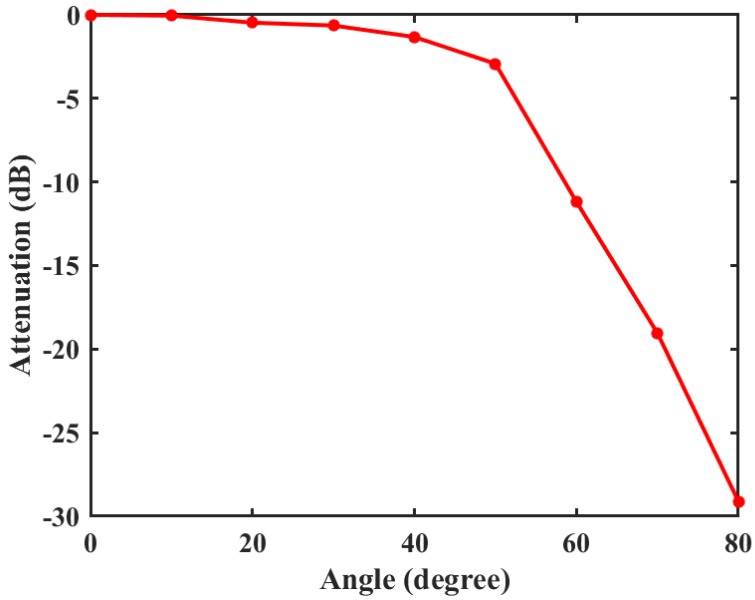

Figure 2.21 Measured FoV of the fluorescent fibre in the concentrator holder.

restricts the field-of-view of the system in one direction. The field of view of the receiver was therefore determined by illuminating the concentrator from different angles and measuring the peak-to-peak amplitude of the APD's output voltage. As anticipated when the axis of the concentrator was horizontal and the light source was moved vertically the FOV of the concentrator was restricted. In

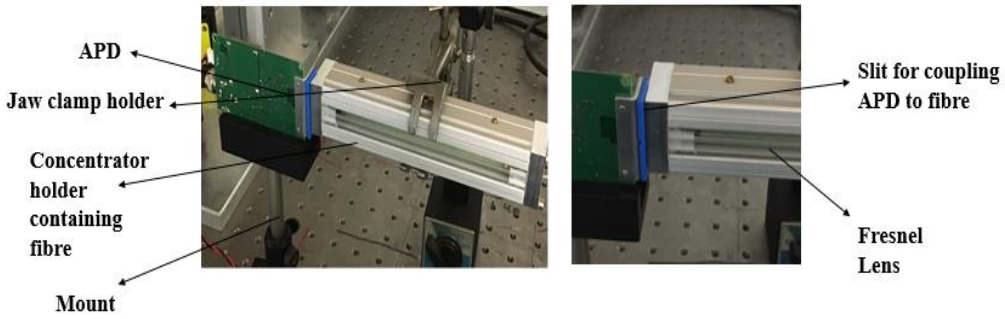

Figure 2.22: The experimental arrangement used to determine the gain and bandwidth of the fluorescent fibre concentrators and to transmit data. The key feature of this experiment is the 3D printed blue cover which reduced the effective area of the APD to the cross sectional area as the fibre. In other experiments, this cover was used to align the APD and fibre.

particular, the field of view in this direction was found to be 14°. The measured FOV of the fibre concentrator in the horizontal direction was found to be 45° as shown in Figure 2.21.

2.13 Measurement of the gain of the fluorescent fibre concentrators

A photograph of the optical set-up used for the gain measurements of fluorescent fibre concentrators is shown in Figure 2.22. The same experimental method and equipment which was described for the gain measurements of a slab concentrator in section 2.6 were also used for the gain measurements of these fibres.

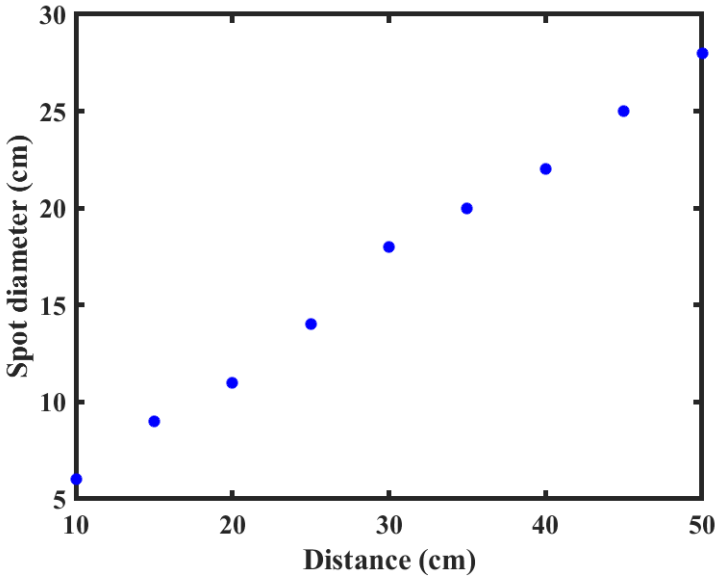

Figure 2.23 Diameter of the beam spot at different distances.

Since the length of the fluorescent fibre concentrator (13 cm) is much larger than the previously described fluorescent slab concentrators, therefore, to take full advantage of the fibre concentrator, it was essential to flood illuminate the entire length of the concentrator. Once a uniform beam was created, the beam diameter at different link distances, shown in Figure 2.23, was measured. As expected the beam diameter increased as the link distance increased, however, as the beam diameter was increasing the intensity at the receiver was decreasing. Since the beam diameter is directly proportional to the exposed length of the fibre concentrator, therefore, it was important to investigate the impact of beam diameter over the length of the fibre and consequently upon the gain (also called concentrating efficiency) of the fluorescent fibre. To understand the relation between the link distance and gain, these experiments were performed for only one fibre, therefore, initially, a green fibre was incorporated into the receiver and at different link distances. The results, in Table 2-2, show that the

gain of the fibre increased until the full length of the fibre was shone by the light source. However, with a further increase in the beam diameter, the gain dropped significantly.

At 10 cm the beam spot was found to be of 6 cm only, which covered less than half of the length of

Table 2-2 The measured gain of the green fibre at different link distances.

Distance (cm)	**Beam Diameter (cm)**	**Gain**
50	28	6.46
40	22	8.2
30	18	7.3
20	11	6.67
10	6	5.88
5	2.9	3.1

the concentrator. At 20 cm, the diameter was still 11 cm, which was unable to cover the entire 13 cm length of the concentrator. However, at 30 cm and 40 cm, the diameter of the spot was 18 cm and 22 cm, which was more than enough to fully illuminate the concentrator (13 cm). Sequentially, the maximum diameter of the spot was 28 cm at a distance of 50 cm. However, the irradiance level at 50 cm link was significantly less to fluorescent the fibre concentrator, therefore, the gain of the fluorescent fibre dropped significantly at 50 cm as shown in Table 2-2. However, at 40 cm, the fibre was fully illuminated due to which fibre got maximum gain. These results suggest that to take the maximum advantage of the concentrator, the link distance should be 30 cm or 40 cm. All other available fibres were, therefore, evaluated at a link distance of 40 cm. The results in Table 2-3, show

Table 2-3 The dimensions of different wavelength absorbing fluorescent fibres used for characterisation.

Fibre	Diameter	Gain
Rounded green	1.2 mm	8.2
Rounded yellow	0.8	5.9
Rounded red	0.8 mm	6.3
Square yellow	1.2 mm	10.35
Square orange	1.4 mm	9.62

that the square yellow and square orange fibre has a higher gain of 10.35 and 9.62 as compared to the other fibres under investigation. Ideally, the fibre with a larger gain provides a higher SNR to achieve a higher data rate, however, Shanon's capacity (described in chapter 1) suggests that the achievable data rate depends upon the combination of SNR and BW. Hence, to choose the suitable fibre for the data transmission experiments, BW characterisation was required.

2.14 Bandwidth characterisation of FCs

Since no technical information such as the type of fluorescent material doped in the fibres and their lifetime was provided by the seller. To ensure that the BW of these concentrators is measured accurately, the whole set of the equipment needed to have a high enough BW so that the BW limitations do not come from the equipment itself. The laser diodes of different wavelengths, depending upon the emission and absorptions spectra of the fibres, which have measured bandwidth of more than 700 MHz were therefore used as light sources. In general, blue, green and violet laser diodes were used for green, red and yellow fibres.

The AWG (Agilent 81150A) used for the previous experiments has a limited BW of 120 MHz only, therefore, it was replaced by an Agilent N8241A arbitrary waveform generator (AWG) which has a BW of above 500 MHz. The sine waves needed for the bandwidth characterisation were generated using the AWG (Agilent N8241A) which has two modes: active and single-ended. The bandwidth of

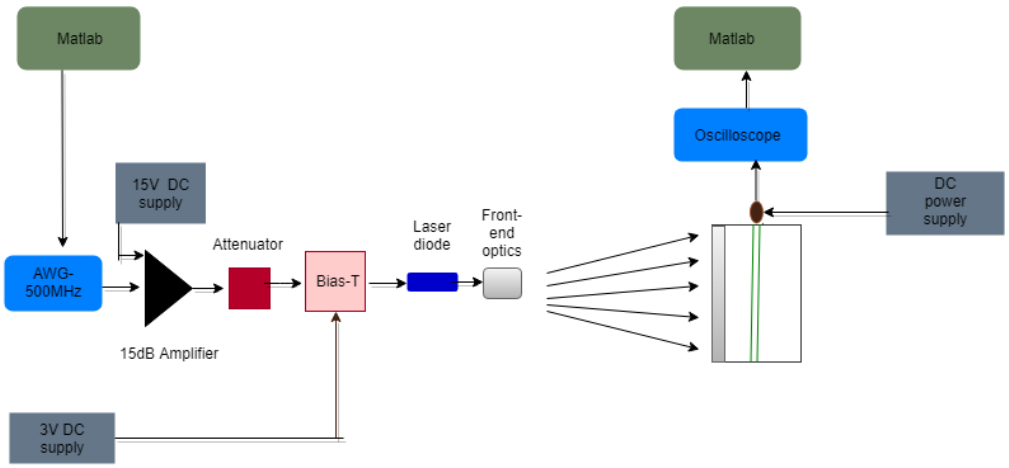

Figure 2.24 The block diagram of the set-up used for the characterisation of the fluorescent concentrators.

these two modes was determined in a back-to-back test and found to be 570 MHz and 520 MHz respectively. The active mode of the AWG, which has an output amplitude of 200 mVpp, was, therefore, used in these experiments.

As shown in the block diagram Figure 2.24, the AWG was used to modulate the input to the laser diode (LD) which acts as the light source. The light output power-current-voltage (LIV) characterisation of PL450B showed that the 200 mV_{PP} signal from the AWG was not enough to drive this LD. A Mini-Circuits ZHL-6A amplifier, which has a bandwidth of 500 MHz, and a 6 dB attenuator were therefore used to create the 2 V_{PP} signal required to drive the laser diode. This modulated signal was added to a 3.8 V_{DC} bias voltage via a Mini-Circuits ZFBT-4R2G bias-T. Although the laser diode bandwidth was 700 MHz, the addition of the amplifier limited the transmitter's bandwidth to 500 MHz. Furthermore, the APD used for the previous experiments has a limited BW of 70 MHz only, therefore, a high-speed photoreceiver with Si-PIN Photodiode (1.4 GHz) by FEMTO (HSPR-X-I-1G4-SI) was used for detecting the signal in these experiments.

To measure the BW of the fibres, it was important to measure their transmission spectra first to ensure that the fluorescent fibres were excited with the suitable LD. The fluorescent fibres were, therefore,

Table 2-4 The measured peak absorption and peak emission values of fluorescent fibres.

Fibre	**Maximum Absorption(nm)**	**Maximum emission(nm)**
Rounded green	450	520
Rounded yellow	440	580
Rounded red	520	650
Square yellow	440	580
Square orange	475	600

characterised for their transmission spectra and the results are shown in Table 2-4. The peak absorption of the fibres lies within the range of blue and green LD, therefore, the results suggest that two LDs PL450B and PL520 are required for the BW characterisation of the fibres.

The fluorescent fibres were inserted individually inside the concentrator holder system and the BW characterisation was performed by using the same method explained in section 2.2 In order to avoid any possible leakage of light from the LD directly to APD, a screen was placed at the APD end of the holder.

The measured frequency response of the fibres is shown in Figure 2.25 shows that rounded green and rounded yellow fibres have higher BW as compared to the other available fibres. However, since the aim was to use the FC which gives a higher gain and BW to maximize the achievable data rate. The results of the gain and BW shown in Figure 2.25 shows that although the square orange fibre has ta significant gain of 9.62 however its BW was only 13 MHz. Similarly, yellow fibre has a higher BW

of 24 MHz but its gain was 5.9, therefore the rounded green fibre which has a gain of 8.2 and a large BW of 24 MHz among the available fibre was chosen for the data transmission experiments.

2.15 Data transmission with and without fluorescent fibre concentrator at the receiver

The optical fibre was further investigated for its performance in the communication link and a comparison of the performances of a receiver with an APD alone and a receiver with a fluorescent fibre concentrator coupled to an APD was investigated. The optical power was varied by the polariser to achieve a BER of 10^{-3} at different data rates. The same equipment described in section 2.14was

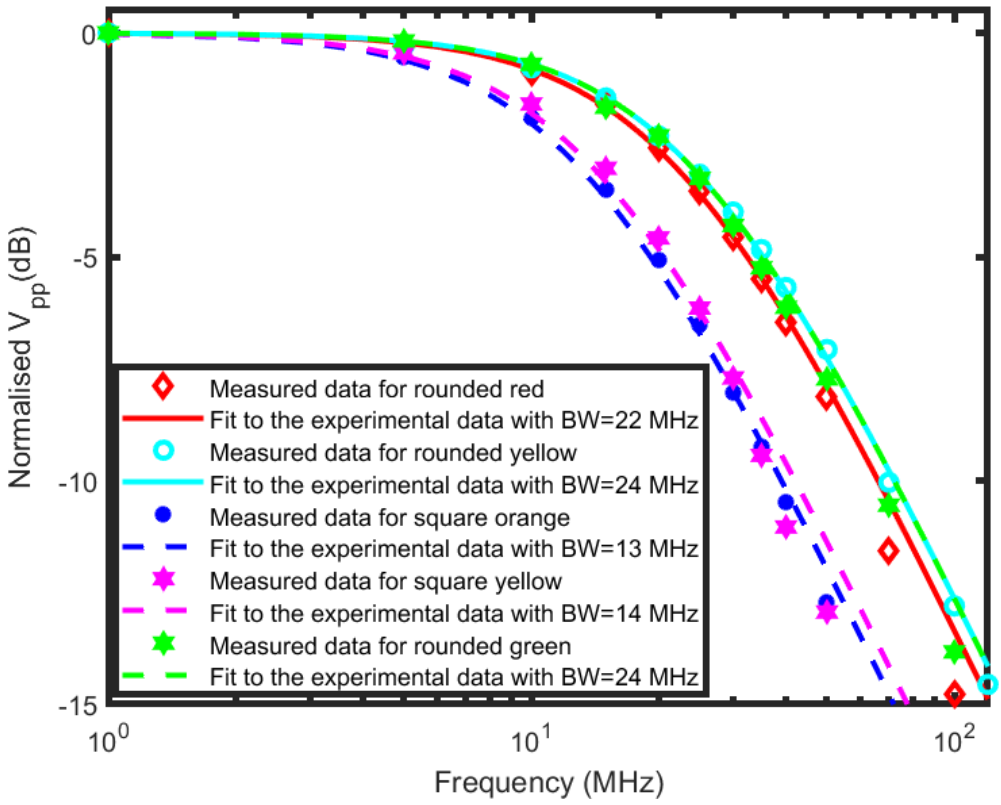

Figure 2.25 The measured bandwidth of the fibres compared to the expected response of the corresponding single pole filter.

also used for these experiments. The achievable data rates at different power levels with a targeted bit to-error rate (BER) of 10^{-3} at a 40 cm long link distance are shown in Figure 2.26

In this figure, the results are shown for two cases: first when APD alone was used to detect the transmitted data and second when APD received concentrated light from one edge of the fibre concentrator. For APD alone, two times more power was required to achieve the same data rate as

with a fluorescent antenna as shown in Figure 2.26. This was a convincing performance by the

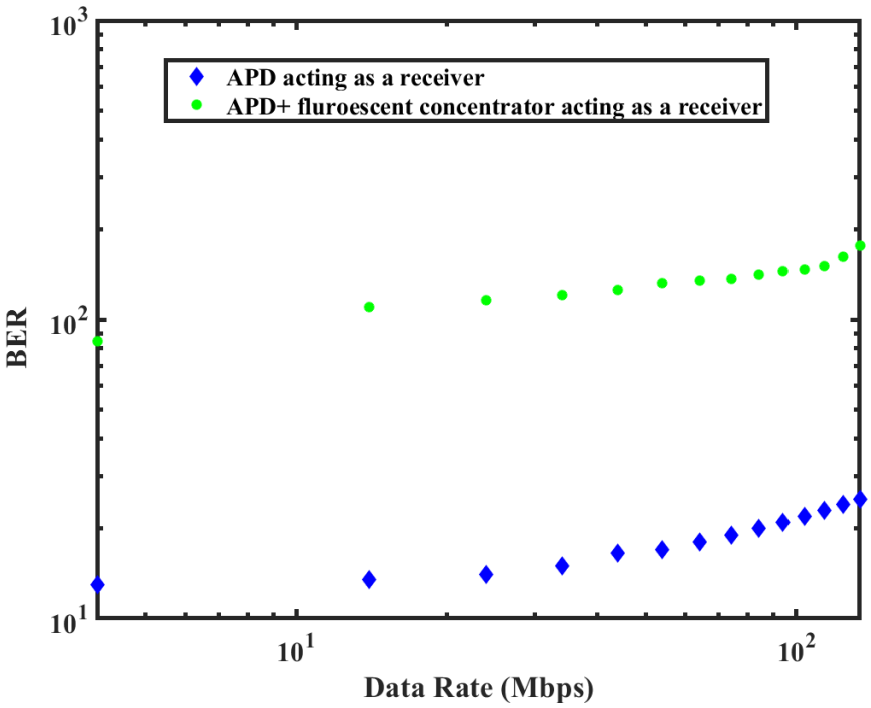

Figure 2.26 OOK communication test with and without concentrator.

fluorescent optical fibre, through which a data rate of 120 Mbps was transmitted over the optical power of less than 50 µW. On the contrary to this APD required more than 100 µW (three times the concentrator) to transmit the same data rates. These results validate the importance of FC in terms of increasing higher SNR and achieving a higher data rate.

2.16 Summary

The effectiveness of a blue filter depends upon two main characteristics: bandwidth and signal strength of white light compared to blue (filtered) light. In this Chapter, the characterisation of a WLED with and without blue filters is discussed along with the experimental results. Due to the addition of a blue filter, the BW of the channel increased, however, the maximum achievable data rate decreased. This drop in the data rate of APD with filter happened due to a significant decrease in the SNR. Although the filter increased the BW of the LED, however, due to a 70% reduction in optical power reduction, the BER increased thereby lowering the achievable data rates. The experimental

investigation demonstrates that if the SNR is not enough, the blue filtering effect would not be sufficient to increase the data rate of the communication channel.

In addition to that, results have been presented which show that the measured bandwidth, 24 MHz, of a fluorescent slab concentrator is higher than the bandwidth of WLEDs even when WLED was filtered by using a blue filter. Furthermore, although they only absorb the faster modulated blue light from a WLED, their larger collecting area means that the receiver's output signal is not reduced when a fluorescent concentrator is used. Results have been presented which show that although the receiver output voltage signal remains unchanged, using the concentrator increased the achievable OOK data rate from 70 Mbps to 120 Mbps. Finally, experimental results have been discussed which show that the concentrator makes the receiver 4 times less sensitive to the presence of varying levels of ambient light.

Furthermore, in this Chapter, the characterisation of multiple inexpensive fluorescent fibres is described along with a novel concentrator holder system. Finally, a green FC which has a gain of approximately 8 and a BW of 24 MHz was chosen for the data transmission experiments. The use of a fibre concentrator with APD at the receiver lowered the optical power requirements of APD by a factor of 3. It seems that the data rate could be increased by approximately three times the APD (which is almost equal to the square root of gain).

3 Wavelength division multiplexing (WDM)

In optical communication systems, wavelength division multiplexing (WDM) is a technique to enhance channel capacity. WDM enables the multiplexing of multiple optical wavelength carriers, each carrying an independent data stream and consequently improving the overall channel capacity [96]. However, the optical components that combine (multiplex) and split (demultiplex) distinct wavelength channels are critical in these systems. Combining multiple wavelengths can be accomplished by using multiple transmitters with various emission wavelengths driven independently e.g. LEDs and LDs [97]. In particular, RGYB LED luminaries have been a popular choice for WDM, however, due to these, the WDM demonstrations tend to limit the number of colours up to four (RGB, RGYB) [98]. In addition to that, [99] showed a novel WDM technique based on polymer-based colour-converters and GaN micro-LEDs. Since the emission of a polymer-based colour-converter may be set to different colours, the number of WDM channels can be considerably increased, however, the receiver in has a small field of view [99].

To separate the transmitted data at the receiver, optical bandpass filters with a centre wavelength that matches the transmitter emission are mostly utilised, however, most of them have a limited field of view [100]. Different fluorescent fibre concentrators which act as a receiver for visible light communications offer a large FOV with a variety of gain-bandwidth combinations and most importantly they absorb different wavelengths. These receivers created by the FC have significantly overcome the theoretical etendue limit in terms of the combination of a wide FOV and a large gain it can achieve [as discussed in Chapter 3]. In addition to that, they are also capable of enabling wavelength division multiplexing (WDM) for data communication, thereby, increasing the channel capacity with a very large FOV.

This significant advantage of a wide FOV and large channel capacity is achieved by creating a receiver that includes different fluorescent fibre concentrators in which each fibre absorbs a different wavelength of the light spectrum which, therefore, enables separable communication channels.

In this chapter, an inexpensive, simple and practical receiver, based on fluorescent optical concentrators, is described for its ability to facilitate WDM in the VLC. In section II of the chapter, the possibility of using FC for a WDM system is described while a method to evaluate the possible cross-talk (H-matrix) is discussed in section III. Section IV then contains the initial characterisation of the FCs and the LDs which includes transmission spectra, bandwidth characterisation of fibres and the optimisation of the biasing and amplitude voltage of the LDs. In addition to that, the data transmission results of the FCs are discussed in section V of this chapter followed by the WDM experiments performed on the FCs in section VI. Finally, the results are discussed in section VII and section VIII contains the summary of the chapter.

3.1 FC for Wavelength division multiplexing (WDM)

The selective absorption spectra of different fluorophores within the fluorescent concentrators offer the opportunity to employ wavelength division multiplexing (WDM) to further enhance the link capacity. However, in a WDM system, to facilitate a reliable communication link, an important factor is to separate the data streams carried by multiple wavelengths while maintaining a minimal link loss and the lowest possible cross-talk between these data streams. In the past, different techniques were employed to counter this challenge of minimising the cross-talks between the channels. One of the most popular approaches is the application of different absorbing or reflecting optical colour filters in front of each photodetector [101] e.g. individual colour selective dichroic filters are used to separate individual WDM data streams which only allows point-to-point applications that restrict the FOV to approximately 25° [101]. Fluorescent concentrators provide much wider FOV and have different fibres that have different absorbance peaks which makes them a better choice for WDM systems.

3.2 H-Matrix

In a communication system, if there are multiple transmitters and multiple receivers, the receivers may receive a signal which is a linear combination of the signals of all the used transmitters as shown in Figure 3.1. Ideally, every receiver should receive a signal from one transmitter only, therefore, in an ideal MIMO system, the receiver which is responsive to one wavelength should not be responsive to any other wavelength. However, in reality, there might be some leakage of unfavored wavelength, which will cause cross-talk. Consequently, the response of each receiver is a linear combination of its response to each of the transmitted signals. Mathematically, this means that a column vector of received output signal (ROS) values, *R*, can be calculated from a column vector of transmitted signal *T* via

$$R = H.T \qquad (3.1)$$

where *H* is a square matrix, known as the H-matrix, which is ideally an identity matrix.

This concept of the H matrix can be applied to a WDM setup with fluorescent fibres to evaluate the level of possible interference caused by each fibre. A block diagram in Figure 3.1 shows MIMO-based systems for the FCs to enable the WDM. For an ideal WDM system, the fibres which have a

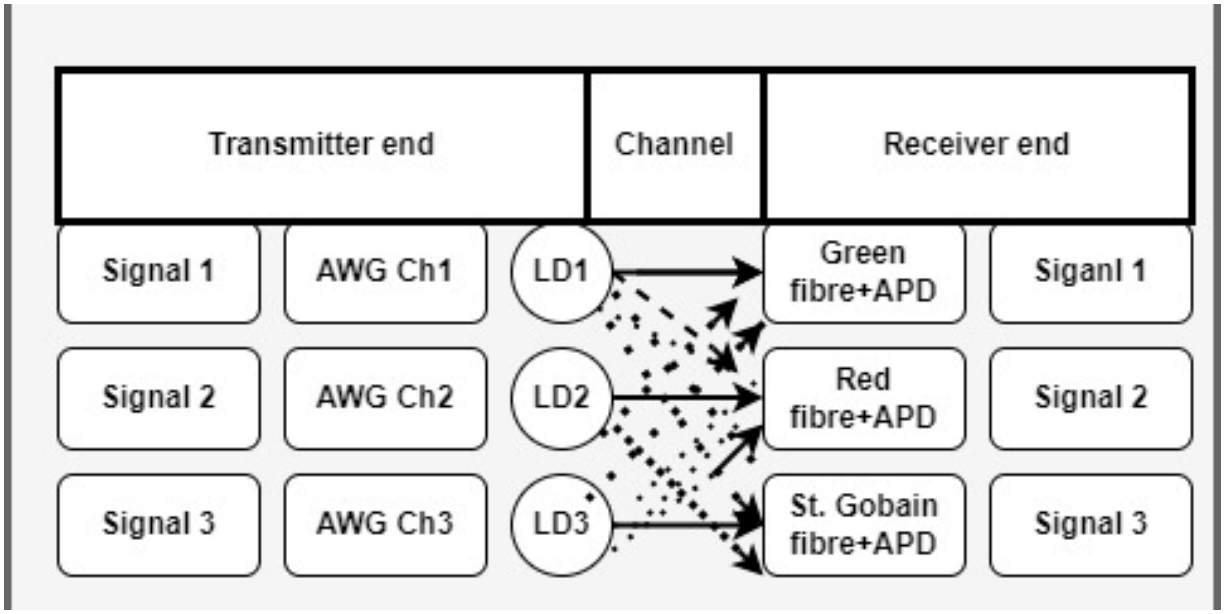

Figure 3.1 A MIMO based system for FC based receiver.

peak absorbance at one particular wavelength should not absorb any other wavelength. Three different fibres at three different transmitters were, therefore, tested to investigate the response of each fibre to the three available transmitters.

$$\begin{bmatrix} Rx_1 \\ Rx_2 \\ Rx_3 \end{bmatrix} = \boldsymbol{H} \begin{bmatrix} Tx_1 \\ Tx_2 \\ Tx_3 \end{bmatrix} \qquad (3.2)$$

where *Rx1, Rx2* and *Rx3* represent the received output from the receiver 1, 2 and 3, whereas, *Tx1, T2* and *Tx3* are transmitted signals from transmitters 1, 2 and 3. Furthermore, to investigate the de-multiplexing capabilities of different receivers in a WDM set-up, the H matrix is used which evaluates the cross-talk between the WDM channels [102]. The H matrix of a channel depicts the levels of light measured by the photodiodes for each laser diode which eventually indicates the proportions of the original data stream and the cross-talk. For an ideal MIMO system, the H matrix should be an identity matrix as it indicates zero cross-talk from the unwanted channels.

When there is crosstalk between channels in a WDM system with multiple fibres-based receivers, a particular receiver cannot determine which transmitter is transmitting. This leads to a poor matrix condition number, in turn leading to poor performance. For example, the model presented in [102] was not an ideal MIMO system. In that paper, two different wavelength absorbing fluorescent concentrators were used to build a WDM system. However, in terms of cross-talk, the H matrix indicated that the cross-talk was about 30% for both layers, which was not ideal for a WDM setup [102]. The matrix presented in [102] is as follows

$$\begin{bmatrix} S_{Cm6} \\ S_{DCM} \end{bmatrix} = H \begin{bmatrix} S_{blue} \\ S_{green} \end{bmatrix} \qquad (3.3)$$

$$H = \begin{bmatrix} 0.91 & 0.36 \\ 0.43 & 1 \end{bmatrix} \qquad (3.4)$$

Hence, it was particularly important to do an H-matrix before building a WDM system.

3.3 Initial Characterisation

Ideally, to achieve an entire eye-safe high-speed data rate communication, the optical irradiance at the receiver cannot be enhanced beyond a certain limit. Few other methods such as optimisation of LD, pre-equalisation [80] and polishing the fibre ends could be utilised to increase the achievable data rate without increasing the irradiance at the receiver.

Consequently, some initial experiments were required for the selection of suitable fibres for the WDM experiments which includes absorption spectra, BW measurements, optimisation of the LD and polishing of fibre tips.

3.3.1 Absorption spectra

As the desirable features for the fluorophore in an FC include a minimum or no overlap between absorption spectra. Similarly, for enabling a WDM system with the FC two features are particularly important which comprise selective absorption spectra and effective separation and emission of multiple wavelengths.

As explained in the previous section, to construct a reliable WDM link, the key challenge is to separate the individual data streams carried by different wavelengths while minimizing link loss and cross-talk between these data streams, on the receiver side. To investigate this characteristic the easiest method is by studying the transmission properties of the FCs to be used in a WDM channel link. Initially, five fibres that absorb different components of the light spectrum were selected for their potential evaluation as an FC in the WDM system. Three of these fibres were red, yellow and green fluorescent fibres purchased from Nanoptics, whilst the fourth (BCF-20 SC1.00), and the fifth were purchased from St Gobain and Kuraray respectively.

Each of these fibres except Kuraray[1] was, therefore, evaluated for their absorption spectra. Broadly categorising the fibres; green and St. Gobain (BCF-20 SC1.00) have strong absorption in the region of the blue laser as shown in Figure 3.2. The y axis represents the fraction of light absorbed by the fibres at a wide range of wavelengths shown on the x-axis.

The absorption of the red and yellow fibres, as shown in Figure 3.3, extends into the region of the green LD's emission which creates an opportunity to demodulate the green part of the light. It is anticipated that Kuraray fibre has a better absorption at approximately 405 nm. Although the absorbance data looks noisy and is not up to the mark as it should be[2] , however, they indicate the range of the wavelengths that are absorbed.

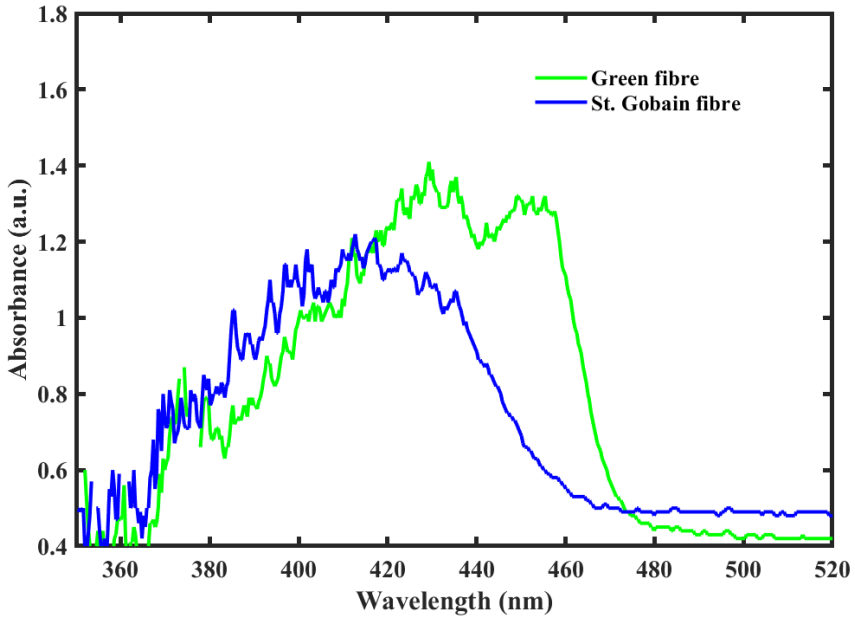

Figure 3.2 Absorption Spectrum of green fibre and St Gobain fibre.

Green and St. Gobain fibre have a strong overlap in their absorption spectrum around 450 nm wavelength which means they cannot be selected together for a WDM system. As bandwidth plays

[1] Due to the labs closure due to COVID-19 pandemic, the author was not able to do the absorption spectrum of the Kuraray fibre.
[2] unfortunately due to lab closure, the author was not able to repeat these experiments

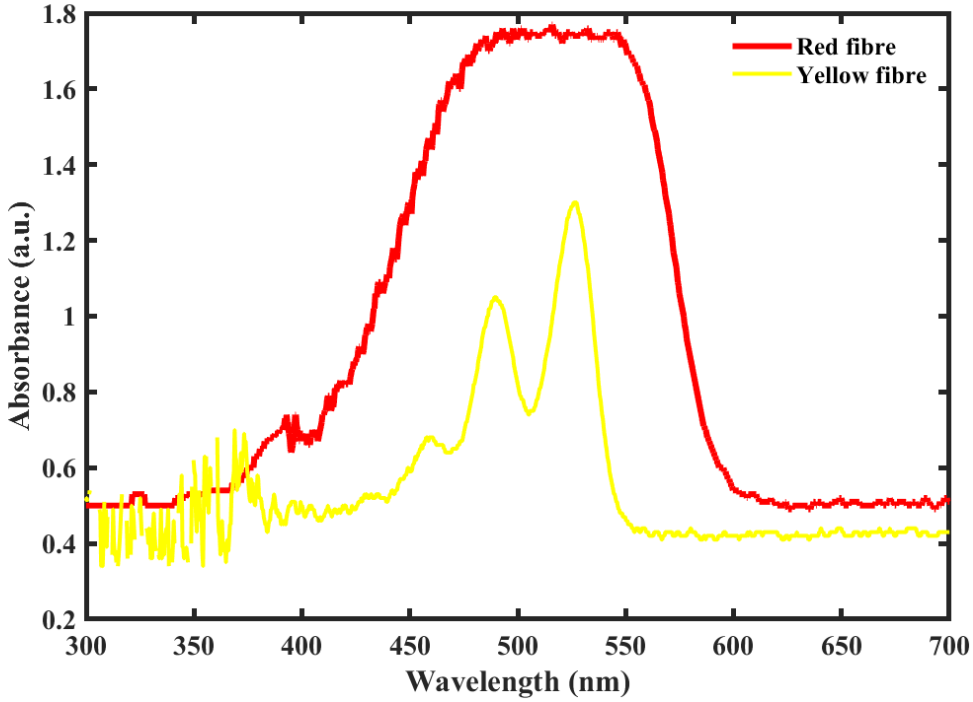

Figure 3.3 Absorption Spectrum of Red and yellow fibre.

an important role in enhancing the channel capacity, therefore, these results suggest that in these two fibres the one with the highest BW shall be selected. Similarly, as green and red both have a peak absorption of around 520 nm, to avoid crosstalk between different channels of WDM one fibre has to be chosen. Based on the results of absorption spectrums, two fibres that are responsive to two different transmitters can be selected. However, it was extremely important to do BW characterisation and data transmission evaluation of these fibres for a more logical decision.

3.3.2 Emission spectrum

Since the absorption and emission spectra both are fundamentally important for the operation of FC, the emission spectrum of the fibres was measured by collecting the light emitted from the edge of the fibres. The equipment and the method to perform the emission spectrum experiment has already been described in section 2.1. The measured responses of these fibres, as shown in Figure 3.4, showed an overlap in the emitted wavelengths of the Saint Gobain and the Green fibre. Both of these fibres have an emission peak between 500 nm to 520 nm approximately. Similarly, as expected the red fibre as shown in Figure 3.4 has a peak emission at 650 nm.

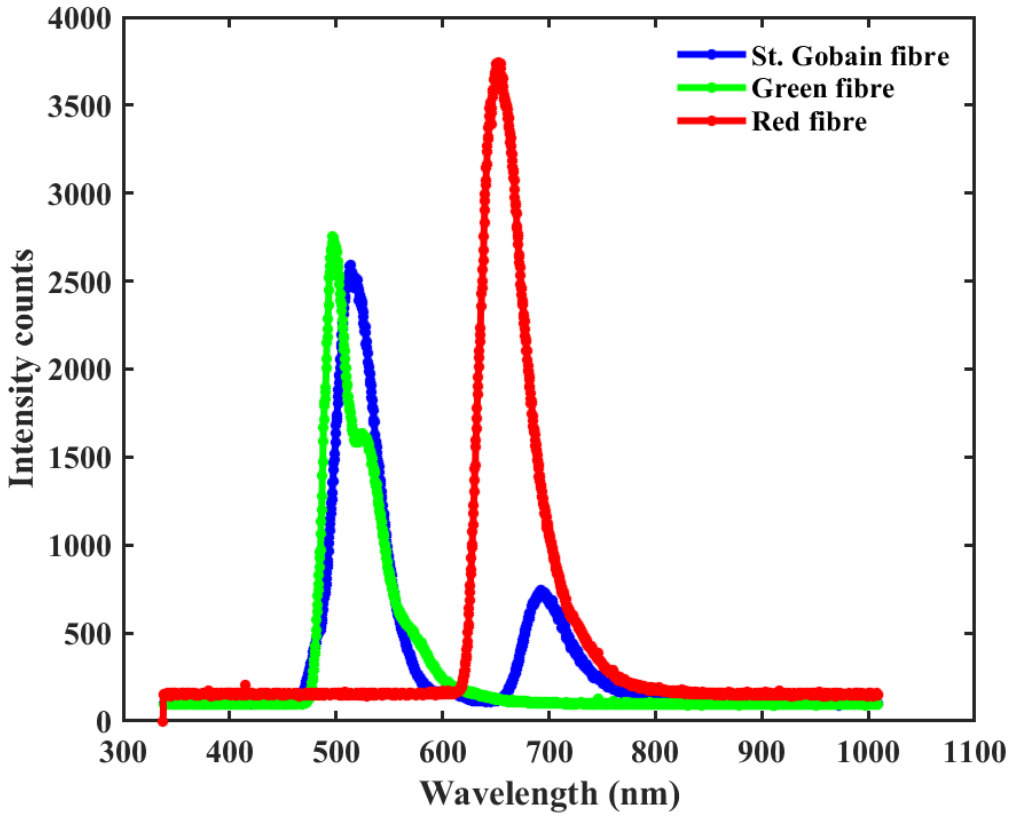

Figure 3.4 Emission spectra of green, St. Gobain and red fibre.

3.3.3 Bandwidth characterisation

In this experiment, the 3 dB bandwidth of the channel with different fibre concentrators was measured. The yellow and the red fibre absorbed the 520 nm light, so a PL520B laser diode (green-LD) was used as a transmitter. Based upon its power-current-voltage (LIV) characteristics the bias of 4.6 V and a 1.5 V_{PP} modulation was applied to this laser diode. Similarly, the green and St. Gobain fibres absorbed the 450 nm and 405 nm light from a PL450B and an L405P20 LD respectively. Based on their LIV characteristics both of these LDs were biased at 4.0 V_{DC} and a peak-to-peak modulation of 1.4 V_{PP}. The Kuraray fibre was only responsive to the 405nm in the current set-up, therefore, its bandwidth was measured using L405P20 LD.

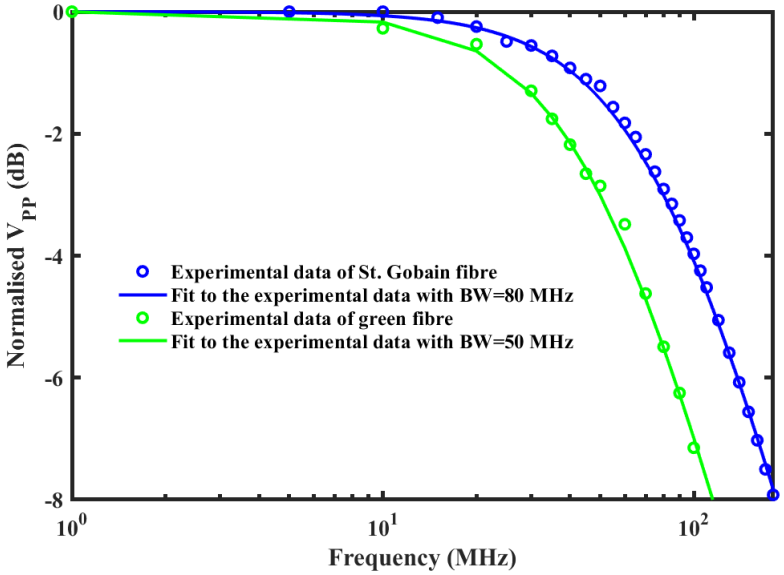

Figure 3.6 BW of St. Gobain and green fibre.

The frequency response of all three LDs was measured by using 1 GHz detectors (Hamamatsu C5658). In these experiments, the AWG was used to modulate the LD with sinusoidal frequencies between 1 MHz and 250 MHz. At each of these frequencies, the frequency response was measured using the same method as described in section 2.2. Using the relevant laser diodes and bias voltages (according to the measured LIV curves of 405 nm, 450 nm and 520 nm LD) the 3 dB bandwidth of each of the fibres was measured individually.

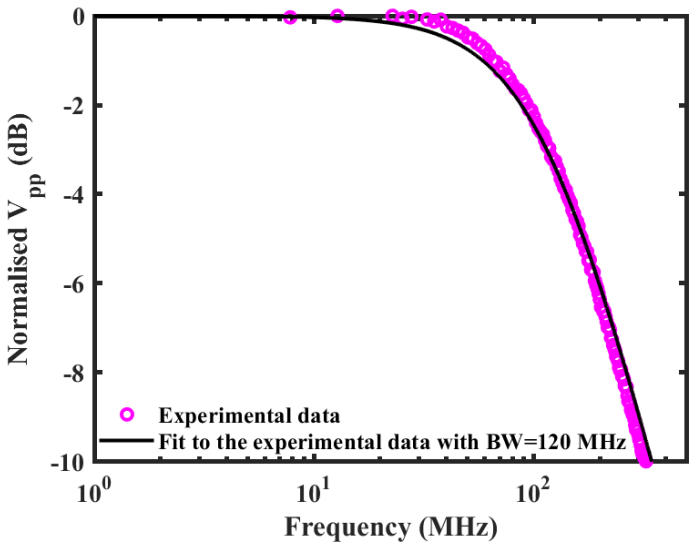

Figure 3.5 Bandwidth of Kuraray fibre.

The results show that, as expected from the lifetimes of the excited states in the fluorophores, all of these fibres have a single-pole response. The results, in Figure 3.6, show that the St. Gobain and Nano-optics green fluorescent fibre have a single-pole response with a 3 dB bandwidth of 80 MHz and 50 MHz respectively. Furthermore, other fibres also have a single-pole response with 3 dB

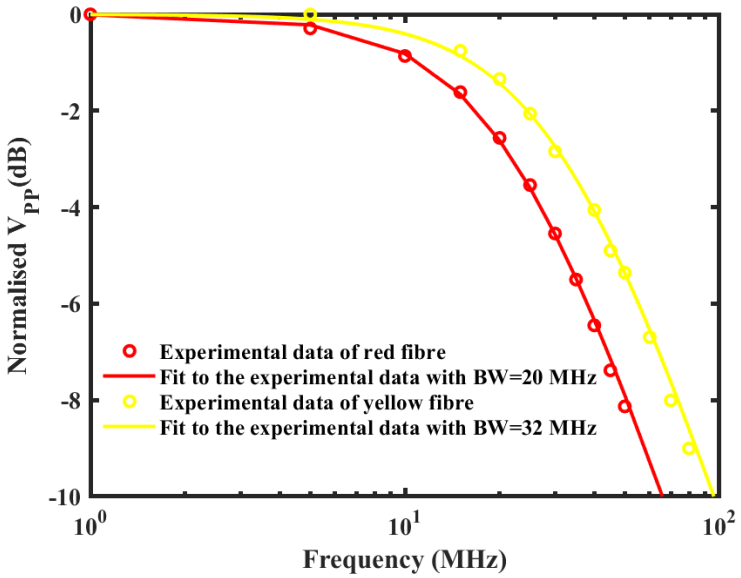

Figure 3.7 BW of the yellow fibre and red fibre.

electrical-optical electrical bandwidths of 20 MHz (red) and 32 MHz (yellow) and 120 MHz (Kuraray) as shown in Figure 3.5 and Figure 3.7 respectively.

Table 3-1 Transmission and bandwidths of fibres.

Fibre	Peak Absorbance (nm)	Bandwidth (MHz)
Nano-optics Red	520	20
Nano-optics Yellow	520	32
Nano-optics Green	450	50
St. Gobain	405	80
Kuraray	380 (not confirmed)	120

Based on the results of the absorption spectrum and bandwidth characterisation of the fibres, shown in Table 3-1, the best choice is Kuraray, St. Gobain and green fibres. However, both green and St. Gobain fibres have a strong overlap in the absorption spectrum, they both have peak absorptions at 450 nm, which means they cannot be used together for a WDM system. St. Gobain fibre has 1.6 times higher bandwidth than the green fibre whilst their gains are approximately the same. Consequently, St. Gobain could be preferred as it can yield a higher data rate at lower irradiance as compared to green. However, for making a fair choice both of these fibres were tested for the data transmission experiments. Similarly, the yellow fluorescent fibre (32 MHz BW) has higher bandwidth than the red fibre (20 MHz BW), however, its gain was approximately 2 times lower as compared to the red fibre. Hence, data transmission experiments were required for a better evaluation of the fibres to be used in the WDM system. In addition to that, Kuraray fibre has the largest bandwidth among all the fibres. In addition to that, from the initial experiments on Kuraray fibre, it was found that it absorbs violet TX more effectively in comparison to green and blue wavelengths, which means there is a fair chance of zero cross-talk while using it in a MIMO setup.

3.3.4 Optimisation of the LDs

To achieve high-speed data transmission with an LD as a light source it is important to optimise the driving conditions of the LD as it impacts the transmission capacity of the LD. A small change in V_{pp} and V_{dc} varies the modulation depth significantly which consequently influences the achievable

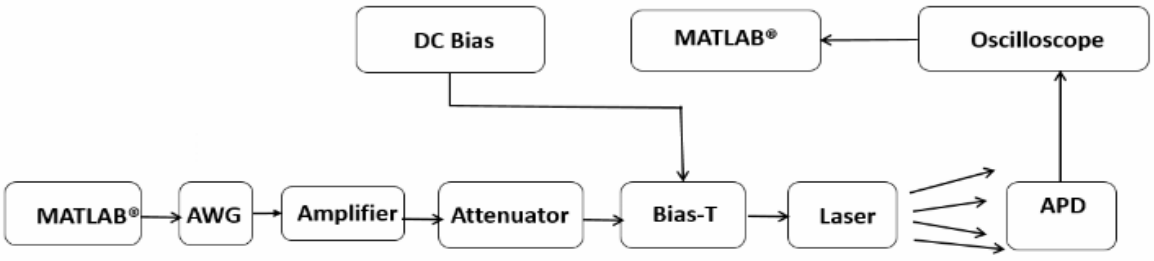

Figure 3.8 System block diagram to show the experimental setup used to evaluate the performance of the lasers at different V_{pp} and $V_{bias.}$

data rate [103][104][105]. To achieve the best possible data transmission results at lower irradiance it is extremely important to optimise the driving conditions of the laser diodes or LEDs. The impact of changes in V_{pp} and V_{bias} on the optical power required to achieve a BER of 10^{-3} for two laser diodes; PL520B (green) and L405P20 (violet) which will be used for the WDM experiments has, therefore, been investigated.

A schematic diagram of the experimental setup used to investigate the impact of varying the peak-to-peak and a bias voltage of the laser diode is shown in Figure 3.8. In this experimental set-up, a 10 GHz arbitrary waveform generator (AWG- Tektronix 70000) was used as the transmitter which generated a pseudorandom binary sequence (PRBS). The maximum peak-to-peak output voltage from the AWG was limited to only 500 mV which was not sufficient to modulate a laser diode, therefore, a 2.5 GHz Mini-Circuits amplifier (ZFL-1000H+) was used to amplify the output peak to peak voltage signal of the AWG. As shown in Figure 3.8, a 6 dB attenuator (BW-S6 2W263) was added to adjust the voltage used to modulate the LD. A 6 GHz Mini-Circuits bias-T (ZFBT-6GW) was then used to add a d.c. bias to the output from the AWG. This combined signal from the Bias-T was then applied to a PL520 laser diode and L405P20 laser diode which have peak output wavelengths of 520 nm and

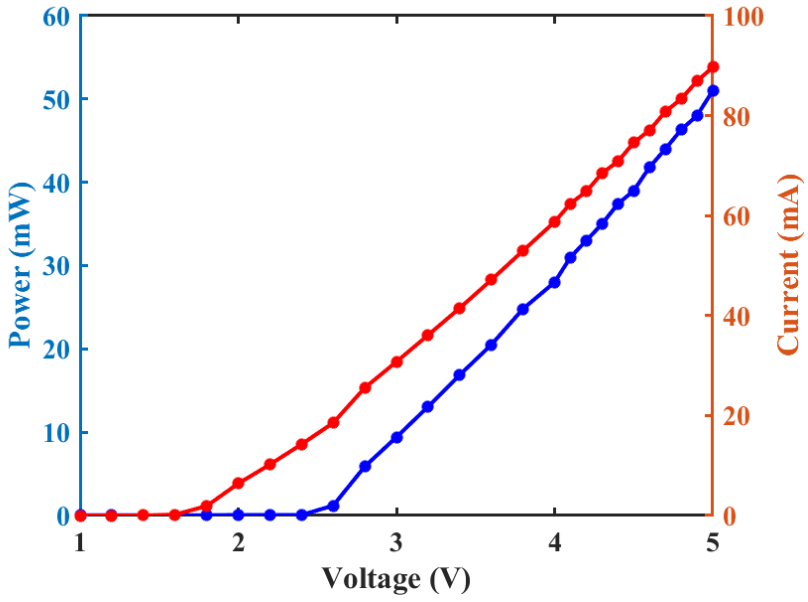

Figure 3.9 LIV curve of the blue laser diode.

405 nm. These particular wavelength LDs were chosen considering the absorption spectrum of the fibres. The irradiance needed to achieve a BER of 10^{-3} at 1Gbps has therefore been measured at

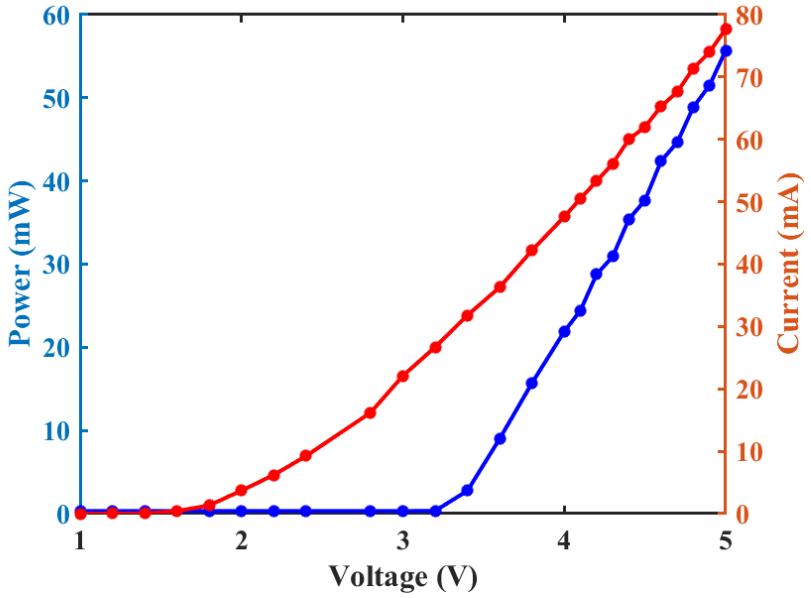

Figure 3.10 LIV curve of the green laser diode.

different bias voltages.

Figure 3.12 shows the impact of bias level on BER performances for the violet and green laser diodes. By considering the LIV curve of the LDs shown in Figure 3.9, Figure 3.10 and Figure 3.11, the

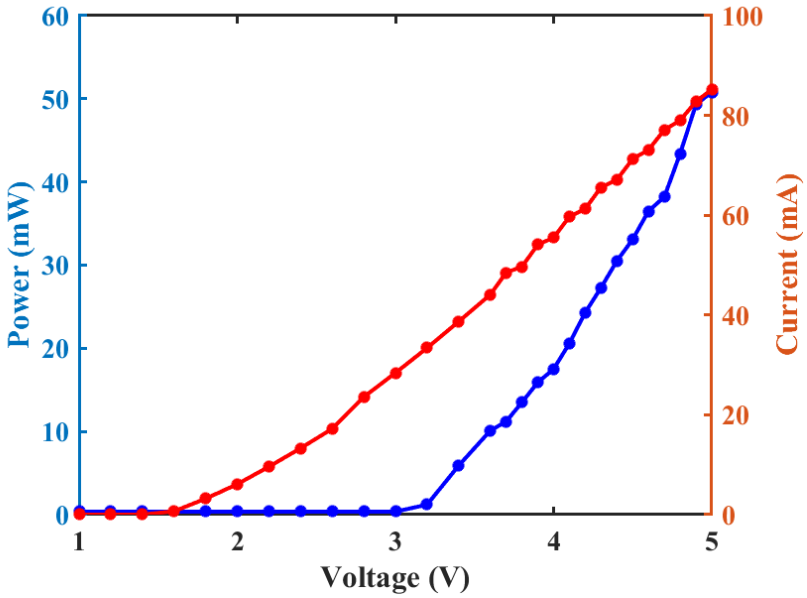

Figure 3.11 LIV curve of the violet laser diode.

amplitude voltage swing was maintained at $1V_{PP}$ (optimized by a quick experiment) and the bias level was increased from 3.8 V_{bias} to 5.4 V_{bias} (to avoid the upper limit at 8 V_{dc} bias voltage which could damage the LD). The results show that a small increase in the bias voltage level causes the output optical power to increase significantly due to the steep slope in the L-I curve for the lasers. [105].

Therefore, a minor increase in bias level leads to a much better SNR for the receiver side and thus a smaller BER [106] [107]. It can be observed from the results, in Figure 3.12, that either the bias voltage is lower or higher than the optimal bias voltage, it shrinks the dynamic range is smaller due to serious signal distortion.

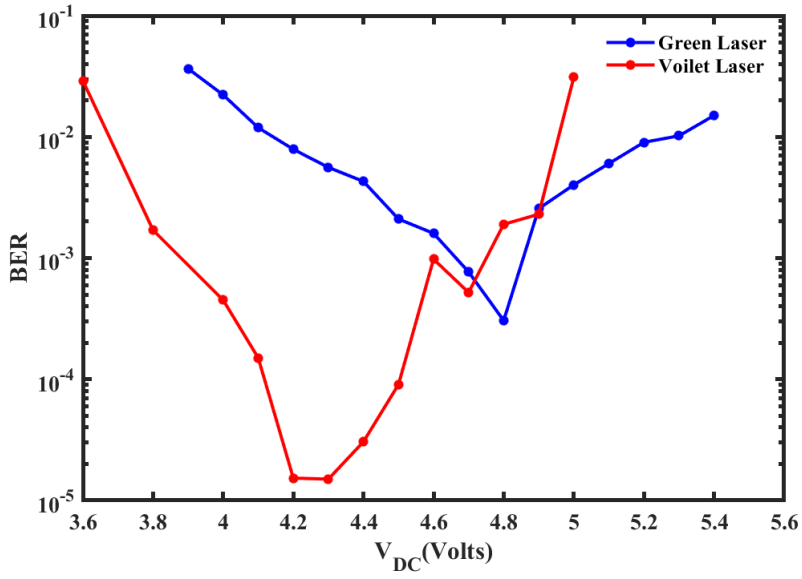

Figure 3.12 BER as a function of V_{bias} of the green laser diode and violet LD.

A prominent improvement in the BER can be observed in Figure 3.12 from bias levels 4.4 V and 5 V. The corresponding measured BER versus V_{dc} show that a 4.8 V_{dc} for green LD and 4.2 V_{dc} for violet LD shall be used.

Furthermore, to determine if BER can be improved by varying the V_{PP} and setting the V_{dc} constant, the d.c. bias voltage on the green laser diode was set to 4.8 V_{dc} and the ac voltage was varied by

keeping the data rate at 1.4 Gbps. Initially, the BER decreased with the increase in peak to peak voltage as shown in Figure 3.13. However, after the optimum voltage, the BER decreased sharply.

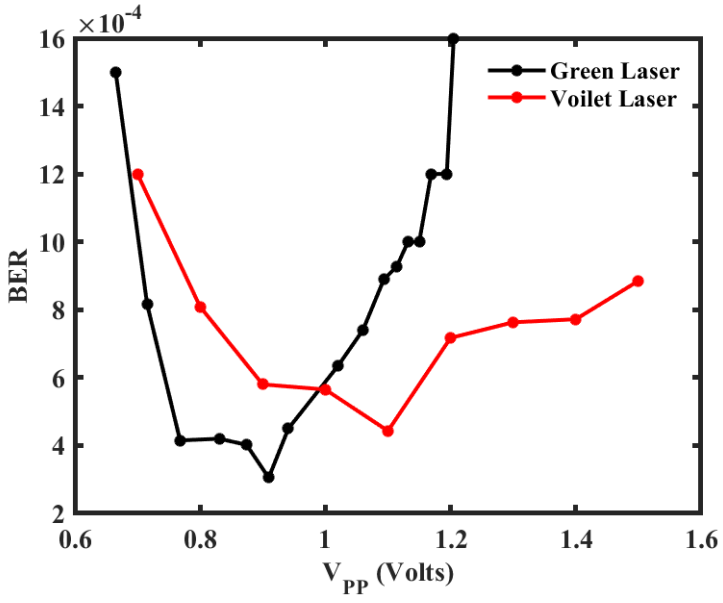

Figure 3.13 V_{PP} Optimisation of green LD and violet LD.

The V_{PP} associated with the minimum BER was then determined and this value, 1.1 V_{PP}, was therefore used in data transmission experiments. Similarly, for the violet LD, the V_{dc} was fixed to 4.2 V_{dc} and V_{PP} was varied at 1.4 Gbps as shown in Figure 3.13. The V_{PP} associated with the various BER was then determined, the results shown in Figure 3.13 suggest that for the minimum BER the violet LD and green LD should be operated at 0.9 V_{PP} and 1.1 V_{PP} respectively.

3.3.5 Impact of polishing on the performance of the fibre

Avoiding additional scattering caused by any rough surfaces is key to guiding the emitted light onto the detector. There are several ways to minimise the surface roughness on the fibre tip like hot blade cutting, fibre polishing, chemical treatments and radiation treatments. However, fibre polishing is a far easier and more efficient method to improve the received output voltage without increasing the irradiance at the receiver.

The use of scissors to cut the plastic optical fibres (POFs) to their correct lengths caused two main issues which needed to be addressed. The shear forces of the scissors changed the cross-section of the fibre from circular to elliptical. Moreover, as PMMA (host matrix of the POF) is mechanically rather soft, the cut fibre is not square. To resolve these two issues the fibre tip was polished as described in the following section. Another benefit of polishing the fibre tips is the reduction of the surface roughness leading to improved light detection [108]. Consequently, increased sensitivity of the detection system can be achieved allowing for higher SNRs of a communication link.

To facilitate the polishing process, the length of the fibre was approximately 0.2.mm larger than the desired length for the optical setup. The fibre was mechanically held by a holder designed in Fusion 360 software, shown in Figure 3.14 in which one end of the fibre was glued into the holder to build a firm grip. It is important to note here that, after cutting the polymer fibres become extremely soft due to mechanical deformations, therefore, the use of adhesive locks the fibre in the holder and prevents fibre damage. Moreover, the glue helps to maintain a firm position of the fibre and provides support during the cleaving and polishing process. After the application of glue, the adhesive was let to sit for a few minutes. Furthermore, the polishing procedure must be performed on a hard flat surface as it can otherwise generate uneven polished edges. Hence, once the fibre within the holder was ready to use, the polishing procedure was performed on a flat and hard surface of a wooden table.

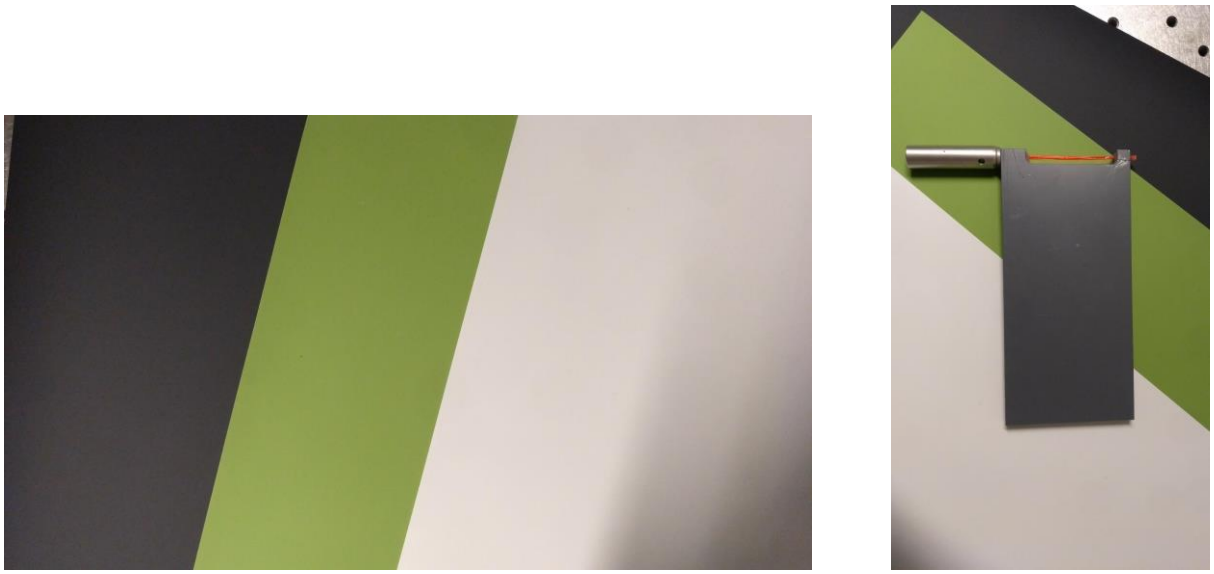

Figure 3.14 Sheets and holder used for fibre polishing.

LF5P sheet with 5 µm grit was used to make the outer coating of the fibre straight. Finally, to obtain a further uniform and even surface, an LF1P polishing sheet with 1 µm grit was used. The minimum recommended grit for polishing PMMA-based fibres was found to be 1µm [109].

According to the measured data, the detected light from a polished fibre tip has a reduced divergence as compared to an unpolished fibre tip. This change (at a fixed link distance) could be associated with a reduction in surface roughness which consequently leads to an increased detection efficiency as more light is guided towards the detector coupled on one edge of the fibre. When the fibre polishing was performed, the received output signal (ROS) increased 1.51 times (i.e. the ROS increased from 70 mV_{pp} to 110 mV_{pp}) as compared to the unpolished ends at the fixed irradiance of 1 mWm^{-2}. Hence it can be concluded that the polished fibre ends connected to the APD, allow higher ROS and SNR without increasing the optical irradiance at the receiver.

3.4 Data Transmission results

To select the best fibres for the WDM experiments, it was important to perform the data transmission experiments on each of them, therefore, the impact of using different fibres as an FC was further investigated by sending On-off keying (OOK) signal. Since these fibres have better BW, so a high BW system (which consists of all the equipment used) whose detail is listed in

Table 3-2 was used. The same experimental method for the data transmission experiment described in section 2.3 was used for these experiments. However, Since DFE is a nonlinear process (DFE is non-linear because the decision circuit is part of the equalizer structure) the number of taps required to compensate for the impact of ISI was determined experimentally. Based upon the experimental investigation, 40 feed-forward and 20 feed-backwards taps were therefore used for all the data rates. For the communication experiments described in this chapter, the irradiance of each LD was initially set under-eye safe limits [110] (reference [110] was used for the eye-safe values), however, optical

power at the receiver was not enough to fluorescent any fibre except the red fibre which was able to

Table 3-2 Equipment used for the characterisation of three fluorescent fibres for WDM experiments used in this chapter

Equipment	Part number	Bandwidth
AWG	Tektronix 70000	10 GHz
LD	PL450B	750 MHz
LD	L405P20	800 MHz
LD	PL520B	800 MHz
Amplifier	DR-AN-20-MO	20 GHz
Attenuator	BW-S6 2W263	26 GHz
Photodetector	C5658 Hamamatsu	1GHz
Oscilloscope	MSOV334A	33 GHz

transmit 200 Mbps. Therefore the irradiance of each LD was increased to the maximum to investigate the maximum achievable data rate through each fibre. The received output voltage signal was not measured for these sets of experiments due to the potential impact of saturation of the receiver (as

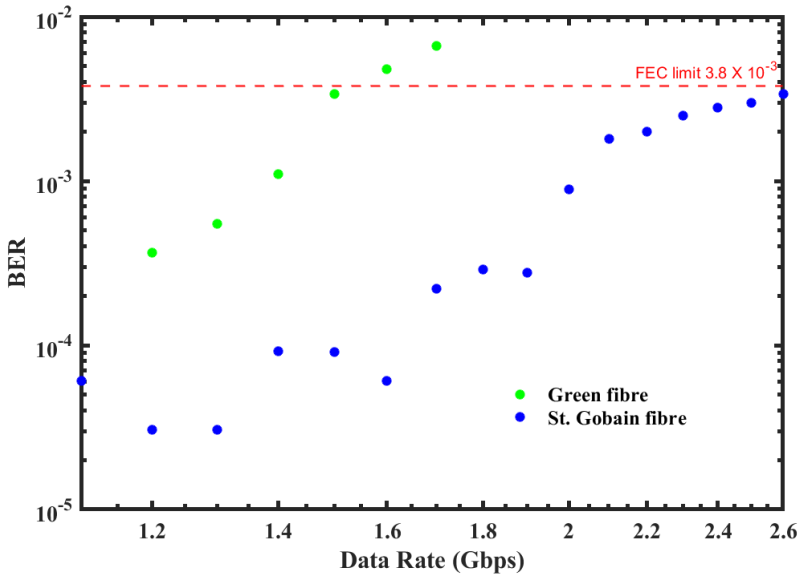

Figure 3.15. Data Transmission results of green fibre and St Gobain

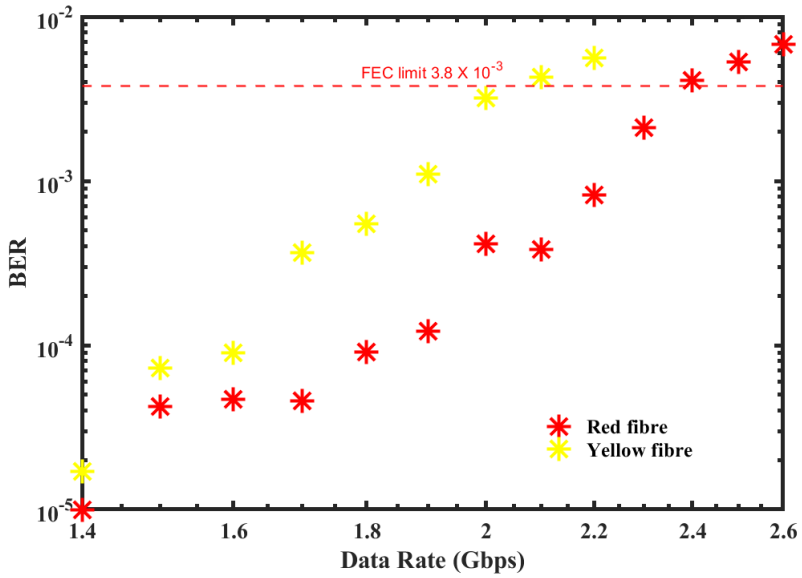

Figure 3.16 Data Transmission results of red and yellow fluorescent fibres

much higher optical power from the LD was used). The BER was measured at different data rates for each fibre and the results are shown in Figure 3.15, Figure 3.16 and Figure 3.17.

The BW of St. Gobain fibre is approximately 1.6 times larger than green fibre and their ROS was approximately the same. When an intense beam of light from the LD was shone on the Rx, Figure 3.15 shows that 2.6 Gbps at a BER of 3.8×10^{-3} (forward error correction threshold) was achieved by using St. Gobain fibre, whereas 1.5 Gbps with a BER of 3.8×10^{-3} was possible through the green fibre.

Furthermore, although the red fibre has a low BW of 20 MHz, the ROS was approximately 3 times higher as compared to the yellow (32 MHz) so the impact of BW difference could not yield advantage for the yellow fibre. Figure 3.16 shows that 2.4 Gbps was achieved at a BER of 3.8×10^{-3} (these high data rates were achieved at an intense beam from the LD) by using the receiver created with the red fibre, whereas, 2 Gbps was achieved with a BER of 3.8×10^{-3} when the yellow fibre was used as an optical concentrator. These results show that although BW is important, however, according to the Shannon Capacity theorem it is the combination of BW and SNR which determines the maximum achievable data rate. Furthermore, when the Kuraray fibre was used for data transmission

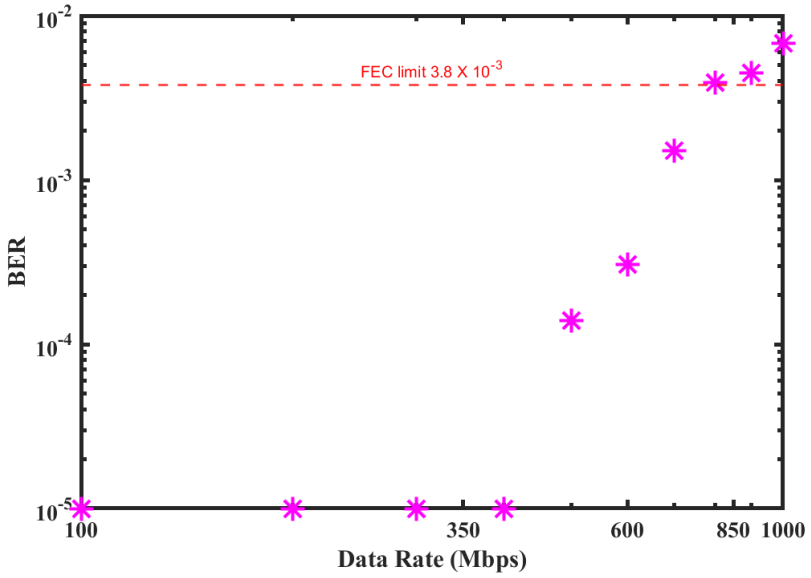

Figure 3.17 Data Transmission results of Kuraray fibre

experiments, a very small amount of fluorescence of the Kuraray fibre, a small output voltage signal, therefore, only 700 Mbps at a BER of 3.8×10^{-3}, as shown in Figure 3.17 was achieved. It is important to note here that the transmitter power was increased to maximum. This lower data rate was particularly due to lower ROS.

Therefore, red and St. Gobain fibres were selected from the two groups based on their better performance in data transmission experiments, whereas Kuraray fibre was chosen because of its effectively better absorption at 405 nm as compared to 450 nm and 520 nm wavelengths (which means lower chances of cross talk or interference).

3.5 Experimental Set-up for WDM experiments

The WDM data link consisted of the WDM fluorescent fibre concentrators coupled to a detector (APD) placed at a link distance of 30 cm from an optical transmitter. The experimental setup along with equipment detail has already been described in section 3.4 All three fibres were tested independently with the three laser sources (405nm, 450nm and 520 nm) to evaluate the H-matrix.

For a fair comparison, it was mandatory to investigate the ROS of each TX at a fixed irradiance, therefore, all the laser diodes were, therefore, operated at 100 mWm^{-2}. The ROS of all three fibres

against the three LDs was measured at the fixed irradiance and the results are shown in Table 3-3. The table suggests that, for the red fibre, about seven times more light is collected by the photodiode when the FC was shone by the green LD as compared to the blue LD. Similarly, for the green LD, approximately 11 times more light was collected by APD as compared to the violet LD.

Table 3-3 The receiver output signals (ROS) from different combinations of fibres and laser

Fibre	Laser diode transmitter	Irradiance (mWm^{-2})	ROS (mV_{PP}) averaged	ROS/ Irradiance
Red	L405P20 (405 nm)	100	1.82	0.018
Red	PL450B (450 nm)	100	2.90	0.029
Red	PL520B (520 nm)	100	28.14	0.281
St Gobain	L405P20 (405 nm)	100	22.65	0.227
St Gobain	PL450B (450 nm)	100	23.16	0.232
St Gobain	PL520B (520 nm)	100	1.02	0.010
Kuraray	L405P20 (405 nm)	100	0.00	0.00
Kuraray	PL450B (450 nm)	100	0.00	0.000
Kuraray	PL520B (520 nm)	100	0.00	0.000
Kuraray	L405P20 (405 nm)	790	19.42	0.025
Kuraray	PL450B (450 nm)	3100	0.00	0.000
Kuraray	PL520B (520 nm)	2100	0.00	0.000

Furthermore, for St. Gobain fibre, the APD absorbs approximately 1.4 times more light with the blue LD as compared to violet LD as shown in Table 3-3, while For the green LD, it is 30 times less compared to the blue LD.

Unfortunately, no received output signal was detected when Kuraray fibre was coupled to the APD at the irradiance of 100 mWm^{-2} regardless of the laser source being used as shown in Table 3-3. To investigate the performance of Kuraray fibre for scientific purposes the irradiance was increased beyond 100 mWm^{-2} taking safety precautions and covering the whole coverage area of LD. A pair of collimating lenses (ACL1210U) were used to create a highly focussed beam for shining on the Kuraray fibre. The results in Table 3-3 show that even at very high irradiances from the three LDs, Kuraray was only responsive to 405 nm with a very low optical gain, which could cause a huge difference in the data rate among the different fibres. Unfortunately, the performance of Kuraray at 405 nm was worse than that of St Gobain at 405 nm.

If the column vector of receiver outputs is the responses of the red, St Gobain fibre and Kuraray fibre and the column vector of transmitter signals is the signals from the 520 nm laser diode, the 450 nm laser diode and the 405 nm laser diode then the data in the last column of Table I means that the H matrix is

$$\boldsymbol{H} = \begin{bmatrix} 0.281 & 0.029 & 0.018 \\ 0.010 & 0.232 & 0.227 \\ 0 & 0 & 0.025 \end{bmatrix} \qquad (3.5)$$

The H matrix indicates the levels of fluorescent light measured by the photodiodes, for each LD.
The Kuraray fibre was included in the experiments because it has a relatively large bandwidth and the Shannon-Hartley Theorem suggests it will support a high data rate. However, the diagonal elements of this H matrix show that it has a significantly smaller output signal than the other fibres when exposed to the same irradiance. This relatively weak response could be accommodated by using a higher irradiance at the receiver from the 405 nm transmitter. However, this would cause a significant amount of interference in the St Gobain fibre. When also taking into consideration the

added cost of supporting three channels, a two-channel system may be a better option. If the two-channel system uses 450 nm and 520 nm transmitters and a receiver containing a St Gobain and a red fibre then the normalised H Matrix would be

$$\mathbf{H} = \begin{bmatrix} 1 & 0.103 \\ 0.043 & 1 \end{bmatrix} \qquad (3.6)$$

Consequently, the interference between these two channels is less than a third of the interference suffered by the two channels in the previous fluorescence-based WDM receiver [101]. More importantly, an important characteristic of any communications system is the achievable bit error rate (BER) and when forward error correction is employed the BER needs to be less than 3.8×10^{-3}. This BER corresponds to a signal to noise ratio of approximately 3. Consequently, assuming that the irradiance from the two transmitters at the receiver is equal, the interference between these two channels will be negligible compared to the existing noise.

Surprisingly, although the bandwidth of the St Gobain fibre is four times the bandwidth of the red fibre the larger ROS of the red fibre means that they can support comparable data rates. In particular, the maximum achievable data rates for the St. Gobain and red fibres are 2.6 Gbps and 2.4 Gbps. The similar data rates and negligible interference between the two channels mean that using WDM should double the data rate that can be supported.

3.6 Results and discussions

It can be seen from Table 3-3, that different WDM fluorescent concentrators have different impacts on the interferences. Kuraray fibre was illuminated with a highly focussed beam of 405 nm LD, a small output voltage signal was obtained and the fibre did fluorescence. However, the collection efficiency of Kuraray fibre was not very good, it only collected $1/10^{th}$ of the signal, as compared to the other fibres which means to use the Kuraray fibre in this WDM system, a very high irradiance (approx. $1000mW/m^2$) would be required for data transmission.

It is important to note here that according to the IEC 62471:2006 safety standard, the blue light hazard limits the permissible irradiances at wavelengths less than 520 nm [110]. The results described in [110] show that green light is 8 times safer than violet light and it is 10 times safer than blue light. This allows more irradiance of 520 nm wavelength as compared to 405 nm and 450 nm wavelengths. Hence, due to a significantly larger power from the transmitter, the red fibre receives 8 times more green light from the 520 nm LD which consequently leads to a much larger ROS and hence a higher data rate. This difference in terms of collection efficiency advocate that Kuraray fibre is not an ideal choice for this WDM system. However, it might be a better option for those applications where interference from other sources is a problem and irradiances above the eye-safe limits are permissible.

Furthermore, for a MIMO system, in light of the H Matrix, it can be concluded that St. Gobain and red fibre with a 450 nm and 520 nm laser diode would be better choices. The H matrix with these two materials (St. Gobain and red fibre) is close to ideal. Although both fibres have a massive difference in the BW, however, due to the much larger ROS of the red fibre, the maximum achievable data rates for St. Gobain and red fibres are very close i.e. 2.6 Gbps and 2.4 Gbps respectively, which means that the implementation of WDM will be helpful in further increasing the capacity of the channel.

3.7 Summary:

The experimental study described in this chapter helps in the selection of the most beneficial type of fluorescent fibre for a WDM system. Furthermore, this chapter presents an inexpensive, novel, compact yet simple and efficient receiver, which could enable WDM with a very large FOV and high gain as compared to the optical filters. Results of initial testing for a WDM system are discussed which include the study of transmittance properties and the frequency responses of the fibres along with the optimisation of the LD. Furthermore, it was demonstrated that the gain of the fibre was increased by 1.51 times when the edge of the fibres were polished by using polishing papers.

Three fibres that have a peak absorption at 520 nm, 450 nm and 405 nm were selected for a WDM setup. The receiver created by these fibres outperforms the challenges created due to the limited FOV

caused by using optical filters. H matrix of these fibres is close to the identity matrix, which means fluorescent fibres maintain minimum cross-talk combined with a large FOV. Unfortunately, the smaller optical gain of Kuraray shows a very high irradiance requirement for the WDM system as compared to the red and the St. Gobain fibre. Results of experiments have been presented which show that if two selected fluorescent fibres are incorporated into a receiver the interference between the two channels would be negligible compared to the existing noise. The result is expected to be a doubling of the achievable data rate by creating a 2 × 2 MIMO system by using the red and St. Gobain fibres.

Furthermore, this investigation opens an opportunity for spectrally efficient fluorescent concentrator-based receivers for a WDM system that could be integrated into the smartphone and other smart devices in the future. In addition to that, it was demonstrated experimentally that the optimum choice of fibre is fundamentally important for an efficient WDM system, therefore, FC could genuinely enable practical WDM VLC receivers.

4 A wide field of view concentrator for a smartphone

An important aim while designing a receiver for the VLC is to achieve a particular data rate with the lowest possible optical irradiance at the receiver [111]. However, field-of-view is also important to ensure connectivity, particularly in devices such as smartphones. The constantly changing orientation of the smartphones in the hands of a mobile user means that the connection links are vulnerable. Due to growing mobile users, the importance of the directionality of the receiver is even higher [112][113]. However, due to rapidly increasing users, it will be difficult to address the challenges of future mobile phone users [114]. Previously, an omnidirectional configuration was proposed to increase the robustness of the link to a smartphone [115]. However, this solution employed several transceivers which not only increases the complexity of the system but also enhances the power consumption and cost.

A VLC receiver that includes a fluorescent optical fibre acting as an optical concentrator for a dummy smartphone has been described. In this chapter, it is shown how an FC-based receiver could be incorporated into the front edge of even the thinnest smartphone. The results of experiments of data transmission are presented which show that it is possible to transmit 1.1 Gbps with a BER of less than the FEC limit of 3.8×10^{-3} to the receiver at a wide angle of ±120°. The most important result which is described is that the receiver has a wide field of view of ±120° in one direction which is the largest reported FOV for the FCs for a smartphone application.

The chapter is organized as follows; Section I contains a brief overview of related work and the importance of the need for a wide FOV in optical wireless communication to ensure connectivity. A fluorescent fibre-based receiver for a smartphone is described in section II, along with the description of the equipment used for the experiments. Moreover, the results of the initial characterisation of the fluorescent fibres which includes the measurement of the field of view are included in section III.

Section IV then contains a description of the results of three different data transmission experiments performed at different angles of incidence and the maximum achievable data rates followed by the summary of the chapter.

4.1 Importance of an Omni directional FOV in VLC

While designing a receiver for optical communication one of the most important aim is to achieve the highest possible data rate at a particular BER (lower than FEC limits) by using the lowest optical irradiance at the receiver. However, usually, these receivers have a relatively smaller collection area which means that there is a constant struggle in the light collection and coverage capabilities of the receiver. Hence, for a mobile user, the coverage mobility support and constant connection switching among multiple access points are the problems that need to be addressed [114]. To solve this problem, multiple studies on handover (HO) and load balancing in optical channel links have been presented [115].

A recent study [116] presented an omnidirectional receiver for a mobile phone user. It was presumed that the normal orientation of the smartphone in the hands of the user is usually slightly tilted while its orientation constantly keeps on changing in random directions. Furthermore, along with this

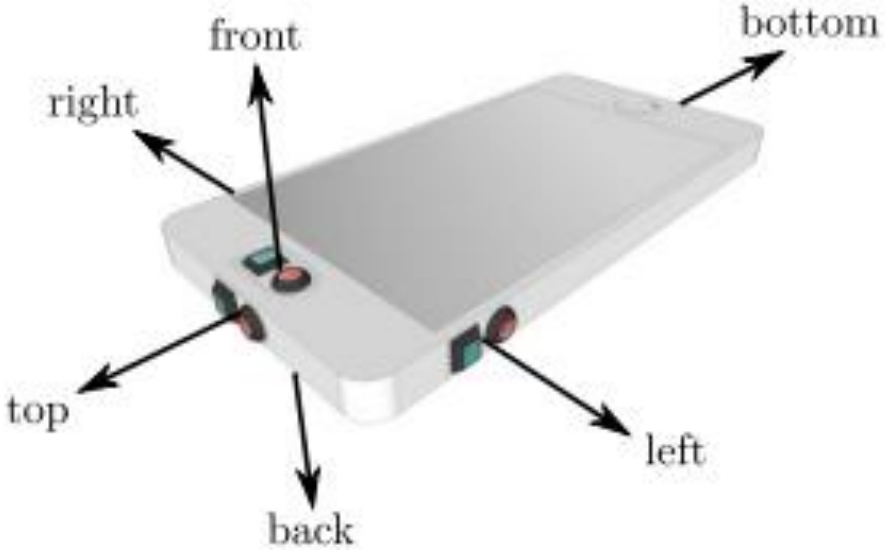

Figure 4.1 Omnidirectional UE configuration for a smartphone presented in [116].

random orientation, multiple factors such as link blockage and variations in the user position may occur. Consequently, these movements result in unreliable link connections for mobile users.

To ensure connectivity in a smartphone, it is important that the receiver in a smartphone is designed to support robust links, irrespective of the random orientation of the smartphone [114]. The suggested model in [116], shown in Figure 4.1, was aimed to improve the coverage and angular diversity.

The simulation results of four different cases discussed in [116] suggested that when a single detector was used as a receiver at the top end of the smartphone, the range of coverage probability lies between 40% and 70%. However, when six detectors, shown in Figure 4.1, were used to create an omnidirectional receiver, the coverage varies between 80% and 95%. More importantly, the maximum achievable data rate increased by 50%. However, there are a few important disadvantages of the proposed omnidirectional configuration such as it needed six transmitters and six receivers which increased the power consumption along with the complexity and the cost of the system [116].

In chapter 2 of this thesis, it is described how an inexpensive fluorescent fibre could be utilised to create an optical receiver to increase the coverage area of the receiver without losing SNR. These fluorescent fibres can also be incorporated into smartphones to provide wide FOV and a higher SNR. One important feature of these fibres is that they are considerably thinner and can be as long as required which helps them to fit into the edge of thin smartphones. Furthermore, these fibres are not limited by etendue which means that they can have both a wide field of view and a significant gain at the receiver.

4.2 Fluorescent concentrators in a dummy smartphone

A 150 mm × 75.7 mm × 8.3 mm dummy smartphone was designed in Fusion 360 software. These dimensions were selected according to the latest phone available on the market at the time of experiments, therefore, these dimensions are the same as of iPhone XR. However, unlike a real smartphone, this dummy phone has two small pillars at one end. In addition to that, each of the two

pillars contains a hole of 1.11 mm in diameter. These holes were created to thread the fibres at the top end of the smartphone as shown in Figure 4.2.

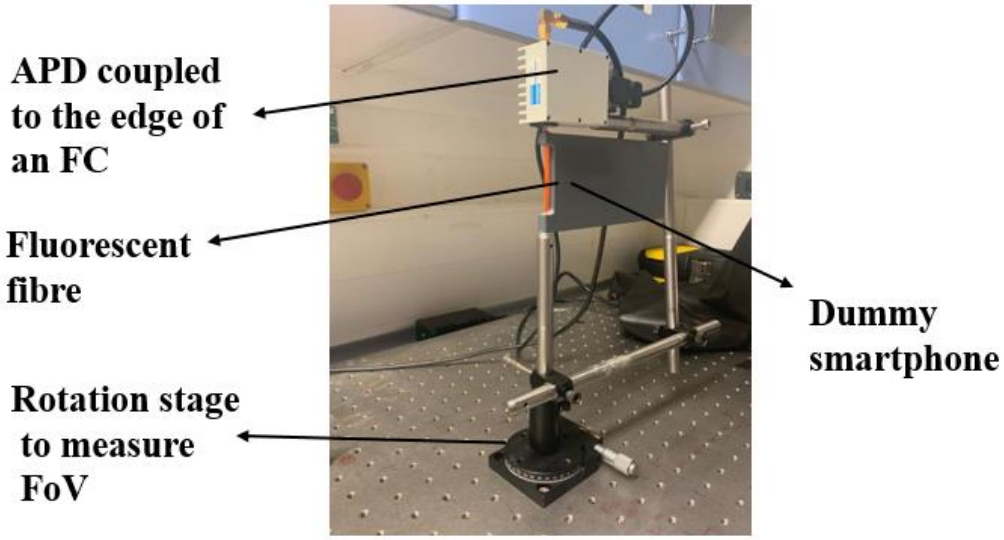

Figure 4.2 Structure to hold the fibre concentrator coupled to the dummy smartphone.

The first experiment which was performed on this setup was the confirmation of BW of the Saint Gobain fibre. The method along with the equipment used for the BW experiment is already described in the previous chapter (section 3.4.3). The results, in Figure 3.6, show that this fluorescent fibre has a single-pole response with a 3 dB bandwidth of 80 MHz, which is significantly higher than the BW of most of the state of art APDs with an active area of more than 1.5 mm^2.

In the experiments reported in this chapter, a blue wavelength absorbing fluorescent fibre from St. Gobain (BCF-20 SC1.00) with a diameter of 1.1 mm was threaded through the two holes in the dummy smartphone. This fibre was chosen due to its higher bandwidth (discussed in section 3.4.3) along with better light collection efficiency as compared to the other available fibres. Although the choice is not important to demonstrate the FOV, however, for the data transmission experiments described later in this chapter, both the bandwidth and light collection efficiency play a critical role. As the St. Gobain fibre has maximum absorption at blue (described in section 3.3.1), therefore, a PL450B 450 nm laser diode (LD) was used as the transmitter.

The holes in the dummy smartphone were created in a position, that they hold the fibre 5 mm from the body of the smartphone. Moreover, the holes were positioned so that the centre of the fibre which has a diameter of 1.11mm was located in the middle of the 6 mm dimension (across the width) of the dummy smartphone. This fibre position was selected so that the FOV of the fibre covered the fields of view of the two receiver configurations presented in [116]. In the configuration presented in [116], two transceivers were deployed on the top and front faces of the smartphone, as these two faces are most likely to be visible to the different access points of a mobile user.

The smartphone with the receiver module was then mounted on the rotation stage with the help of a post (TR3-Thorlabs) as shown in Figure 4.2. While designing the experimental set-up to measure the FOV of the fibre in the dummy smartphone, it was important to maintain an intact coupling between one end of the fibre and the APD photodetector in multiple orientations. A slight change in the alignment could cause a major impact on the results which means the fibre and APD unit should be so robust that they can be held in any possible orientation without any misalignment. To fulfil this requirement four TR4 posts from Thorlabs were used to construct a structure, shown in Figure 4.2, which keeps the centres of both APD and the fibre along the axis of rotation of Thorlabs PR01 rotation

Table 4-1 Details of the experimental equipment used for characterising the Saint Gobain fibre concentrator in a smartphone set-up

Equipment	**Part number**	**Bandwidth (GHZ)**
AWG	Tektronix 7000	10
APD	Hamamatsu C5658	1 (biased with 5 V_{DC})
Oscilloscope	Agilent MSO9254A	2.5
Amplifier	Mini-Circuits ZFL-2500VH+ amplifier	2.5 (biased with 15 V_{DC})
Attenuator	Mini-Circuits BW-S6 2W263	26
Bias T	Mini-Circuits ZFBT-4R2G	4.2

stage (this structure eliminates any chances of misalignment). The whole receiver unit was mounted on the rotation stage to measure the FOV of the receiver.

4.3 Measured FOV of the FCs in a dummy smartphone setup

The first experiment performed with this equipment was to determine the FOV of the receiver (RX). To measure the FOV, the angular positions of the RX were changed by increments of 10° and the corresponding received output peak to peak voltages at 1 MHz were recorded. To improve the accuracy of the results, and ensure that they were reliable, the FOV experiment was repeated twice for a full rotation of 360°.

The detail of the equipment used for the experiments described in the Chapter is included in Table 4-1. The APD was coupled at one end of the fluorescent fibre which was once arranged in the system and goes on the top edge of the FC as shown in Figure 4.3. This APD was chosen to make sure that it has higher BW than the fibres and has a higher responsivity in the emission range of the available fluorescent fibres. It is important to note here that the diameter of the active area of the APD is only 0.5 mm^2 (with 1 GHz BW) which means that a precise alignment between the fibre and APD is fundamentally important. A slight misalignment results in a huge impact on the measurement results, therefore, the structure which held fibre and the APD was made robust. The APD was connected to

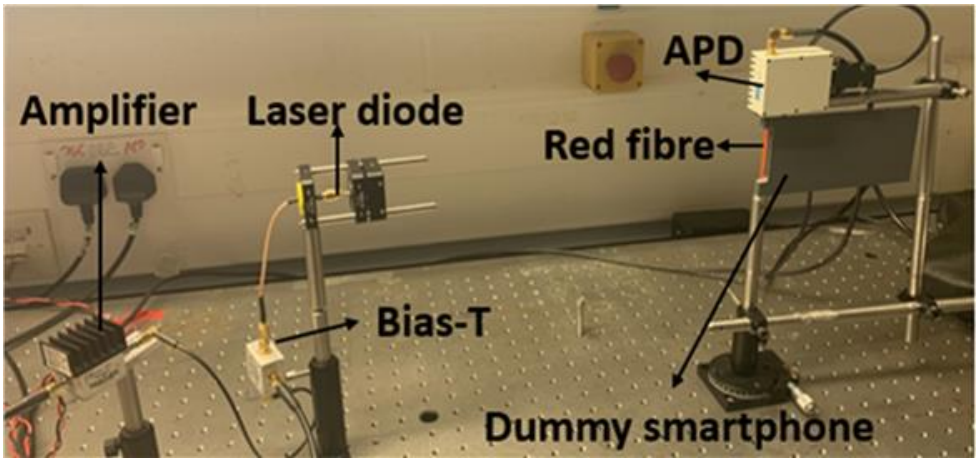

Figure 4.3 Photo of the optical link created to characterise the FC in a dummy smartphone setup.

the oscilloscope. This oscilloscope was used to capture the received output signal (ROS) from the APD at different orientations (angles).

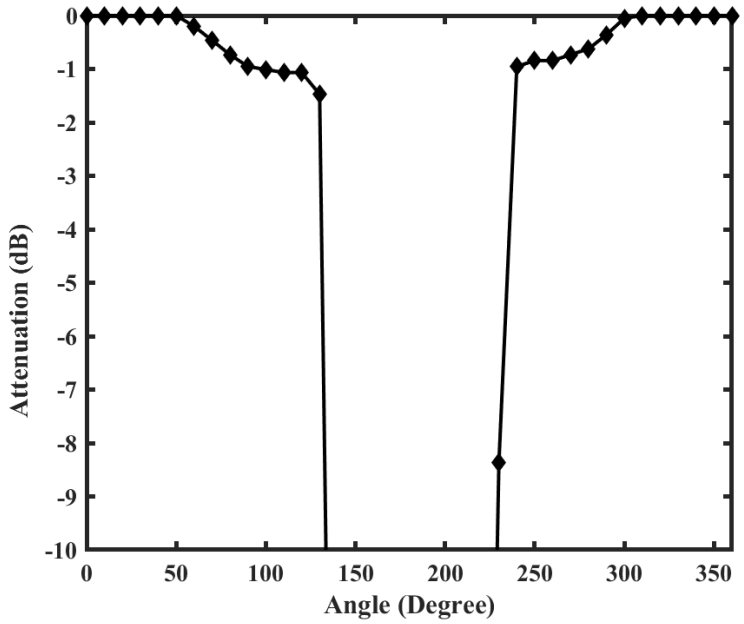

Figure 4.4 Measured field of view of the fibre concentrator coupled to the dummy smartphone.

Another important requirement for the experiments described in this chapter was to ensure that light could not enter the APD directly from the LD. A 3D printed cover that has a hole of 1.1 mm diameter was therefore included in the setup. This cover was coupled in between the fibre and the APD so that when the fibre was inserted into this hole the centre of the fibre was located directly over the centre of the APD. In this way, the only light that could get detected by the photodetector was the light emitted from the edge of the fibre. Furthermore, before doing FOV measurement, it was ensured that the beam is uniform by adding the diffusers and aspheric lenses (explained in chapter 2) in front of the LD.

The results, in Figure 4.4 show that by adding the fluorescent fibre to the dummy smartphone, the FOV of the RX was found to be ±120°. Moreover, there is a sharp dip in the received voltage signal at the angles from 120° to 240°, this is because the line of sight between the transmitter and the fibre is partly blocked by the thickness of the dummy mobile phone body. At these particular angles, most

of the light from the transmitter was unable to reach the fibre i.e. the body of the smartphone was blocking the incident light from the transmitter. This suggests that in the future when the body of the smartphone is expected to be thinner, the FOV would be even larger. This creates an opportunity for the receivers that use fluorescent fibres and it means they will have even wider fields of view in the further thin smartphones that will be launched in the near future. This ±120° FOV ensures the connectivity for a wide range of user movements and this concept could be further applied to different handheld devices. Moreover, with a wide FOV of 240° in one direction, the effects of user movement, user device random orientation, and link blockage will be small.

4.4 Communication Performance

In order to achieve a more realistic communication link, it is particularly important to use a receiver with a wide FOV so that the problems like user blockage, receiver's random orientation and enhanced mobility could be solved. The proposed dummy smartphone configuration is expected to significantly improve the communication performance with better coverage at different angles of orientations of smartphones. It was, therefore, important to investigate the data communication performance of this receiver in an optical link. In the subsequent experiments, three data transmission experiments were performed to evaluate the benefits of the receiver.

4.4.1 Maximum achievable data rate when the FC was used in a dummy smartphone at 0°

The impact of the changes in peak to peak output voltage for the FOV experiment was investigated by determining the relationship between the peak-to-peak voltage at the output of the receiver and the On-Off keying (OOK) data rate, The modulated light from the LD was then directed towards the receiver. For the communication experiments described in this chapter, the same method which was described in chapter 2 was used. For these experiments, the output from the LD was diffused with the help of diffusers and a polarizer to create a uniform beam on the FC, whose maximum irradiance was 2.5 mWm^{-2} at the receiver.

The received output signal was measured at different data rates with a BER of 1×10^{-3}. For this purpose, to vary the ROS, the irradiance at the RX was varied by covering the length of the fibre and by changing the angles of the polariser. A polariser was used because it provides an efficient way of varying power which does not have an impact on the modulation BW of the channel. However, as the BER is extremely sensitive to the SNR, therefore, in a few cases the change of angle of the polariser was not sufficient to obtain a BER of $1x10^{-3}$ exactly. Hence, in those cases in addition to changing the angle of the polariser, different lengths of fibre were also covered/shadowed to evaluate the implications of the angle dependence of the received output voltage signal from the receiver. At the irradiance of $2.5mW/m^2$. When the full length of the fibre was illuminated and full the irradiance coming from the polariser was set to maximum, a data rate of 1.1 Gbps was achieved with a BER of

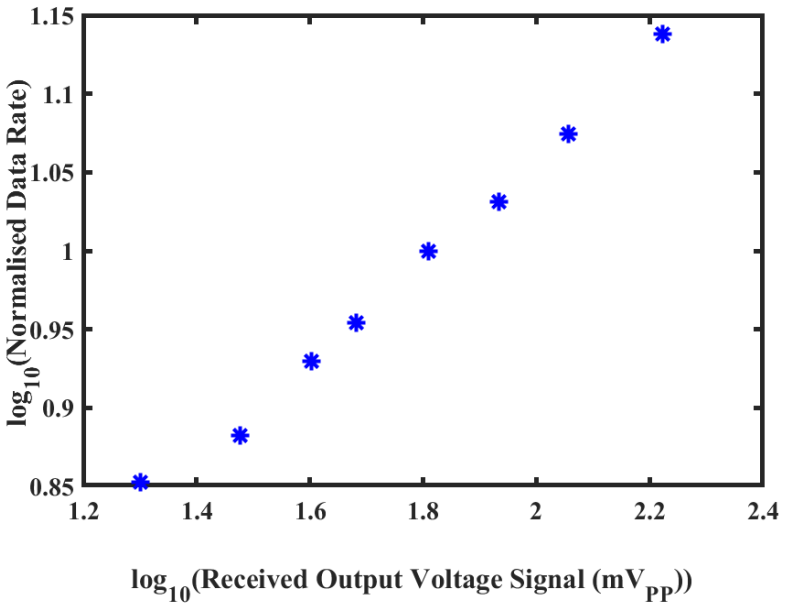

Figure 4.5 The voltage needed to support various data rates normalized by BW with a BER of 1×10^{-3}

10^{-3} as shown in Figure 4.5. The vertical axis in Figure 4.5 represents the data rate normalised by the 3-dB bandwidth of Saint Gobain fibre (BW- 80 MHz). An interesting feature of these results is that the data rate increased linearly with the increase in the received signal as shown in Figure 4.5.

4.4.2 The maximum achievable data rate when FC was used in a dummy smartphone setup at a wide FOV of 120°

The results of FOV experiments, in Figure 4.4 suggests that the worst performance occurred at the highest angles. To evaluate the communication performance of the RX, the angle between the receiver and the transmitter was, therefore, set at 120° and the data transmission experiments were performed. In these experiments, the data rates varied between 600 Mbps and 1.1 Gbps, and the corresponding BER was measured. The results in, Figure 4.6, show that as expected at lower data rates the BER was smaller, however, it deteriorates as the data rate increases. More importantly at this large FOV of 120°, a data rate of 1.1 Gbps was achieved at a BER of 3.7×10^{-3} with DFE. This means that at

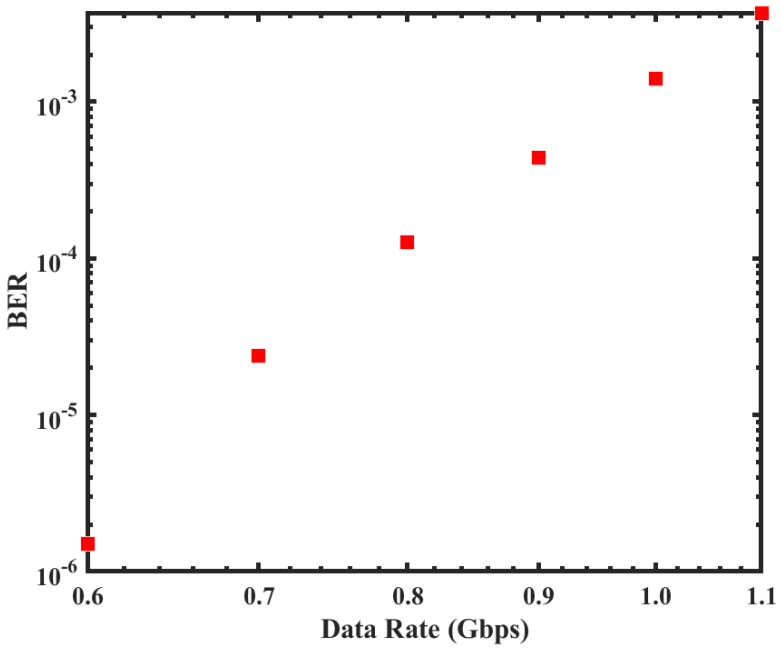

Figure 4.6 Bit error rate measured against different data rates at a wide angle of 120°.

1.1 Gbps the BER is under the threshold of the forward error correction (FEC) so these errors can be corrected.

4.4.3 The BER performance at a fixed data rate and a different angle of incidences

To investigate the impact received output voltage signal in regards to changing the relative orientation of the dummy smartphone and the transmitter, the data rate was fixed at 1.1 Gbps. The angle between

the receiver and the transmitter was then varied while the corresponding BER was measured. The results of these experiments, in Figure 4.7, showed the expected symmetry, i.e. the lowest BER of 1.8×10^{-3}, was obtained when the dummy smartphone was directly in front of the transmitter. As the angle between the transmitter and the normal to the front of the dummy smartphone increased, as expected from the results of FOV experiments, Figure 4.4, the receiver output voltage signal reduced which consequently lead to a higher BER. The BER dropped significantly at 70° transmitted signal from the transmitter was mostly blocked by the body of the dummy smartphone, which means that a very limited amount of light was reaching the FC and eventually the photodetector. However, at a very large angle of 120°, as shown in Figure 4.7, the BER remained less than the forward error correctable limit of 3.8×10^{-3}. If the BER is used to define the field of view of the receiver, it could be interpreted that this receiver has a FOV of ±120°.

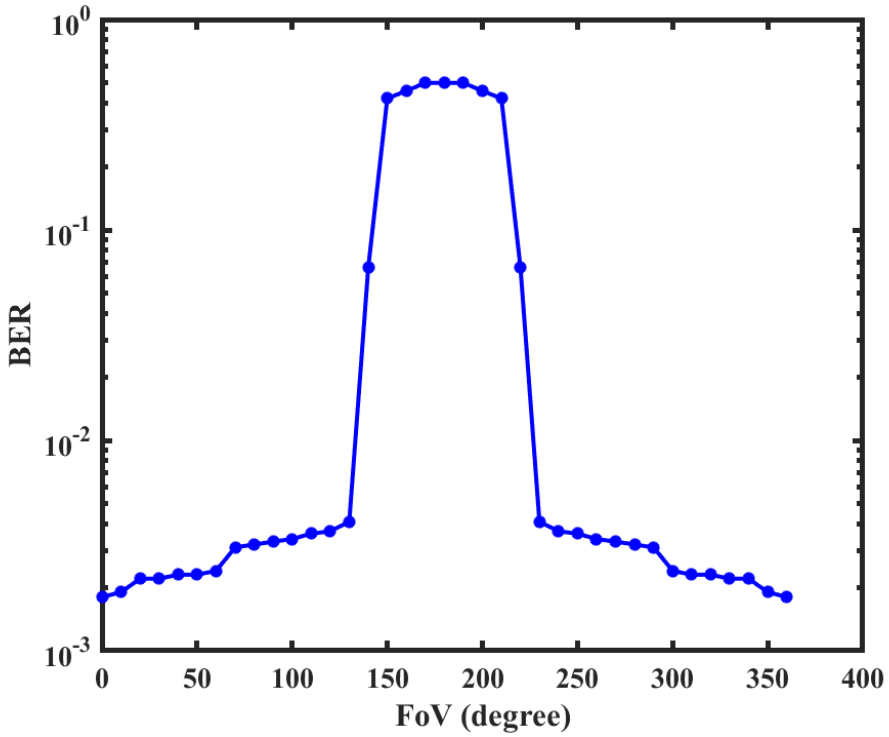

Figure 4.7 Bit error rate measured against the angle of the RX at a fixed data rate of 1.1Gbps.

The results presented in [116] showed that the field of view in the orthogonal direction was ±40° which means that the receiver proposed for a smartphone in this chapter has approximately three times larger FOV as compared to the previous results reported in [116].

4.5 Summary

Recently it has been pointed out that a major challenge that might prevent the deployment of VLC to smartphones is the unpredictable orientation of a smartphone held by a moving user. To overcome this particular challenge, an omnidirectional receiver that incorporates several detectors in a smartphone was proposed. Moreover, the configuration with the best results needed six receivers, which could cause a significant increase in power level consumption and costs. To address this challenge an inexpensive and simple receiver created from a fluorescent fibre concentrator for a smartphone is proposed in this chapter. It has been demonstrated how a fluorescent fibre could be incorporated into the smartphone to create receivers with a FOV of ±120°.

Furthermore, the results of data transmission experiments are presented which show that by using the fluorescent fibre as a receiver in a smartphone and at an irradiance of 2.5 $mWcm^{-2}$ it was possible to transmit 2.3 Gbps with a BER that is below the forward error correction limit. However, the maximum achievable data rate depends upon a variety of factors, such as angle of incidence and the irradiance, therefore, the results of the data rate achieved a FOV of 120° and the relation of BW and irradiance was also discussed. At a wide FOV of 120°, 1.1 Gbps was achieved with a BER less than FEC limits. Further work is now required to exploit the various opportunities created by these thin receivers with extremely wide fields of view.

5 Predicting the OOK data rate achievable with fluorescent concentrators

In order to select the best fibre to use as an FC, the most challenging factor of all is that when the optical concentrator is a fluorescent optical concentrator it has an ability to change both the received output voltage (ROS) at the receiver and the bandwidth of the channel link. In contrast to optical concentrators like CPC and PC, the FC has a trade-off between ROS and bandwidth, a method is, therefore, required that predicts the impact of changes to both ROS and bandwidth.

If the bandwidth of the FC is larger than the existing VLC channel then the 3 dB bandwidth of the VLC channel will remain the same. In these circumstances, the FC will simply increase the ROS. Alternatively, when the bandwidth of the fluorescent fibre is less than the bandwidth of the existing VLC channel an increased data rate can still be obtained if the increase in ROS compensates for the reduction in the channel bandwidth. Most importantly, achieving data rates significantly higher than four times a fibre's 3 dB bandwidth requires large increases in ROS. When selecting a fluorescent fibre, or a fluorophore that might be incorporated into an FC plays an important role in determining the ROS and bandwidth

In this chapter an equation for the SNR needed to support decision feedback equalization (DFE) at different data rates [95] is used as the starting point for a numerical method of determining the relationship between increases in the (ROS) obtained by using an FC and ratio between the achievable OOK data rate and the bandwidth of the FC. Section-I contains the derivation of equations related to signal-independent and signal-dependent noise. The accuracy of this method is confirmed using the results of experiments with one FC, which was later validated by two more fibres independently. In section two of this chapter, the experimental results are also compared with two equations that approximate the results from the numerical method. In addition to being a convenient way to estimate

the benefits of including an FC in a receiver, these equations emphasise the importance of the bandwidth of the FC. The impact of changing the FCs bandwidth is then investigated using two other FCs. Furthermore, the impact of these results on the selection of fluorophores, or existing fluorescent fibres, for use in FCs is discussed. Furthermore, an analysis to investigate the dominant source of the noise present in the optical link is described followed by a brief summary in the last section.

5.1 Derivation of the relationship used for predicting data rate

The starting point for deriving a relationship between the received output signal (ROS) and OOK data rate and predicting the impact of the FC's bandwidth is the SNR needed when a decision feedback equalizer (DFE) is used which is [95]

$$SNR_{DFE} = \frac{2E_S}{N_o} \exp\left\{\frac{1}{f_s}\int_{-\frac{f_s}{2}}^{\frac{f_s}{2}} \ln[Y(f)]df\right\} \qquad (5.1)$$

where E_s is the received energy per symbol and $N_0/2$ is the variance of the Gaussian distributed noise [95]. In addition,

$$Y(f) = \sum_{n=-\infty}^{\infty} |S(f - nf_s)\, H(f - nf_s)|^2 \qquad (5.2)$$

in which *S(f)* is the Fourier transform of the signal and *H(f)* is the frequency response of the channel. If the signal is OOK data, which is a sequence of rectangular pulses with a bit rate of f_s sampled at one time per bit then

$$S(f) = \sin(\pi f/f_s)/(\pi f/f_s) \qquad (5.3)$$

When the channel's frequency response is characterized by a single pole, such as that created by the FC, then

$$H(f) = (1 + jf/f_{3dB})^{-1} \qquad (5.4)$$

This definition of *H(f)* and equation 5.2 mean that the results obtained from equation 5.1 depend upon the ratio f_s/f_{3dB}. In addition to that, since f_s is the OOK data rate, therefore, this is the ratio of the data rate to the bandwidth in equation 5.4. Hence, the results obtained from equation 5.4 are represented as a function of the ratio between the OOK data rate and the 3 dB bandwidth of the channel.

The power penalty that occurs when transmitted OOK data across a channel with a single-pole response has been determined by using equation 5.2 to equation 5.4 to evaluate the power penalty

$$PP_{DFE} = \exp\left\{\frac{1}{f_s}\int_{-\frac{f_s}{2}}^{\frac{f_s}{2}} \ln[Y(f)]df\right\} \qquad (5.5)$$

When the data rate is less than the 3dB frequency the power penalty is small. However, it rapidly increases once the data rate is larger than the 3 dB bandwidth.

Another factor that causes power penalty in a receiver is the bandwidth limiting filter integrated into them, which is incorporated to limit the bandwidth of noise. There is a variety of different types of filters, which could be used for this purpose, however, their probable impact on the power needed to transmit data can be represented by filters whose responses take the form

$$H(f) = (1 + jf/f_{3dB})^{-\mathrm{p}} \qquad (5.6)$$

where *p* is the number of identical poles used to create the filter. In order to avoid power penalty, the filter's characteristic frequency should be higher than the transmitted OOK data rate. However, the main question here is how large the filter's BW should be. If the BW of the filter is much larger that the signal waveform remains undistorted, and results in a lot of noise which contributes to the reduced sensitivity of the receiver. Alternatively, if the filter's BW is narrow to filter the noise, the signal

distortion called ISI will occur. Similar to noise the ISI also reduces the sensitivity of the receiver. Due to these two factors, typically an optimum 3dB BW value of the filter is set to 60 to 70 % of the BER i.e. BW3dB ≈ 0.6BER…0.7BER [119][120][121].

$2E_s/N_0$ in equation 5.1 shows that the measure of SNR is the ratio of the received energy per bit and the variance of the Gaussian noise. However, this is not the only way to calculate the signal to noise ratio (described in Chapter 1). Generally, for Gaussian noise, if the threshold used to determine the transmitted bit at each sample time is optimal, then the bit error rate (BER) is calculated by using equation 1.2.

Equation 1.2, shows that the measure of the Q parameter, that is most directly related to the BER is

$$Q = \frac{v_s^{PP}}{v_{noise,0}^{rms} + v_{noise,1}^{rms}} \qquad (5.7)$$

where the numerator is the peak-to-peak voltage difference between the average receiver output voltage signal when a zero and a one are transmitted [118] and the denominator is the sum of the root mean square noise when a zero is transmitted and a one is transmitted. Furthermore, in some conditions, particularly, when a fluorescent concentrator is involved, this SNR is more easily determined experimentally due to larger resulting ROS.

In particular, if the OOK data rate is *D* and $f_s = D$ then changing the measure of *SNR* to *Q* in equation 5.1 leads to

$$Q(D) = \mathrm{Q}\left(D_{ref}\right) \exp\left\{\frac{1}{\mathrm{D}} \int_{-\frac{\mathrm{D}}{2}}^{\frac{\mathrm{D}}{2}} \ln[Y(f)] df\right\} \qquad (5.7)$$

where *Q(D)* is the value of *Q* needed to support an OOK data rate of *D* and $Q(D_{ref})$ is the *Q* value at a data rate at which the DFE power penalty equals one. Alternatively, the BER at a convenient data rate can be measured after the decision threshold has been optimized and then equation 1.2 means

that if the value of ROS is known, then it is possible to determine the denominator of Q in equation 1.3.

It is important to note that as the irradiance at the receiver is a direct measure of ROS, therefore, in order to determine a relationship between OOK data rate and the irradiance at the receiver, it is essential to consider all the changes to noise at the receiver output. Generally, a noise filter is added to improve the performance of the receiver, however, it is important that the bandwidth of the noise filter is higher than the data rate to avoid a significant power penalty. Hence, an ideal receiver has a bandwidth higher than the desired data rate.

If the dominant source of noise is independent of signal (ROS) and has a uniform power spectral density then the denominator in equation 1.3 will be proportional to the square root of the bandwidth of this filter, and hence the data rate. Under these conditions

$$\frac{\mathrm{ROS}(D)}{(\mathrm{sigma}_0+\mathrm{sigma}_1)\sqrt{D}} = \frac{\mathrm{ROS}(D_{low})}{(\mathrm{sigma}_0+\mathrm{sigma}_1)\sqrt{D_{low}}} PP(D) \qquad (5.8)$$

which can also be written as

$$ROS(D) = \mathrm{ROS}(D_{low}) \frac{\sqrt{D}}{\sqrt{D_{low}}} PP(D) \qquad (5.9)$$

In some situations, it may not be possible to determine the performance of a system at a low data rate or information may already be available at a particular data rate. If information is known a particular data rate is D_{known} then the received output signal (ROS) needed to support a data rate D is

$$ROS(D) = ROS(D_{known}) \frac{\sqrt{D} \times PP(D)}{\sqrt{D_{known}} \times PP(D_{known})} \qquad (5.10)$$

If the dominant noise source is thermal noise in the receiver or shot noise from ambient light only then the noise signal independent model will be valid. However, in some conditions, the noise in a receiver is dominated by shot noise from the transmitter. In that case, the noise at each data rate is proportional to the square root of the product of the data rate and ROS.

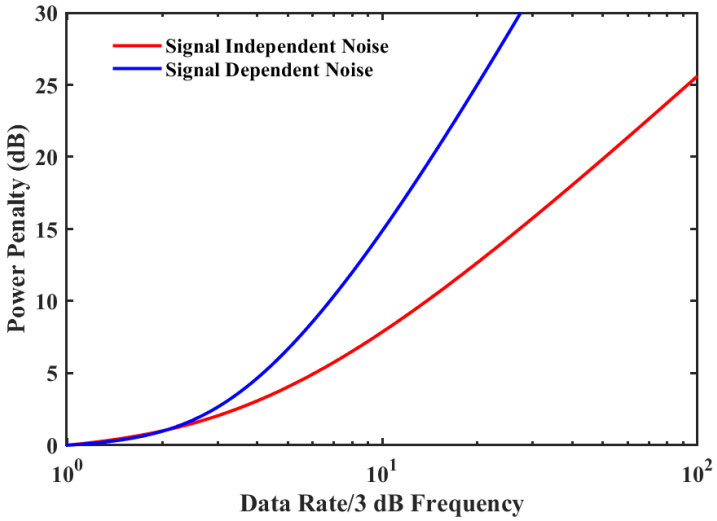

Figure 5.1 The power penalty for a channel with a single pole frequency response from DFE combined with signal independent noise and signal dependent noise.

In this case

$$ROS(D) = ROS(D_{known})\frac{D \times PP^2(D)}{D_{known} \times PP^2(D_{known})} \qquad (5.11)$$

The results obtained by evaluating (5.10) and (5.11), for a channel with a single-pole response are shown in Figure 5.1, in this figure the power penalty when the data rate equals the 3 dB frequency of the channel has been set to one. These results show that the power penalty when the noise is signal-dependent is significantly larger than the power penalty when the noise is signal-independent.

5.2 Experimental results

The validity of equation 5.10 has been investigated by transmitting an OOK data to a receiver that incorporates an FC formed from a fluorescent fibre. For each series of experiments, one of these fibres was threaded through the front end of a holder that represented a dummy smartphone. Once in position, one end of the fibre was coupled to the APD (Hamamatsu C5658) and the data transmission experiments were performed in that optical link. One of the important features is that fibres have a large field of view (FOV) largely 240° as explained in chapter 4, section 4.3.

For these sets of experiments, three fibres were used in total. Two of these fibres were a red and a green fluorescent fibres purchased from Nano-optics, whilst the third fibre (BCF-20 SC1.00) was

purchased from St Gobain. The frequency responses of these fibres along with the emission spectrum are discussed in detail in Chapter 3 of this thesis. Based upon their LIV characteristics (described in chapter 3) and experimentally optimized V_{pp} and V_{dc} (discussed in chapter 3) PL450B and L405P20 LDs were biased with a DC bias of 4.0 V and a peak-to-peak modulation of 1 V_{pp}, whereas a DC bias of 4.8 V and a 1V_{pp} modulation was applied to the green laser diode (PL520B).

When OOK data was transmitted the first step in MATLAB® was to filter the received signal with a 4^{th} order Butterworth low pass filter, which has a bandwidth proportional to the data rate. Decision feedback equalization (DFE), with 40 feed-forward and 20 feed-backwards taps, was applied to the signal to compensate for inter-symbol interference (ISI). The processed received signal was then compared to the transmitted signal, which was simultaneously captured using channel two of the oscilloscope. The bit error rate (BER) was, therefore, calculated by comparing the received signal to the transmitted signal.

As discussed in the previous chapters, the addition of an FC increases the ROS which is a combination of the increase in the number of photons reaching the receiver and a higher photodetector responsivity. The impact of adding an FC to a receiver in an optical link has, therefore, been determined by measuring the ROS. In order to determine the ROS independent of the fibre's bandwidth, the average peak-to-peak receiver output voltage at 1 MHz sine wave was measured. The maximum OOK data rate at which a BER of 10^{-3} could be achieved with DFE and this ROS was then measured.

Furthermore, to investigate if the method of predicting the data rate is general and not limited to one particular fibre, the impact of other FCs in an optical link has been investigated using FCs formed from three different fluorescent fibres individually. The results in Figure 5.2, show that the experimental results all fall close to the curve formed by the numerical evaluation of equation 5.10.

To compare (6.10) to experimental results a reference data rate and ROS at that data rate are both required. The most logical data rate to use as a reference is the one that is numerically equal to the

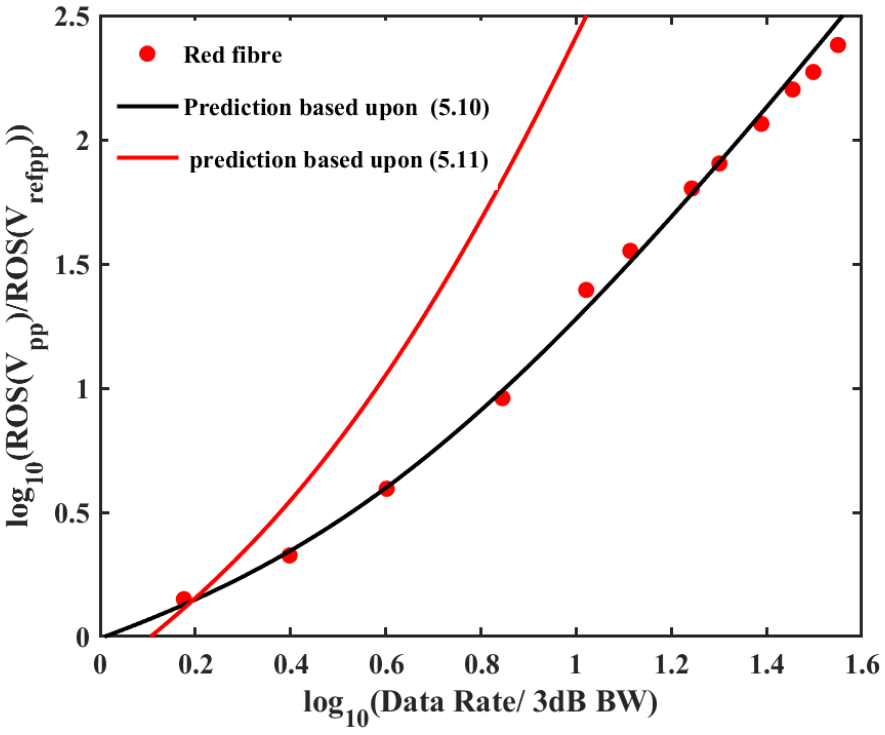

Figure 5.2 The experimental data from the red fibre compared to the results obtained using equations (5.10) and (5.11) This figure has been obtained using ROS(V_{refpp})=2.8 mV and the bandwidth of the red fibre is 20 MHz.

3dB bandwidth of the FC. However, the BER is extremely sensitive to a small fraction of change of ROS and hence Q, so it was difficult to obtain a BER of 10^{-3} at this data rate experimentally. The ROS for this reference data rate was, therefore, obtained by assuming that (5.10) predicts the ROS at the lowest measured data rate, which was 30 Mbps. The peak to peak voltage at 1 MHz required to obtain this data rate, which is the chosen measure of ROS, was 4.0 mV. This data together and (5.10) resulted in an estimated value of ROS needed to obtain the data rate numerically equal to the bandwidth equal to 2.8 mV.

Figure 5.3 shows the experimental data obtained for data rates between 30 Mbps and 170 Mbps, which is 8.5 times the fibre's bandwidth. The y-axis in this figure is the logarithm of the ratio between the ROS at different data rates and the ROS at the reference data rate, which is 2.8 mV. Similarly, the x-axis in Figure 5.3 is the logarithm of the ratio between the OOK data rate and the bandwidth of the red fibre. In addition to the experimental data, this figure also includes the curve obtained using

equations (5.10) and (5.11). The most important feature of Figure 5.3 is that the curve based upon signal independent model passes very close to all the experimental data. The performance of the

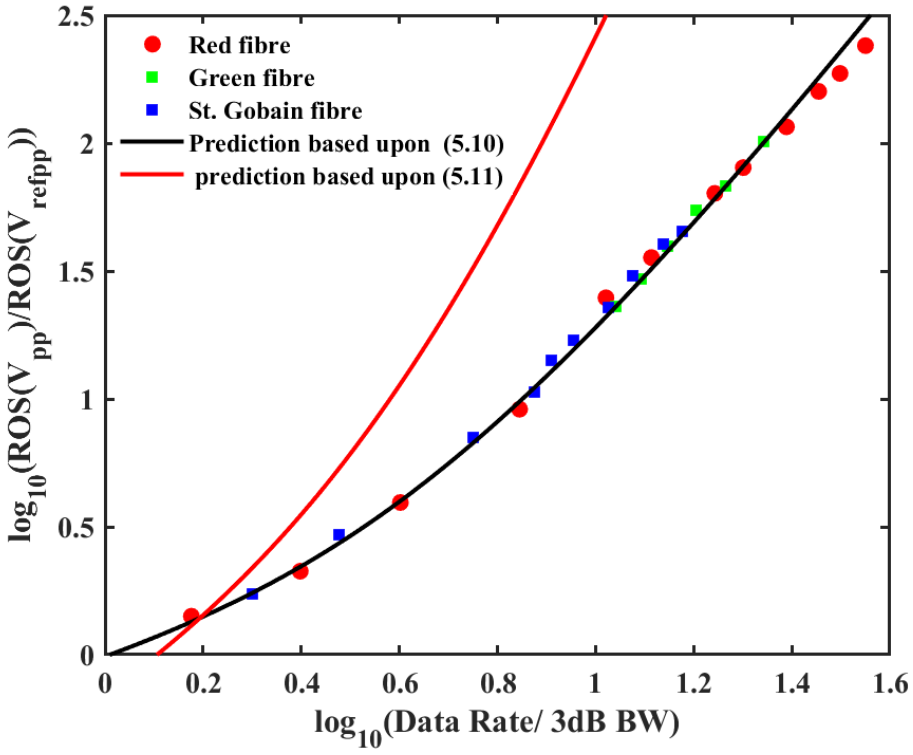

Figure 5.3 The experimental data from the red fibre, green fibre and St. Gobain fibre compared to the results obtained using equations (5.10) and (5.11) This figure has been obtained using $ROS(V_{refpp})$=2.8 mV and the bandwidth of the red fibre is 20 MHz.

receiver for data rates up to almost 40 times the fibre's bandwidth can therefore be accurately predicted by numerically evaluating (5.10) as shown in Figure 5.3 (the BW of the red fibre is 20 MHz, and the achievable data rate with red fibre is approximately 800 Mbps, which means the predictions were correct until 40 times of the BW of the fibre). More importantly, these equations can be used to predict the relative performance of FCs with different bandwidths and increases in ROS.

5.3 Evidence of signal-independent noise

In a channel link with an APD as a receiver, the APD's avalanche gain can only be enhanced at the cost of adding more detector noise [117]. Usually, the avalanche noise's amplitude distribution, which is crucial for computing the BER of the received signal is non-Gaussian. It is, therefore, anticipated

that the dominant source of the noise (in an APD link) will be a shot noise. However, the experimental results described above showed an agreement with the signal-independent noise model, therefore, it was important to investigate the behaviour of noise from the saved experimental data.

The receiver which is more prone to signal-dependent noise is the one created by coupling an APD to a red fibre which has a lower bandwidth (20 MHz) among the three fibres, therefore, requires a much higher ROS to support a given data rate, Hence, the red fibre at different data rates is investigated for signal dependence behaviour.

One way to evaluate the noise is by simply looking at the extinction ratio/modulation depth of the LD used for these experiments [118]. If the modulation index is low, the difference between level zero and level one will be small, therefore, even if shot noise is dominant, a small extinction ratio will generate noise that is almost signal independently [118]. However, the LIV curves as shown in Figure 3.9, Figure 3.10 and Figure 3.11 suggest that a relatively higher modulation index was used, therefore, to prove that noise is signal independent further analysis of noise is required.

The nature of noise can also be investigated by evaluating the histograms [118].

i. Histograms

Histograms are important in the determination of the Gaussian behaviour of noise. If the noise on the ones is bigger than the noise on the zeros, then the two distributions have different standard deviations. For example, if one distribution is narrow with a standard deviation of 0 for the zeros and the other distribution is a wider one with a standard deviation of 1 for the ones. The distribution for the zeros should be taller as compared to the distribution for the ones because both probability distributions must have a total area equal to 1. In that case, the noise will be non-Gaussian and signal-dependent. However, if the standard deviations of ones and zeros are the same and the distribution of ones and zeros, therefore, has the same width and height it will be Gaussian or signal-independent [118].

However, in the determination of the Gaussian nature of the noise the tails of bit one and bit zero which cross the decision point are more important. If the noise is Gaussian, it is fundamental that the Gaussian fits the tail and the tails are rather symmetric [118]. Histograms of bit ones and bit zeros were plotted at the down-sampled data without DEF and after the DFE. Furthermore, a Gaussian with the corresponding variance and mean was also plotted as shown in Figure 5.6 to Figure 5.9.

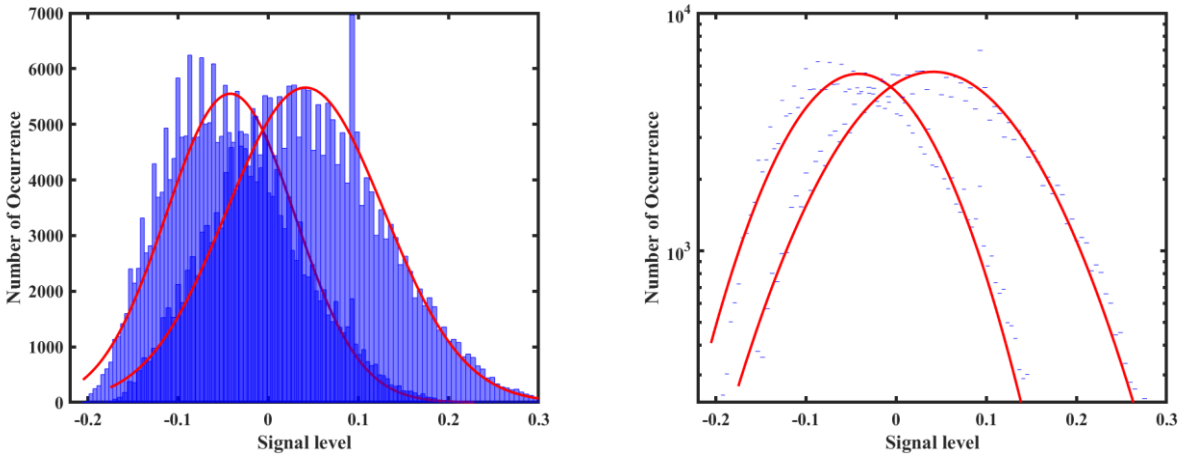

Figure 5.4 Comparison of the histogram of noise and a Gaussian pdf at the data rate of 710 Mbps for red fibre without DFE.

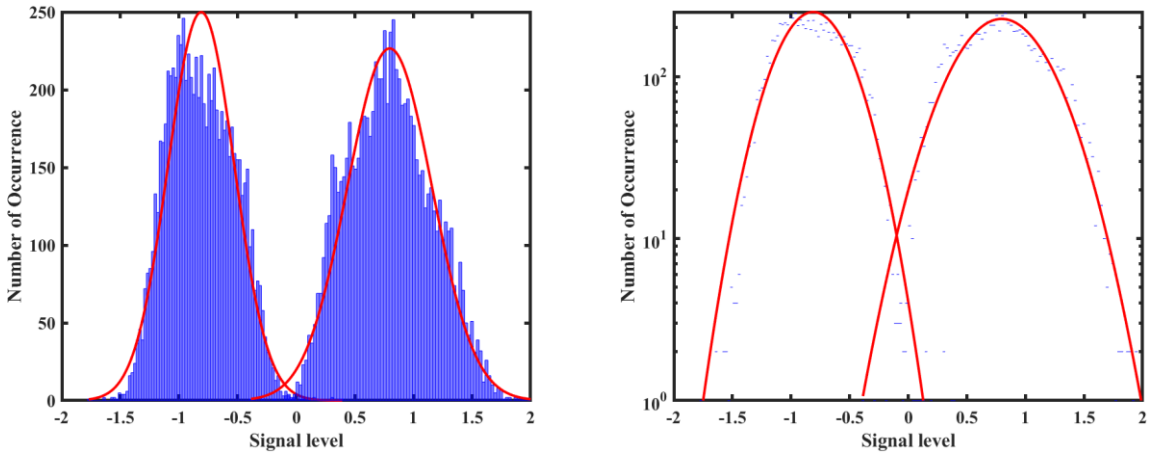

Figure 5.5 Comparison of the histogram of noise and a Gaussian pdf at the data rate of 710 Mbps for red fibre with DFE.

In these figures, the histograms with a fit at different data rates are shown on the left-hand side (the fit is plotted using the Gaussian equation) while on the right-hand side the y-axis is converted in log scale to display the tails of the one and zeros more efficiently. The shaded areas in Figure 5.6 to Figure 5.9, under the Gaussian tails represent the error probabilities, which determine the BER, so these are most critical in determining if the noise is Gaussian or not. As expected, the error probabilities were much higher for the data rates without DFE, however, the error counts do not matter in the evaluation of noise. Therefore, the histograms at key data rates were plotted without

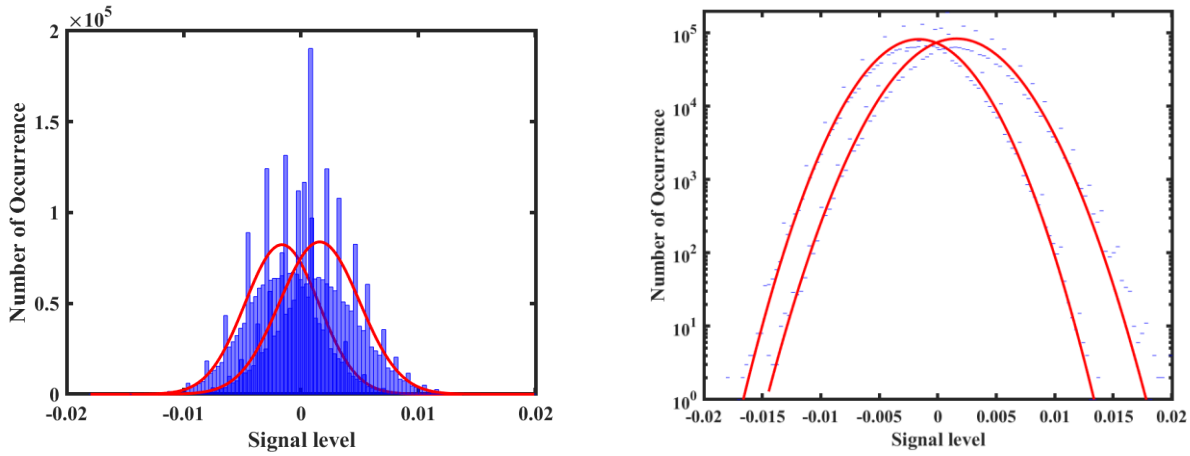

Figure 5.6 Comparison of the histogram of noise and a Gaussian pdf at a data rate of 80 Mbps without DFE.

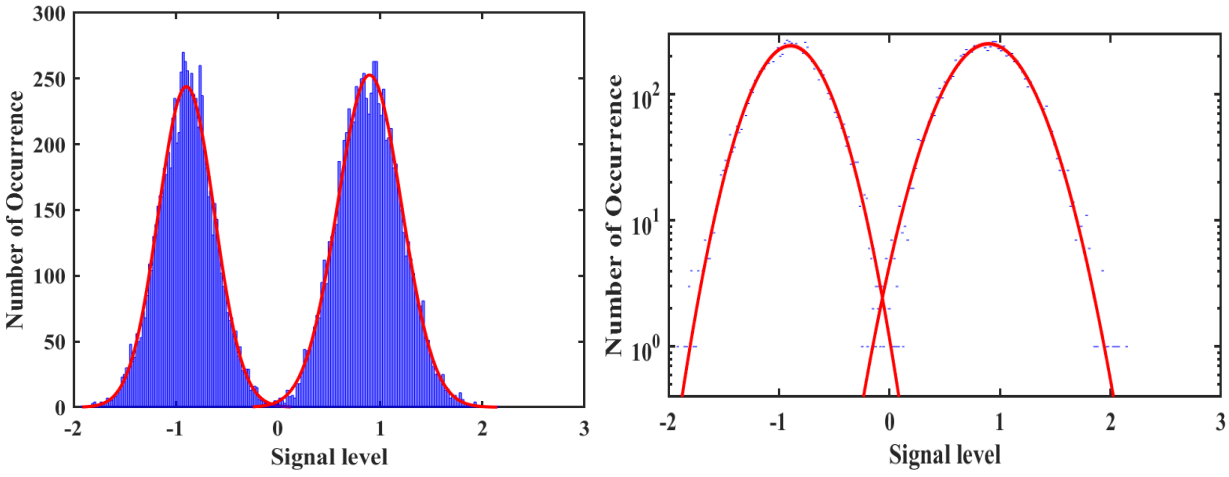

Figure 5.7 Comparison of the histogram of noise and a Gaussian pdf at a data rate of 80 Mbps with the DFE.

DFE as well.

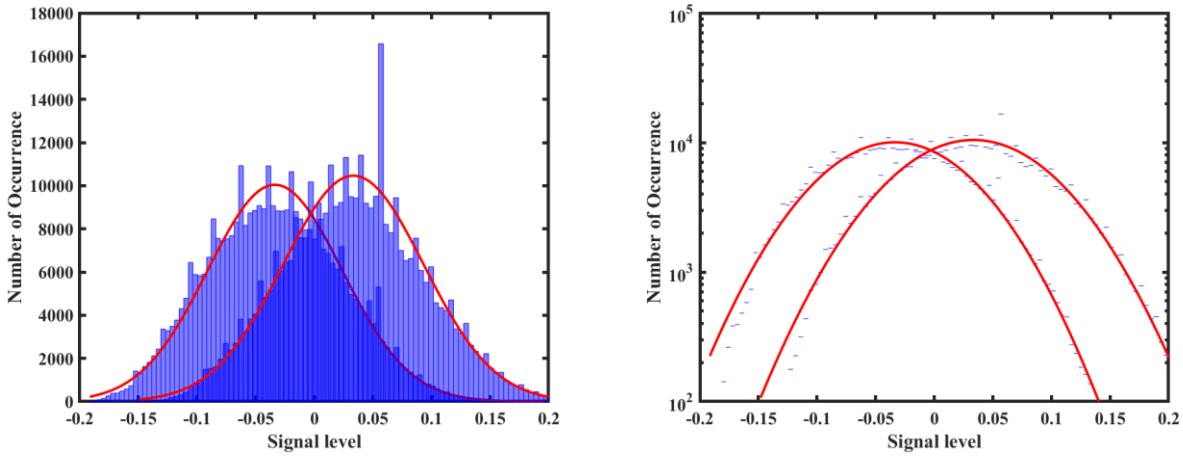

Figure 5.8 Comparison of the histogram of noise and a Gaussian pdf at 1100 Mbps for green fibre without DFE.

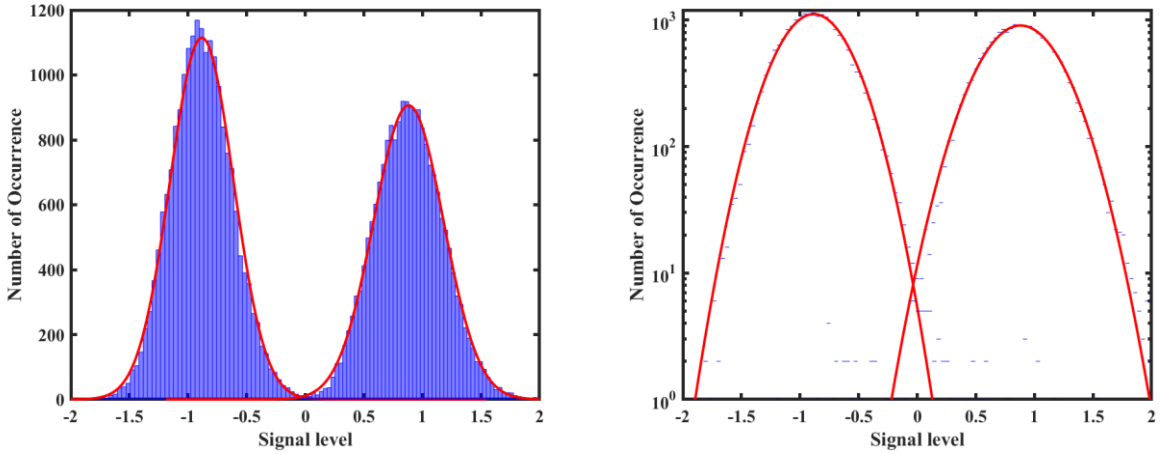

Figure 5.9 Comparison of the histogram of noise and a Gaussian pdf at 1100 Mbps for green fibre with DFE.

This analysis was performed on each fibre used for the irradiance (ROS) versus data rates experiments, however, due to limited space, the histograms of three key data rates with and without DFE are shown here. As mentioned earlier, the chances of signal dependence behaviour increase when the value of ROS is significantly larger. Of the three fibres, red fibre had the highest values of ROS (due to a small BW-20 MHz), therefore, histograms of red fibre data at the lowest and highest data rates are shown in Figure 5.6 to Figure 5.5 respectively. The third histogram is of the green fibre at 1100 Mbps, shown in Figure 5.8 to Figure 5.9, which was also vulnerable to signal dependence noise (due to a much larger data rate and hence the irradiance).

Figure 5.6 and Figure 5.8 (80 Mbps and 1100 Mbps) show that Gaussian fits quite accurately to the tails and has the same area under the tails. As expected, due to significantly higher values of ROS, a few distortions, as shown in Figure 5.4, represents a negligible impact of signal-dependent noise. Since the histograms, shown in Figure 5.6 to Figure 5.9 have a close resemblance to the Gaussian distribution, therefore, it proves that the noise distribution model is reasonably close to signal independent. Moreover, the histograms without DFE, shown in Figure 5.6, Figure 5.4 and Figure 5.8, show agreement with the signal independence model of the noise.

In addition to this, the values of the standard deviation of bits ones and bit zero at the different data rates of red fibres along with the mean of zeros and ones are shown in Table 5-1.

Table 5-1 Values of measured standard deviations and variance of the experimental data at different data rates

Data Rate (Mbps)	STD Bit 1	STD0 Bit 0	Mean Bit 0	Mean Bit 1	Ratio of STD
710	0.36	0.28	0.81	0.80	1.28
570	0.34	0.27	0.84	0.83	1.28
490	0.34	0.26	0.87	0.88	1.32
400	0.33	0.26	0.88	0.87	1.28
350	0.34	0.26	0.88	0.88	1.31
260	0.32	0.26	0.88	0.87	1.23
210	0.32	0.26	0.89	0.89	1.23
140	0.31	0.26	0.89	0.89	1.21
80	0.32	0.27	0.90	0.90	1.15

The nature of the noise can also be determined by comparing the statistical distributions of ones and zeros if the ratio of the standard deviation (STD) is the same, the noise is Gaussian. The ratio of STD

in Table 5-1 shows that the values of standard deviations predominantly stay the same irrespective of the data rate and hence ROS. Therefore, it can be concluded, that the values of STD are independent of the signal, even in the worst case the difference is only 30%. Table 5-1 also contains the mean value of zeros and ones which is required for the calculation of the Q factor explained in the next section

5.4 Summary

To conclude, an expression for the SNR needed to support DFE has been used to develop a method of predicting the maximum achievable OOK data rate when an FC is integrated into a receiver. The validity of this method has been demonstrated using the results of experiments with FCs. In addition, the ability to take into account the bandwidth of the FC has been demonstrated using experimental results from two other FCs. Consequently, the maximum OOK data rate that can be achieved when an FC is added to a receiver can be predicted. However, these predictions are based on numerical calculations. Two equations which are an accurate approximation to the results of the numerical calculation, which can easily be used to predict the impact of adding an FC to a receiver, have therefore been presented. These equations clearly demonstrate that when selecting a fluorophore for use in an FC, or fluorescent fibre to use as an FC, the resulting bandwidth is an important characteristic.

Furthermore, a detailed analysis of the experimental data was performed to investigate whether the dominant source of noise is signal-dependent or signal-independent. The findings of this work further validate that the noise in the system is significantly signal-independent. Even at the highest ROS the impact of signal dependence is quite negligible. The histograms and measured standard deviations of the experimental data at different data rates further validate the assumption that noise in the system is Gaussian. The specific reason why it is still unknown, however, it could be an impact of trans-impedance amplifier in the APD.

6 Summary and Future work

6.1 Summary

The growing indoor data demand made a challenging situation to serve the user's requests. Wi-Fi is the most popular technology that is currently used for indoor communication. However, the progress in these technologies is not enough to meet user expectations. Visible light communication (VLC) is a potential candidate for short-range and indoor communications in meeting this challenge by accompanying conventional RF transmission. VLC uses LEDs as a transmitter which is already part of the existing infrastructure. So, VLC can provide a cheap and efficient solution, as LEDs can work both for illumination and communication simultaneously. The receiver, on the other hand, follows the principle of direct detection in which the photodetector generates an electric current depending upon the incident optical power. This kind of transmission is generally known as intensity modulation/ direct detection, IM/DD.

A better receiver in VLC means a wide field of view and a more extensive collection area. However, increasing the detector’s area ended up having a higher capacitance and low bandwidth (BW) which are not desirable. So, an optical concentrator can be used to improve the SNR and system capacity (BW and data rate). A geometrical property called etendue limits the efficiency of these optical concentrators. This conservation of etendue means that the concentrating factor (maximum gain) of these concentrators limits the maximum acceptance angle. This problem can be solved by using fluorescent concentrators (FC), which do not only depend upon the phenomenon of reflection and refraction alone. The fluorophore in FC absorbs light at a lower wavelength and emits it at a higher wavelength. As the responsivity of most of the APDs is higher at a longer wavelength, the wavelength shifting property of an FC brings an advantage by increasing their gain as compared to other optical concentrators.

The effectiveness of blue filtering is subject to the SNR required to push the data rate this concept has been demonstrated experimentally. If the SNR is not large enough, just an increase in BW alone will not be helpful in increasing the achievable data rate. A commercially available wide FOV slab concentrator with the inherent capacity of blue filtering was introduced which has the capability of replacing CPC and PC, given the fact it has larger FOV and better communication performances. FC acts as a natural filter and cuts the slow phosphor component of WLED and only allows the faster (blue component of light) to transmit. which makes the receiver more robust to the impact of ambient light. Moreover, multiple fibres-based FCs were characterised for their performances in a VLC link, a green colour fibre with 24 MHz BW and a gain of approximately 8 was selected for data transmission which shows the data rate with FC increased by a factor of 3.

Furthermore, a simple and inexpensive receiver that was created by using fluorescent fibres was investigated to evaluate its ability to perform WDM. The ultimate benefit of the FC-based WDM system is that they not only provide a large FOV but also yields a higher gain as compared to the typical optical filters. Three different wavelength absorbing fluorescent fibres were therefore tested for a WDM link. Initial results demonstrated a very low cross talk which is an ideal condition for enabling a WDM system along with a wide FOV. Unfortunately, due to a significant difference in the light collection efficiency and hence the data rates of the three fibres means that adding three channels via WDM would not further improve the link capacity under eye safe limits. However, an ideal H-matrix of the red and the Saint Gobain fibre predicts that a 2 ×2 WDM channel be developed by using the existing fibre. This study emphasises the importance of the selection of a suitable choice of FC for a WDM optical link.

In addition, the constantly changing orientation of receivers at the user end creates problems with connectivity. In the past, an omnidirectional receiver that incorporates six detectors was presented, which unnecessarily increases the cost and complexity of the system. To overcome this challenge, a simple fluorescent fibre-based receiver is presented which offers a large FOV of ±120°. Furthermore, with this receiver, a gigabit data transmission was achieved at the worst angle of 120°.

A method to determine the benefits of using a concentrator is not available. The equations which could be used to predict the impact of adding FC in an optical link are discussed with the experimental results. The results suggest that while selecting fluorescent concentrators the most important characteristic is the bandwidth. Finally, the method to predict the maximum achievable OOK data rate is validated on three different wavelength absorbing fibres. A detailed analysis of noise is also presented which proves that the dominant source of the noise is signal-independent. The results histograms and standard deviations of the experimental data are discussed which further confirms the Gaussian nature of noise even at the highest ROS levels.

6.2 Future work

The fluorescent concentrator-based receiver offers several advantages for VLC which suggests that they have a promising future for VLC. Due to their large FOV, higher collection efficiency, low cost and simple structure, FCs will remain in demand. In this project, different types of fluorescent concentrators are discussed and a comparative study of low BW FCs and a blue filter is presented. Furthermore, a wide range of fibre fluorescent concentrators was evaluated for their performances in a communication link along with a method to predict the data rate by adding an FC.

At present, the experiments reported in chapters 3 and 6 were performed on four different systems which had a dominant single-pole. Further work could be done to investigate links between a fixed single pole and a pole that is introduced at a variable frequency within MATLAB. This can be used to determine when the bandwidth of an FC is so large compared to the existing link bandwidth that the FC effectively adds gain (just like a CPC).

The experimental investigation in this thesis is limited to 2-PAM-based modulation on-off keying (OOK) with a decision feedback equaliser. A number of other modulation schemes like 4-PAM and OFDM which may or may not offer further improvement in the system's performance could be investigated. In addition, imaging MIMO schemes and WDM with the FCs (by using multiple TX, RX and FCs) which have similar optical gain is an area worthy of investigation. One prominent

advantage of using an FC is the increase in RX output voltage. This could be exploited to increase the transmitted data rate by using PAM, which increases the data rate by using more than two levels in a symbol period. It is anticipated that channels with multiple poles will require large optical gains to achieve a high OOK data rate. In these circumstances, the same data rate might be achieved more efficiently by using a longer symbol time but more levels. Moreover, since the links that employ LEDs can have very small bandwidths but a large SNR OFDM is a popular modulation scheme. Therefore the use of an FC with a WLED transmitter with OFDM can be investigated. The performance of an optical link when OOK, 4-PAM and OFDM are employed alternatively with an FC could be evaluated to investigate which modulation scheme performs better with an FC.

Some additional work could be done to make the smartphone receiver work that has already been presented in this thesis more comprehensive, for example by demonstrating that fibres can have a FOV of almost 360°. One possibility can be to use a couple of fibres on all 4 ends of the smartphone so that the incident light is not blocked by the body of the smartphone. This can be demonstrated by coupling a fibre concentrator on the edges of a smartphone or the top edge of the laptop. Further work on improving the sensitivity and the random orientation of the hand-held device in a room and the impact of this on the FOV needed in the two directions can be done. Additional research can be carried out focusing on increasing the ROS by making fibre bundles etc. Finally, incorporating FC in a real smartphone could also be done, however, in a real system, for a better coverage the fibre may be put closer to the front edge rather than in the centre.

References

[1] Wang, C.X., Haider, F., Gao, X., You, X.H., Yang, Y., Yuan, D., Aggoune, H.M., Haas, H., Fletcher, S. and Hepsaydir, E., 2014. Cellular architecture and key technologies for 5G wireless communication networks. IEEE communications magazine, 52(2), pp.122-130.

[2] Matheus, L.E.M., Vieira, A.B., Vieira, L.F., Vieira, M.A. and Gnawali, O., 2019. Visible light communication: concepts, applications and challenges. IEEE Communications Surveys & Tutorials, 21(4), pp.3204-3237.

[3] Kavehrad, M., 2013, February. Optical wireless applications: A solution to ease the wireless airwaves spectrum crunch. In Broadband Access Communication Technologies Vii (Vol. 8645, pp. 109-115). SPIE.

[4] Abuella, H., Elamassie, M., Uysal, M., Xu, Z., Serpedin, E., Qaraqe, K.A. and Ekin, S., 2021. Hybrid RF/VLC systems: A comprehensive survey on network topologies, performance analyses, applications, and future directions. IEEE Access.

[5] Hranilovic, S., 2005. On the design of bandwidth efficient signalling for indoor wireless optical channels. International Journal of Communication Systems, 18(3), pp.205-228.

[6] Wang, S., Lei, T., Zhang, L., Hsu, C.H. and Yang, F., 2016. Offloading mobile data traffic for QoS-aware service provision in vehicular cyber-physical systems. Future Generation Computer Systems, 61, pp.118-127.

[7] Arnon, S., Barry, J., Karagiannidis, G., Schober, R. and Uysal, M. eds., 2012. Advanced optical wireless communication systems. Cambridge university press.

[8] Saadi, M., Wattisuttikulkij, L., Zhao, Y. and Sangwongngam, P., 2013. Visible light communication: opportunities, challenges and channel models. International Journal of Electronics & Informatics, 2(1), pp.1-11.

[9] Medina, C., Zambrano, M. and Navarro, K., 2015. Led based visible light communication: Technology, applications and challenges-a survey. International Journal of Advances in Engineering & Technology, 8(4), p.482.

[10] Liao, C.L., Chang, Y.F., Ho, C.L., Wu, M.C., Hsieh, Y.T., Li, C.Y., Houng, M.P. and Yang, C.F., 2015, August. Light-emitting diodes for visible light communication. In 2015 International Wireless Communications and Mobile Computing Conference (IWCMC) (pp. 665-667). IEEE.

[11] Feng, L., Hu, R.Q., Wang, J., Xu, P. and Qian, Y., 2016. Applying VLC in 5G networks: Architectures and key technologies. IEEE Network, 30(6), pp.77-83.

[12] Gancarz, J., Elgala, H. and Little, T.D., 2013. Impact of lighting requirements on VLC systems. IEEE Communications Magazine, 51(12), pp.34-41.

[13] Arnon, S. ed., 2015. Visible light communication. Cambridge University Press.

[14] Jovicic, A., Li, J. and Richardson, T., 2013. Visible light communication: opportunities, challenges and the path to market. IEEE Communications Magazine, 51(12), pp.26-32.

[15] Komine, T. and Nakagawa, M., 2004. Fundamental analysis for visible-light communication system using LED lights. IEEE transactions on Consumer Electronics, 50(1), pp.100-107.

[16] Haas, H., 2015, March. Visible light communication. In 2015 Optical Fiber Communications Conference and Exhibition (OFC) (pp. 1-72). IEEE.

[17] Xia, F., Mueller, T., Lin, Y.M., Valdes-Garcia, A. and Avouris, P., 2009. Ultrafast graphene photodetector. Nature nanotechnology, 4(12), pp.839-843.

[18] Forrest, S.R., 1986. Optical detectors: Three contenders: Depending on the application, the photoeonductor, pin diode, or avalanche photodiode may prove the best choice. IEEE Spectrum, 23(5), pp.76-85.

[19] Karunatilaka, D., Zafar, F., Kalavally, V. and Parthiban, R., 2015. LED based indoor visible

light communications: State of the art. IEEE communications surveys & tutorials, 17(3), pp.1649-1678.
[20] Ghassemlooy, Z., Popoola, W. and Rajbhandari, S., 2019. Optical wireless communications: system and channel modelling with Matlab®. CRC press.
[21] Rajagopal, S., Roberts, R.D. and Lim, S.K., 2012. IEEE 802.15. 7 visible light communication: modulation schemes and dimming support. IEEE Communications Magazine, 50(3), pp.72-82.
[22] Carruther, J.B. and Kahn, J.M., 2000. Angle diversity for nondirected wireless infrared communication. IEEE Transactions on Communications, 48(6), pp.960-969.
[23] Marsh, G.W. and Kahn, J.M., 1996. Performance evaluation of experimental 50-Mb/s diffuse infrared wireless link using on-off keying with decision-feedback equalization. IEEE Transactions on Communications, 44(11), pp.1496-1504.
[24] Chi, N., Zhang, M., Zhou, Y. and Zhao, J., 2016. 3.375-Gb/s RGB-LED based WDM visible light communication system employing PAM-8 modulation with phase shifted Manchester coding. Optics express, 24(19), pp.21663-21673.
[25] Mesleh, R., Elgala, H. and Haas, H., 2011. On the performance of different OFDM based optical wireless communication systems. Journal of Optical Communications and Networking, 3(8), pp.620-628.
[26] Mossaad, M.S., Hranilovic, S. and Lampe, L., 2015. Visible light communications using OFDM and multiple LEDs. IEEE Transactions on Communications, 63(11), pp.4304-4313.
[27] He, C., Ahmed, Z. and Collins, S., 2020, December. Optical OFDM and SiPM Receivers. In 2020 IEEE Globecom Workshops (GC Wkshps (pp. 1-6). IEEE.
[28] Yu, M. and Chun, H., 2022. RCS-OFDM enabling full brightness control with power-efficient visible-light communication. Optics Letters, 47(2), pp.277-280.
[29] Hanzo, L., Ng, S.X., Webb, W.T. and Keller, T., 2004. Quadrature amplitude modulation: From basics to adaptive trellis-coded, turbo-equalised and space-time coded OFDM, CDMA and MC-CDMA systems. IEEE Press-John Wiley.
[30] Korde, R. and Geist, J., 1987. Quantum efficiency stability of silicon photodiodes. Applied Optics, 26(24), pp.5284-5290.
[31] Stillman, G.E. and Wolfe, C.M., 1977. Avalanche photodiodes. In Semiconductors and semimetals (Vol. 12, pp. 291-393). Elsevier.
[32] Ahmed, Z., Singh, R., Ali, W., Faulkner, G., O'Brien, D. and Collins, S., 2020. A SiPM-based VLC receiver for Gigabit communication using OOK modulation. IEEE Photonics Technology Letters, 32(6), pp.317-320.
[33] Ahmed, Z., Zhang, L., Faulkner, G., O'Brien, D. and Collins, S., 2019, May. A shot-noise limited 420 Mbps visible light communication system using commerical off-the-shelf silicon photomultiplier (SiPM). In 2019 IEEE International Conference on Communications Workshops (ICC Workshops) (pp. 1-5). IEEE.
[34] Zhang, L., Chun, H., Ahmed, Z., Faulkner, G., O'Brien, D. and Collins, S., 2019. The future prospects for SiPM-based receivers for visible light communications. Journal of Lightwave Technology, 37(17), pp.4367-4374.
[35] Ali, W., Faulkner, G., Ahmed, Z., Matthews, W., O'Brien, D. and Collins, S., 2020, December. Silicon photomultiplier receivers and future VLC systems. In 2020 IEEE Globecom Workshops (GC Wkshps (pp. 1-5). IEEE.
[36] Gupta, A. and Garg, P., 2018. Statistics of SNR for an indoor VLC system and its applications in system performance. IEEE Communications Letters, 22(9), pp.1898-1901.
[37] Rajbhandari, S., Chun, H., Faulkner, G., Cameron, K., Jalajakumari, A.V., Henderson, R., Tsonev, D., Ijaz, M., Chen, Z., Haas, H. and Xie, E., 2015. High-speed integrated visible light communication system: Device constraints and design considerations. IEEE Journal on Selected Areas in Communications, 33(9), pp.1750-1757.
[38] H. Chun, S. Rajbhandari, G. Faulkner, D. Tsonev, H. Haas, and D. O'Brien, "Visible Light Communication using Laser Diode based Remote Phosphor Technique" IEEE International

Conference on Communications (ICC), June 2015.
[39] Rajbhandari, S., Chun, H., Faulkner, G., Haas, H., Xie, E., McKendry, J.J., Herrnsdorf, J., Gu, E., Dawson, M.D. and O'Brien, D., 2019. Neural network-based joint spatial and temporal equalization for MIMO-VLC system. IEEE Photonics Technology Letters, 31(11), pp.821-824.
[40] Bandara, K.D., Niroopan, P. and Yeon-Ho, C., 2013. Improved indoor visible light communication with PAM and RLS decision feedback equalizer. IETE Journal of Research, 59(6), pp.672-678.
[41] Bandara, K. and Chung, Y.H., 2012, October. Reduced training sequence using RLS adaptive algorithm with decision feedback equalizer in indoor visible light wireless communication channel. In 2012 International Conference on ICT Convergence (ICTC) (pp. 149-154). IEEE.
[42] Khan, L.U., 2017. Visible light communication: Applications, architecture, standardization and research challenges. Digital Communications and Networks, 3(2), pp.78-88.
[43] Kasper, B.L., Mizuhara, O. and Chen, Y.K., 2002. High bit-rate receivers, transmitters, and electronics. Optical Fiber Telecommunications IV-A, pp.784-851.
[44] Shaaban, R., Ranganathan, P. and Faruque, S., 2019, March. Visible light communication security vulnerabilities in multiuser network: power distribution and signal to noise ratio analysis. In Future of Information and Communication Conference (pp. 1-13). Springer, Cham.
[45] Cossu, G., Khalid, A.M., Choudhury, P., Corsini, R. and Ciaramella, E., 2012. 3.4 Gbit/s visible optical wireless transmission based on RGB LED. Optics express, 20(26), pp.B501-B506.
[46] Zhang, C., Wei, Z., Li, X., Li, Y., Wang, L., Wang, L., Fu, H.Y. and Yang, Y., 2022. 3.8 Gb/s PAM-4 UOWC System Over a 2-m Underwater Channel Enabled by a Single-Pixel 175-μm GaN-Based Mini-LED. IEEE Photonics Journal, 14(3), pp.1-7.
[47] Träger, F. ed., 2012. Springer handbook of lasers and optics (Vol. 2). New York, NY, USA:: springer.
[48] Zafar, F., Bakaul, M. and Parthiban, R., 2017. Laser-diode-based visible light communication: Toward gigabit class communication. IEEE Communications Magazine, 55(2), pp.144-151.
[49] Campbell, J.C., Demiguel, S., Ma, F., Beck, A., Guo, X., Wang, S., Zheng, X., Li, X., Beck, J.D., Kinch, M.A. and Huntington, A., 2004. Recent advances in avalanche photodiodes. IEEE Journal of selected topics in quantum electronics, 10(4), pp.777-787.
[50] Piatek, S., 2014. Measuring the electrical and optical properties of the MPPC silicon photomultiplier. Hamamatsu Corporation and New Jersey Institute of Technology.
[51] Grobe, L., Paraskevopoulos, A., Hilt, J., Schulz, D., Lassak, F., Hartlieb, F., Kottke, C., Jungnickel, V. and Langer, K.D., 2013. High-speed visible light communication systems. IEEE communications magazine, 51(12), pp.60-66.
[52] Winston, R., 2005. JC Mi nano, and P. Benítez. Nonimaging Optics.
[53] Winston, R., 1976. Dielectric compound parabolic concentrators. Applied optics, 15(2), pp.291-292.
[54] Winston, R., Wang, C. and Zhang, W., 2009, August. Beating the optical Liouville theorem: How does geometrical optics know the second law of thermodynamics?. In Nonimaging Optics: Efficient Design for Illumination and Solar Concentration VI (Vol. 7423, pp. 92-94). SPIE.
[55] Collins, S., O'Brien, D.C. and Watt, A., 2014. High gain, wide field of view concentrator for optical communications. Optics letters, 39(7), pp.1756-1759.
[56] Hermann, A.M., 1982. Luminescent solar concentrators—a review. Solar Energy, 29(4), pp.323-329.
[57] Batchelder, J.S., Zewai, A.H. and Cole, T., 1979. Luminescent solar concentrators. 1: Theory of operation and techniques for performance evaluation. Applied Optics, 18(18), pp.3090-3110.
[58] Luque, A., Martí, A., Bett, A., Andreev, V.M., Jaussaud, C., Van Roosmalen, J.A.M., Alonso,

J., Räuber, A., Strobl, G., Stolz, W. and Algora, C., 2005. FULLSPECTRUM: a new PV wave making more efficient use of the solar spectrum. Solar energy materials and solar cells, 87(1-4), pp.467-479.
[59] Corrado, C., Leow, S.W., Osborn, M., Chan, E., Balaban, B. and Carter, S.A., 2013. Optimization of gain and energy conversion efficiency using front-facing photovoltaic cell luminescent solar concentratordesign. Solar Energy Materials and Solar Cells, 111, pp.74-81.
[60] Hermann, A.M., 1982. Luminescent solar concentrators—a review. Solar Energy, 29(4), pp.323-329.
[61] Batchelder, J.S., Zewai, A.H. and Cole, T., 1979. Luminescent solar concentrators. 1: Theory of operation and techniques for performance evaluation. Applied Optics, 18(18), pp.3090-3110.
[62] Wittwer, V., Stahl, W. and Goetzberger, A., 1984. Fluorescent planar concentrators. Solar Energy Materials, 11(3), pp.187-197.
[63] Alberto, G., Miletto, I., Viscardi, G., Caputo, G., Latterini, L., Coluccia, S. and Martra, G., 2009. Hybrid cyanine− silica nanoparticles: homogeneous photoemission behavior of entrapped fluorophores and consequent high brightness enhancement. The Journal of Physical Chemistry C, 113(50), pp.21048-21053.
[64] Riaz, A., Faulkner, G. and Collins, S., 2019, June. A fluorescent antenna for white light visible light communications. In 2019 Global LiFi Congress (GLC) (pp. 1-4). IEEE.
[65] RIAZ, A. and COLLINS, S., A green absorbing fluorescent fibre concentrator for VLC.
[66] Riaz, A. and Collins, S., 2020, December. A wide field of view VLC receiver for smartphones. In 2020 European Conference on Optical Communications (ECOC) (pp. 1-4). IEEE.
[67] Zastrow, A., 1994. Physics and applications of fluorescent concentrators: a review. Optical Materials Technology for Energy Efficiency and Solar Energy Conversion XIII, 2255, pp.534-547.
[68] Sottile, M., Tomei, G., Borsacchi, S., Martini, F., Geppi, M., Ruggeri, G. and Pucci, A., 2017. Epoxy resin doped with Coumarin 6: Example of accessible luminescent collectors. European Polymer Journal, 89, pp.23-33..
[69] Sajjad, M.T., Manousiadis, P.P., Chun, H., Vithanage, D.A., Rajbhandari, S., Kanibolotsky, A.L., Faulkner, G., O'Brien, D., Skabara, P.J., Samuel, I.D. and Turnbull, G.A., 2015. Novel fast color-converter for visible light communication using a blend of conjugated polymers. Acs Photonics, 2(2), pp.194-199.
[70] Stone, P.T., 1992. Fluorescent lighting and health. Lighting Research & Technology, 24(2), pp.55-61.
[71] Manousiadis, P.P., Rajbhandari, S., Mulyawan, R., Vithanage, D.A., Chun, H., Faulkner, G., O'Brien, D.C., Turnbull, G.A., Collins, S. and Samuel, I.D., 2016. Wide field-of-view fluorescent antenna for visible light communications beyond the étendue limit. Optica, 3(7), pp.702-706.
[72] Mulyawan, R., Gomez, A., Chun, H., Rajbhandari, S., Manousiadis, P.P., Vithanage, D.A., Faulkner, G., Turnbull, G.A., Samuel, I.D., Collins, S. and O'Brien, D., 2017, January. A comparative study of optical concentrators for visible light communications. In Broadband Access Communication Technologies XI (Vol. 10128, pp. 142-147). SPIE.
[73] Peyronel, T., Quirk, K.J., Wang, S.C. and Tiecke, T.G., 2016. Luminescent detector for free-space optical communication. Optica, 3(7), pp.787-792.
[74] Collins, S., Mulyawan, R., Rajbhandari, S., Chu, H., Faulkner, G.E., O'Brien, D.C., Manousiadis, P.P., Vithanage, D.A., Turnbull, G.A. and Samuel, I.D.W., 2015, July. A simple wide field of view concentrator for free space visible light communications. In 2015 IEEE Summer Topicals Meeting Series (SUM) (pp. 43-44). IEEE.
[75] Kang, C.H., Trichili, A., Alkhazragi, O., Zhang, H., Subedi, R.C., Guo, Y., Mitra, S., Shen, C., Roqan, I.S., Ng, T.K. and Alouini, M.S., 2019. Ultraviolet-to-blue color-converting scintillating-fibers photoreceiver for 375-nm laser-based underwater wireless optical communication. Optics express, 27(21), pp.30450-30461.

[76] Quintana, C., Chun, H., Mulyawan, R., Faulkner, G., Collins, S., O'Brien, D.C., Xie, E., McKendry, J.J., Gu, E., Dawson, M.D. and Manousiadis, P.P., 2018, February. Ultra-wide coverage VLC system with alignment-free receiver. In 2018 Global LIFI Congress (GLC) (pp. 1-4). IEEE.
[77] Mulyawan, R., Chun, H., Gomez, A., Rajbhandari, S., Faulkner, G., Manousiadis, P.P., Vithanage, D.A., Turnbull, G.A., Samuel, I.D., Collins, S. and O'Brien, D., 2017. MIMO visible light communications using a wide field-of-view fluorescent concentrator. IEEE Photonics Technology Letters, 29(3), pp.306-309.
[78] Manousiadis, P.P., Chun, H., Rajbhandari, S., Vithanage, D.A., Mulyawan, R., Faulkner, G., Haas, H., O'Brien, D.C., Collins, S., Turnbull, G.A. and Samuel, I.D., 2020. Optical antennas for wavelength division multiplexing in visible light communications beyond the étendue limit. Advanced Optical Materials, 8(4), p.1901139.
[79] Portnoi, M., Haigh, P.A., Macdonald, T.J., Ambroz, F., Parkin, I.P., Darwazeh, I. and Papakonstantinou, I., 2021. Bandwidth limits of luminescent solar concentrators as detectors in free-space optical communication systems. Light: Science & Applications, 10(1), pp.1-12.
[80] Surampudi, A., Singh, R., Riaz, A., Ali, W., Faulkner, G., O'Brien, D.C. and Collins, S., 2021. A Digital Pre-equalizer for Optical Wireless Links. Journal of Lightwave Technology.
[81] Ali, W., Manousiadis, P., O'Brien, D.C., Turnbull, G., Samuel, I. and Collins, S., 2021. A Gigabit VLC receiver that incorporates a fluorescent antenna and a SiPM. Journal of Lightwave Technology.
[82] Ali, W., Ahmed, Z., Matthews, W. and Collins, S., 2021. The impact of the length of fluorescent fiber concentrators on the performance of VLC receivers. IEEE Photonics Technology Letters, 33(24), pp.1451-1454.
[83] Cho, S. and Chun, H., 2021. Reflection based coupling efficiency enhancement in a fluorescent planar concentrator for an optical wireless receiver. Optics Express, 29(18), pp.28901-28911.
[84] Oh, S., Lee, Y., Yu, M., Cho, S., Javed, S. and Chun, H., 2022. Smart License Plate in Combination with Fluorescent Concentrator for Vehicular Visible Light Communication System. Sensors, 22(7), p.2485.
[85] Wang, Z., Zhang, L., Li, J., Wei, G., Dong, Y. and Fu, H.Y., 2022. Fluorescent concentrator based MISO-NOMA for visible light communications. Optics Letters, 47(4), pp.902-905.
[86] A. H. Azhar, T. Tran, and D. O. Brien, "A Gigabit / s Indoor Wireless Transmission Using," vol. 25, no. 2, pp. 171–174, 2013.
[87] Liao, C.L., Chang, Y.F., Ho, C.L., Wu, M.C., Hsieh, Y.T., Li, C.Y., Houng, M.P. and Yang, C.F., 2015, August. Light-emitting diodes for visible light communication. In 2015 International Wireless Communications and Mobile Computing Conference (IWCMC) (pp. 665-667). IEEE.
[88] Cossu, G., Khalid, A.M., Choudhury, P., Corsini, R. and Ciaramella, E., 2012. 3.4 Gbit/s visible optical wireless transmission based on RGB LED. Optics express, 20(26), pp.B501-B506.
[89] Anous, N., Ramadan, T., Abdallah, M., Qaraqe, K. and Khalil, D., 2018. Impact of blue filtering on effective modulation bandwidth and wide-angle operation in white LED-based VLC systems. OSA Continuum, 1(3), pp.910-929.
[90] Sung, J.Y., Chow, C.W. and Yeh, C.H., 2014. Is blue optical filter necessary in high speed phosphor-based white light LED visible light communications?. Optics express, 22(17), pp.20646-20651.
[91] Yeh, C.H., Chow, C.W., Chen, H.Y., Chen, J. and Liu, Y.L., 2014. Adaptive 84.44− 190 Mbit/s phosphor-LED wireless communication utilizing no blue filter at practical transmission distance. Optics Express, 22(8), pp.9783-9788.
[92] Wang, S.W., Chen, F., Liang, L., He, S., Wang, Y., Chen, X. and Lu, W., 2015. A high-performance blue filter for a white-led-based visible light communication system. IEEE wireless communications, 22(2), pp.61-67.

[93] Chun, H., Rajbhandari, S., Faulkner, G. and O'Brien, D., 2014, September. Effectiveness of blue-filtering in WLED based indoor visible light communication. In 2014 3rd International Workshop in Optical Wireless Communications (IWOW) (pp. 60-64). IEEE.
[94] https://www.saint-gobain.co.uk/
[95] Randel, S., Breyer, F., Lee, S.C. and Walewski, J.W., 2010. Advanced modulation schemes for short-range optical communications. IEEE Journal of Selected Topics in Quantum Electronics, 16(5), pp.1280-1289.
[96] Chun, H., 2015. Multi gigabit/s visible light communications: modelling and demonstrations (Doctoral dissertation, University of Oxford)
[97] Tsai, C.T., Cheng, C.H., Kuo, H.C. and Lin, G.R., 2019. Toward high-speed visible laser lighting based optical wireless communications. Progress in Quantum Electronics, 67, p.100225.
[98] Rajbhandari, S., 2016, July. Spatial and wavelength division multiplexing for high-speed VLC systems: An overview. In 2016 10th International Symposium on Communication Systems, Networks and Digital Signal Processing (CSNDSP) (pp. 1-6). IEEE.
[99] Chun, H., Rajbhandari, S., Faulkner, G., Tsonev, D., Xie, E., McKendry, J.J.D., Gu, E., Dawson, M.D., O'Brien, D.C. and Haas, H., 2016. LED based wavelength division multiplexed 10 Gb/s visible light communications. Journal of lightwave technology, 34(13), pp.3047-3052.
[100] Rajbhandari, S., McKendry, J.J., Herrnsdorf, J., Chun, H., Faulkner, G., Haas, H., Watson, I.M., O'Brien, D. and Dawson, M.D., 2017. A review of gallium nitride LEDs for multi-gigabit-per-second visible light data communications. Semiconductor Science and Technology, 32(2), p.023001.
[101] Vučić, J., Kottke, C., Habel, K. and Langer, K.D., 2011, March. 803 Mbit/s visible light WDM link based on DMT modulation of a single RGB LED luminary. In Optical Fiber Communication Conference (p. OWB6). Optica Publishing Group.
[102] Manousiadis, P.P., Chun, H., Rajbhandari, S., Vithanage, D.A., Mulyawan, R., Faulkner, G., Haas, H., O'Brien, D.C., Collins, S., Turnbull, G.A. and Samuel, I.D., 2020. Optical antennas for wavelength division multiplexing in visible light communications beyond the étendue limit. Advanced Optical Materials, 8(4), p.1901139.
[103] Wang, W.C., Wang, H.Y. and Lin, G.R., 2018. Ultrahigh-speed violet laser diode based free-space optical communication beyond 25 Gbit/s. Scientific reports, 8(1), pp.1-7.
[104] Lee, C., Zhang, C., Cantore, M., Farrell, R.M., Oh, S.H., Margalith, T., Speck, J.S., Nakamura, S., Bowers, J.E. and DenBaars, S.P., 2015. 4 Gbps direct modulation of 450 nm GaN laser for high-speed visible light communication. Optics express, 23(12), pp.16232-16237.
[105] Liu, X., Yi, S., Zhou, X., Fang, Z., Qiu, Z.J., Hu, L., Cong, C., Zheng, L., Liu, R. and Tian, P., 2017. 34.5 m underwater optical wireless communication with 2.70 Gbps data rate based on a green laser diode with NRZ-OOK modulation. Optics express, 25(22), pp.27937-27947.
[106] T. C. Wu, Y. C. Chi, H. Y. Wang, C. T. Tsai, and G. R. Lin, "Blue laser diode enables underwater communication at 12.4 Gbps," Sci. Rep. 7, 40480 (2017).
[107] Shen, C., Guo, Y., Oubei, H.M., Ng, T.K., Liu, G., Park, K.H., Ho, K.T., Alouini, M.S. and Ooi, B.S., 2016. 20-meter underwater wireless optical communication link with 1.5 Gbps data rate. Optics express, 24(22), pp.25502-25509.
[108] Hussey, C.D. and Minelly, J.D., 1988. Optical fibre polishing with a motor driven polishing wheel. Electronics Letters, 24(13), pp.805-807..
[109] Schreier, A., 2020. Distributed Brillouin sensor in polymer optical fibers utilizing BOFDA. Cuvillier Verlag.
[110] Ali, W., Faulkner, G., Ahmed, Z., Matthews, W. and Collins, S., 2021. Giga-bit Transmission between an Eye-safe transmitter and wide field-of-view SiPM receiver. IEEE Access, 9, pp.154225-154236.

[111] O'Brien, D.C. and Zeng, L., 2008. Le-Minh, H. Faulkner, G. Walewski, JW Randel, S.,"Visible light communications: Challenges and possibilities", Indoor and Mobile Radio Communications, 2008. PIMRC 2008. In IEEE 19th International Symposium on.
[112] Komine, T. and Nakagawa, M., 2004. Fundamental analysis for visible-light communication system using LED lights. IEEE transactions on Consumer Electronics, 50(1), pp.100-107.
[113] Tsonev, D., Videv, S. and Haas, H., 2015. Towards a 100 Gb/s visible light wireless access network. Optics express, 23(2), pp.1627-1637.
[114] Soltani, M.D., Purwita, A.A., Zeng, Z., Haas, H. and Safari, M., 2018. Modeling the random orientation of mobile devices: Measurement, analysis and LiFi use case. IEEE Transactions on Communications, 67(3), pp.2157-2172.
[115] Purwita, A.A., Soltani, M.D., Safari, M. and Haas, H., 2019. Terminal orientation in OFDM-based LiFi systems. IEEE Transactions on Wireless Communications, 18(8), pp.4003-4016.
[116] Chen, C., Soltani, M.D., Safari, M., Purwita, A.A., Wu, X. and Haas, H., 2019, May. An omnidirectional user equipment configuration to support mobility in LiFi networks. In 2019 IEEE International Conference on Communications Workshops (ICC Workshops) (pp. 1-6). IEEE.
[117] Janjua, B., Oubei, H.M., Retamal, J.R.D., Ng, T.K., Tsai, C.T., Wang, H.Y., Chi, Y.C., Kuo, H.C., Lin, G.R., He, J.H. and Ooi, B.S., 2015. Going beyond 4 Gbps data rate by employing RGB laser diodes for visible light communication. Optics express, 23(14), pp.18746-18753.
[118] Säckinger, E., 2017. Analysis and design of transimpedance amplifiers for optical receivers. John Wiley & Sons.
[119] Alexander, S.B., 1997. Optical communication receiver design (Vol. 37). SPIE Press.
[120] Couch, L.W., Kulkarni, M. and Acharya, U.S., 2013. Digital and analog communication systems (Vol. 8). Upper Saddle River: Pearson.
[121] Large, D. and Farmer, J., 2004. Modern cable television technology. Elsevier.